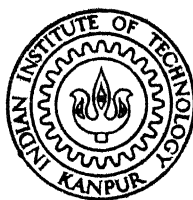


VIBRATIONAL DYNAMICS AND PHASE TRANSITIONS IN TETRAMETHYL AMMONIUM COMPOUNDS

By
MAHENDRA PAL



DEPARTMENT OF PHYSICS

INDIAN INSTITUTE OF TECHNOLOGY KANPUR

MARCH, 1984

PHY
1984
D
PAL
VIB

TH
PHY/1984/D
P17v

7910102

VIBRATIONAL DYNAMICS AND PHASE TRANSITIONS IN TETRAMETHYL AMMONIUM COMPOUNDS

A Thesis Submitted
in Partial Fulfilment of the Requirements
for the Degree of
DOCTOR OF PHILOSOPHY

By
MAHENDRA PAL

to the

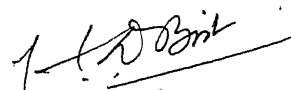
DEPARTMENT OF PHYSICS
INDIAN INSTITUTE OF TECHNOLOGY KANPUR
MARCH, 1984

87525

PHY-1984-D-PAL-VIB

CERTIFICATE

This is to certify that the work presented in this thesis entitled "VIBRATIONAL DYNAMICS AND PHASE TRANSITIONS IN TETRAETHYL AMMONIUM COMPOUNDS" is carried out by Mr. Mahendra Pal under my supervision and has not been submitted elsewhere for a degree or diploma.



H D Bist

Professor of Physics

Date: March 9, 1984.

ACKNOWLEDGEMENT

I express my deep sense of gratitude to Professor H D Bist for introducing me to the field and his stimulating guidance throughout the course of this work.

I feel pleasure in thanking to Professor D P Khandelwal for numerous stimulating discussions and valuable suggestions on the subject.

I thank Professor D D Pant for the timely encouragement during his short visits to this place.

I am indebted to all my colleagues, especially Dr. M B Patel, Mr. G D Tewari, Dr. O P Lamba, Mr. P K Khowash, Dr. Kanik Ram and Dr. S Ram for their cooperation. I am also thankful to Dr. V N Sarin and Dr. P Chand for their timely help during the passage of this work.

Thanks are also due to Mr. K Rajgopalan for recording IR spectra and all others in workshop, glass blowing, graphic arts, central library etc. for their timely help. I wish to thank Mr. L S Bajpai for excellent typing, Mr. G S Thapa for tracing the figures and Mr. H K Panda and Mr. L S Rathaur for cyclostyling the stencils. My thanks are also to Mr. Ram Prakash, the lab. assistant.

Although my thanks, I feel, are in no way capable of expressing my feeling towards my friends, G S Raghuvanshi and his family, Atul Sen, Aruna Rajvanshi and Anshu Agarwal whose company kept me unceasingly enthusiastic and made my days in IIT Kanpur a memorable event, still I thank them to express a part of it.

I express my profound regards to my parents for their constant inspiration. I feel elated in expressing my gratitude to my brothers, Dr. S P Verma and Mr. Virendra Kumar whose suggestions, help and kind wishes gave me vigour to accomplish the present work. I extend my sincere thanks to all my brothers, sisters and other family members for their encouragement.

MAHENDRA PAL

TABLE OF CONTENTS

	<u>Page</u>
SYNOPSIS	vii
CHAPTER 1 INTRODUCTION	1
1.1 The Dynamics of a Molecule	1
1.2 Anharmonicity and Interaction of Vibrations	6
1.3 Fermi Resonance	8
1.4 Isotope Effect	13
1.5 Structural Phase Transitions	15
1.6 Earlier Studies on Tetramethyl Ammonium Halogides	22
1.7 Earlier Studies on Tetramethyl Ammonium Tetrahalo Metallates	24
REFERENCES	25
TABLES	34
FIGURES	36
CHAPTER 2 EXPERIMENTAL	37
2.1 Sample Preparation	37
2.2 Raman Spectra	38
2.3 Infrared Spectra	42
2.4 Resolution of the Overlapping Bands	43
REFERENCES	46
FIGURES	47

CHAPTER 3	VIBRATIONAL STUDIES AND PHASE TRANSITIONS IN NORMAL (d_0) AND PERDEUTERATED (d_{12}) TETRAMETHYL AMMONIUM CHLORIDES	52
3.1	Crystal Structure	52
3.2	Group Theoretical Analysis	54
3.3	Vibrational Spectra of TMACl-d_0 in Aqueous Solutions	55
3.4	Characteristic Raman Spectra of TMACl-d_0 in the Four Phases Above Liquid Nitrogen Temperature and Their Assignments	63
3.5	Infrared Spectra of TMACl-d_0	67
3.6	Raman Spectra of TMACl-d_{12} in Phases III and II	69
3.7	Phase Transitions	72
3.8	Conclusion	74
	REFERENCES	76
	TABLES	78
	FIGURES	91
CHAPTER 4	VIBRATIONAL STUDIES OF TETRAMETHYL AMMONIUM BROMIDE AND IODIDE	101
4.1	Crystal Structure and Group Theoretical Analysis	101
4.2	Characteristic Raman Spectra of Normal (d_0) TMAI and TMAI at 300 and 100 K	103
4.3	Dynamic Disorder of TMA Ion in Normal (d_0) TMA Halides	103

	<u>Page</u>
4.4 Raman Spectra of Selectively Deuterated Tetramethyl Ammonium Iodides	107
4.5 Conclusion	113
REFERENCES	114
TABLES	115
FIGURES	121
CHAPTER 5 INCOMMENSURATE PHASE IN TETRAMETHYL AMMONIUM TETRACHLORO ZINCATE	125
5.1 Crystal Structure and Group Theoretical Analysis	125
5.2 Raman Spectra of $(TMA)_2ZnCl_4$ Crystal	127
5.3 Phase Transitions in $(TMA)_2ZnCl_4$	128
5.4 Conclusion	130
REFERENCES	132
TABLES	134
FIGURES	137
CHAPTER 6 CONCLUSION	140
LIST OF PUBLICATIONS	

SYNOPSIS

VIBRATIONAL DYNAMICS AND PHASE TRANSITIONS IN TETRAMETHYL AMMONIUM COMPOUNDS

MAHENDRA PAL

Ph.D.

DEPARTMENT OF PHYSICS
INDIAN INSTITUTE OF TECHNOLOGY KANPUR

March, 1984.

Tetramethyl ammonium halides (abbreviated as TMACl, TMABr and TMAI for chloride, bromide and iodide, respectively) and tetramethyl ammonium tetrachloro zincate (abbreviated as $(\text{TMA})_2\text{ZnCl}_4$) have been taken up for detailed temperature dependent Raman studies in view of the following facts :

(i) The present vibrational assignments of the modes for the TMA moiety are controversial in solution as well as in the solid phases; (ii) The TMA halides, in general, are isostructural at room temperature with space group D_{4h}^{7-} ($Z = 2$), but only TMACl is known to undergo four successive phase transitions between 4 and 540 K; (iii) The nature and mechanism of these phase transitions in TMACl are not yet clearly understood; and (iv) $(\text{TMA})_2\text{ZnCl}_4$ undergoes several successive phase transitions including an incommensurate phase between 296.65 and 280.95 K. On the basis of these studies we have been able to provide

detailed vibrational assignments for the observed bands in all the salts. Further we have been able to observe all the reported phase transitions in TMA₂Cl above liquid nitrogen temperature and specify their characteristics at each of the transition temperatures. We have also confirmed the incommensurate phase in (TMA)₂ZnCl₄ through Raman spectra.

Chapter 1 of the thesis reviews the various aspects of vibrational spectroscopy, such as vibrations in molecules and crystals, group theoretical analysis, mechanical and electrical anharmonicities, Fermi resonance, isotope effect etc. The different types of phase transitions and various experimental techniques used for their investigations are also reviewed in this chapter.

Chapter 2 contains details of the techniques used with 'Spex Ramalog spectrophotometer system' for Raman spectra and 'Perkin Elmer 580' for infrared spectra, and accessories such as the low and high temperature cells fabricated in our laboratory for Raman studies, and 'Specac variable temperature cell' used for infrared studies. The technique for obtaining temperatures below the normal boiling point of liquid nitrogen (upto 63 K, the freezing point), viz. evaporating the coolant at lower pressure, has also been described here.

In Chapter 3, the vibrational assignments of the observed Raman and infrared bands in aqueous solutions and in various phases of normal (d₀) and perdeuterated (d₁₂) tetramethyl ammonium chloride are proposed on the basis of polarization

data and concentration dependence of intensity in aqueous solutions, and the splitting of the bands on lowering the temperature in the polycrystalline samples. For explaining the occurrence of three intense and polarized bands in the CH_3 stretching region, which switch over intensities on variation of concentration, a model is proposed according to which the T_d symmetry of TMA ion dynamically distorts to C_{3v} . The three phase transitions in TMACl-d_0 above liquid nitrogen temperatures have been confirmed on the basis of these studies. Numbering the phases from high temperature downwards, the following inferences have been drawn from the spectra :

- (i) The phase transition $\text{II} \rightleftharpoons \text{I}$, occurring at 536 K, is due to ionic diffusion in which H atoms of TMA get relatively free.
- (ii) The transition $\text{III} \rightarrow \text{II}$ is irreversible and of the reconstructive type and this transition temperature depends on the rate of heating. The transition occurs at 367 ± 2 K on keeping the sample under continuous vacuum during investigation.
- (iii) The transition $\text{III} \rightleftharpoons \text{IV}$ occurs at 185 K and is due to reorientation of CH_3 groups and tumbling of the whole TMA moiety. In TMACl-d_{12} a phase transition ($\text{III} \rightarrow \text{II}$) at 407 ± 5 K is only observed and it is also irreversible and of the reconstructive type. It is concluded that TMACl-d_{12} lies in between TMACl-d_0 and TMABr-d_0 in the generalized phase diagram of the TMA halides.

Chapter 4 deals with the temperature dependent Raman studies of TMABr and TMAI. The splitting of C_{4N} totally symmetric mode $\nu_3(A_1)$ in the iodide is discussed in terms of a disordered structure. The temperature induced variations of intensities of the components suggests occupation of two different sites which correspond to the different orientations of TMA : parallel and perpendicular. Their energy difference is deduced to be $0.43 \text{ KCal. mol}^{-1}$. The relative behaviours of the three halides are explained if the tumbling motion is governed by the free space available in the lattice in the three salts. It is in the order $I^- > Cl^- > Br^-$. A comparative study of selectively deuterated tetramethyl ammonium iodides (TMAI- d_n ; $n = 0, 1, 3, 9, 10, 11, 12$) samples is also presented in this chapter.

In Chapter 5, the Raman studies of single crystals of $(TMA)_2ZnCl_4$ in six polarization geometries are presented. The behaviour of the internal modes of TMA and $ZnCl_4^{--}$ in the incommensurate phase is particularly discussed.

Chapter 6 outlines the conclusions drawn from our studies and also gives some suggestions and prospects for future work.

1. INTRODUCTION

With the invention of lasers, the Raman scattering technique has become as powerful a tool as infrared absorption for the analysis and identification of materials and for the study of molecular dynamics and molecular structure [1]. Extensive information about the structure and symmetry of molecules as well as their vibrational energies can be obtained from these spectra. This chapter is intended as an introduction to the principles and practice of those aspects of Raman and infrared spectroscopy which are of major interest in our present research work.

1.1 THE DYNAMICS OF A MOLECULE

The dynamics of an isolated N-atomic molecule can be obtained in terms of $3N$ degrees of freedom. These may be classified as 3 translations + 3 rotations + $(3N-6)$ vibrations for a non-linear molecule or 3 translations + 2 rotations + $(3N-5)$ vibrations for a linear molecule. The vibrations of a molecule are described in terms of normal modes. A normal mode has the following properties [2,3] : (i) each atom of the system oscillates about its equilibrium position with simple harmonic motion having the same frequency and phase, and (ii) the relative velocities and amplitudes of individual atoms depend on their masses, and the nature of motion is so governed that no resultant translation or rotation of the

system as a whole takes place.

The vibrations of an isolated molecule in the gas phase are subject only to the symmetry restrictions based on its own intrinsic point group symmetry. The methods of classification of normal modes of a free molecule using group theoretical approach have been discussed by several workers [3-5].

Vibrational assignments of the observed frequencies of different modes of vibration are made by studying the infrared and Raman spectra of a molecule in vapour, liquid and solid phases and the state of polarization of Raman lines. Due to mathematical complexity only in a very few cases of simple molecules it has been possible to determine these vibrational frequencies on a purely theoretical basis. Analytical expressions for force constants as explicit functions of the observed frequencies and geometric parameters cannot generally be obtained. The only way for calculating the force constants from the observed frequencies is to use an iterative method. A starting set of force constants is assumed and refined by successive approximations until the set which yields the calculated frequencies in best agreement with the observed one is obtained. These studies lead to a knowledge of the structure of the molecules, like bond lengths, bond angles etc. The results are not always unique and isotopic substitution is often required to verify the force constants.

When a group of atoms constituting an ion or a molecule goes to build up a crystal, its normal modes usually undergo

three types of modifications : (i) splitting of degenerate vibrations, (ii) multiplicity due to the unit cell containing more than one molecule, and (iii) alternations in the selection rules. The vibrational potential energy (V) associated with a unit cell under harmonic approximation can be expressed as [6,7]

$$V = \sum_j (V_j^0 + V_j') + \sum_j \sum_k V_{jk} + V_L + \sum_j V_{Lj} \quad (1.1)$$

where the summations extend over all the molecular units in the unit cell. The various terms are :

- V_j^0 - the potential energy function of the free j^{th} molecule. It determines the internal mode vibrations.
- V_j' - the perturbation of V_j^0 due to the equilibrium field of the crystal at the site of the j^{th} molecule. It can cause shifts in the fundamental frequencies and changes in selection rules.
- V_{jk} - represents terms involving displacement coordinates in the j^{th} and k^{th} molecules i.e. it encompasses interactions between vibrations in different molecules.
- V_L - contains terms involving the relative displacement and rotational orientation of molecules with respect to each other, and thus represents the lattice potential.
- V_{Lj} - denotes those terms involving interaction between lattice coordinates and the internal coordinates of the j^{th} molecule.

A molecule in a crystalline array can, in principle, be treated as an entity by itself, subject only to symmetry restrictions arising out of the crystalline environment. But the interaction between this entity and rest of the crystal which creates the environment cannot be ignored. For complete rigour, therefore, the entire array of molecule must be analysed as one unit. However, such a completely rigorous approach is essentially impossible for practical reasons. Therefore, the vibrational spectra of crystals are always analysed with some approximations.

1.1.1 Unit Cell Approach

The first systematic approach to explain the solid state spectra was made by Bhagavantam and Venkatarayudu [8,9]. They treated the unit cell as one giant molecule and applied the group theoretical method to examine its vibrations. In this approach the problem of classification of $3nN$ modes of the whole crystal (containing n unit cells of N atoms each) is reduced to the problem of classification of $3N$ modes of the unit cell. Such a simplification is based on the assumption that atoms or molecules at equivalent lattice positions in different unit cells are in the same state of motion without any phase differences.

1.1.2 Local or Site Symmetry Approach

There is another powerful method to distribute the normal modes of ions or molecules in solid state phase.

Assuming the local potentials to be mainly responsible for the dynamics of polyatomic groups in the crystals, Halford [10] suggested the classification of the normal modes into species of local symmetry point group. It is achieved by correlating the symmetry species of the point group of the free molecular group to those of local symmetry point group. A serious limitation of this method is that it neglects the interaction between different groups in the same unit cell. Hornig [11] considered such interactions and showed that by further correlating the species of the site and the crystal symmetry point groups, one obtains the same classification as that obtained by the unit cell approach.

As an illustration consider the case of tetramethyl ammonium halides (TMAX, $X = \text{Cl, Br or I}$) which belong to the tetragonal system with space group D_{4h}^7 ($Z = 2$) at room temperature [12-14]. The TMA ion has the point group symmetry T_d . In the unit cell the TMA and X^- ions have site symmetries D_{2d} and C_{4v} , respectively; whereas the unit cell is invariant only under the operations of the factor group D_{4h} . Since D_{2d} and C_{4v} are the local or site symmetries for TMA and X^- ions, respectively, a correlation between the species of T_d , D_{2d} and D_{4h} gives the distribution of the modes of TMA ions, while the modes of X^- ions are distributed by correlating the species of C_{4v} and D_{4h} .

Winston and Halford [15] derived both the methods by considering the motions of a crystal segment composed of an

arbitrary number of unit cells and subjecting it to the Born-Von Karman boundary conditions [16]. The applications of these methods (unit cell approach and site symmetry approach) have been discussed in depth [17-23]. However, we will discuss in detail the distributions of the modes of tetramethyl ammonium halides and tetramethyl ammonium tetrachlorozincate in Chapters 3 and 5, respectively.

1.2 ANHARMONICITY AND INTERACTION OF VIBRATIONS

Anharmonicity affects molecular vibrations in two important ways [3,24]. Firstly, the selection rule derived for the harmonic oscillator $\Delta v = \pm 1$ (v - vibrational quantum number) ceases to be a rigorous selection rule and transitions with $\Delta v = \pm 1, \pm 2, \pm 3 \dots$ become allowed. Secondly, the vibrational energy levels are not spaced apart equally by the quantity $h\nu$. And finally, combination bands are also allowed. The intensity of the overtone or combination bands is directly related to the anharmonicity character of the vibrations. If overtones or combination bands are not observed, the harmonic approximation is an excellent one. Observation of strong overtone or combination bands indicate the presence of anharmonic character in the vibration.

The anharmonicities are of two types : mechanical and electrical [25,26]. The mechanical anharmonicity is associated with the deviation of the potential function for a given mode from the harmonic form. Normal vibrations rest

on the assumption that in the range of amplitude of oscillations involved the quadratic term in the potential energy plays the dominant role in the motions. But in actual vibrations the cubic, quartic and higher terms in the potential energy may be appreciable to make the oscillations anharmonic. The potential energy function for a particular vibration is written as

$$V = \frac{1}{2} K_2 Q^2 + K_3 Q^3 + K_4 Q^4 + \dots \quad (1.2)$$

where Q is the relevant normal coordinate and K_i the force constant.

Electrical anharmonicity depends on the quadratic and higher terms in the expression of the instantaneous dipole moment given by

$$\mu = \mu_0 + \mu_1 Q + \mu_2 Q^2 + \dots \quad (1.3)$$

There are cases where the mechanical vibration is harmonic ($K_3, K_4, \dots = \text{zero}$), but the changes in μ are anharmonic ($\mu_2, \mu_3, \dots = \text{finite}$).

The mechanical anharmonicity is related to vibrations through the well known equation [3]

$$G(v) = (v + \frac{1}{2}) w_e - (v + \frac{1}{2})^2 w_e x_e + \dots \quad (1.4)$$

where $G(1)-G(0)$, $G(2)-G(0)$, ... give the observed band frequencies ν , 2ν etc. Conversely, the observed values of ν and 2ν [not the same as $2(\nu)$] lead to w_e , $w_e x_e$ [3] and cubic potential constant K_3 [25]. Also the relative

intensities of ν and 2ν bands lead to μ_2/μ_1 [26]. The relations are :

$$w_e X_e = \frac{2(\nu) - 2\nu}{2} \quad (1.5)$$

$$w_e = \nu + 2w_e X_e \quad (1.6)$$

$$K_3 = \pm \left[\frac{4}{15} w_e |w_e X_e| \right]^{1/2} \quad (1.7)$$

$$\frac{\mu_2}{\mu_1} = \frac{-(K_3/w_e) \pm [I_{2\nu} \cdot \nu / I_\nu \cdot 2\nu]^{1/2}}{1 \pm 5(K_3/w_e) [I_{2\nu} \cdot \nu / I_\nu \cdot 2\nu]^{1/2}} \quad (1.8)$$

where \pm sign in the last two equations refers to a negative value of $w_e X_e$ and vice versa.

1.3 FERMI RESONANCE

Fermi observed that two or more quasi-degenerate vibrational levels of the same symmetry repel each other. The interaction is due to the presence of anharmonic terms in the vibrational potential function and consequent mixing of the related vibrational wave functions [3,27]. The phenomenon is called Fermi resonance.

1.3.1 Two Levels Fermi Resonance

Consider two quasi-degenerate energy levels having unperturbed wave functions ψ_1^0 and ψ_2^0 with unperturbed energies E_1^0 and E_2^0 , respectively. The first order perturbation wave function will be

$$\Psi_1 = a\psi_1^0 + b\psi_2^0$$

$$\Psi_2 = -b\psi_1^0 + a\psi_2^0 \quad (1.9)$$

where $a^2 + b^2 = 1$.

According to the first order perturbation theory, the perturbed energies (λ) and eigenfunctions can be obtained by solving the secular equation

$$\begin{vmatrix} E_1^0 - \lambda & |H'_{12}| \\ H'_{21} & E_2^0 - \lambda \end{vmatrix} = 0 \quad (1.10)$$

where H' is the interaction hamiltonian. This gives

$$\lambda = \frac{1}{2} (E_1^0 + E_2^0) \pm \frac{1}{2} [4|H'_{12}|^2 + (E_1^0 - E_2^0)^2]^{1/2} \quad (1.11)$$

Thus the perturbed levels separation (which is the observed one) is

$$\delta = [4|H'_{12}|^2 + \delta_0^2]^{1/2} \quad (1.12)$$

where $\delta_0 (= E_1^0 - E_2^0)$ is the separation of the unperturbed levels and $|H'_{12}|$ is called Fermi coupling coefficient.

Bertran et al. [28] calculated the coefficients a and b of eq. (1.9) to be

$$a = \left[\frac{\delta + \delta_0}{2} \right]^{1/2}, \quad b = \left[\frac{\delta - \delta_0}{2} \right]^{1/2} \quad (1.13)$$

The matrix elements of the actual transitions are

$$\langle 0 | A | 1 \rangle = a \langle 0 | A | 1^0 \rangle + b \langle 0 | A | 2^0 \rangle$$

$$\langle 0 | A | 2 \rangle = -b \langle 0 | A | 1^0 \rangle + a \langle 0 | A | 2^0 \rangle \quad (1.14)$$

where A is polarizability (α) for Raman transitions and dipole moment (p) for infrared transitions.

The ratio of intensities of the transitions is, thus,

$$R = \frac{I_1}{I_2} = \frac{|\langle 0 | A | 1 \rangle|^2}{|\langle 0 | A | 2 \rangle|^2} = \left\{ \frac{a\sqrt{I_1^0} + b\sqrt{I_2^0}}{-b\sqrt{I_1^0} + a\sqrt{I_2^0}} \right\}^2 \quad (1.15)$$

Here I_1^0 and I_2^0 are the unperturbed intensities of the resonating bands. Setting $I_1^0/I_2^0 = R_0$ and using equations (1.15), (1.13) and (1.12) we obtain

$$R = \left[\frac{\{\delta + (\delta^2 - 4|H'_{12}|^2)^{1/2}\}^{1/2} R_0^{1/2} + \{\delta - (\delta^2 - 4|H'_{12}|^2)^{1/2}\}^{1/2}}{-\{\delta - (\delta^2 - 4|H'_{12}|^2)^{1/2}\}^{1/2} R_0^{1/2} + \{\delta + (\delta^2 - 4|H'_{12}|^2)^{1/2}\}^{1/2}} \right]^{1/2} \quad (1.16)$$

The above equation contains two unknowns, R_0 and H'_{12} and, therefore, cannot be solved without further information. However, Fermi resonance occurs mostly in the cases where one of the transitions of the Fermi doublet is a strong fundamental and the other is a very weak harmonic or combination transition (i.e. $I_2^0 \simeq 0$). Then

$$R = \frac{I_1}{I_2} = \frac{\delta + \delta_0}{\delta - \delta_0} \quad (1.17)$$

Thus the observed δ and R lead to δ_0 , and hence to $|H'_{12}|$ from eq. (1.12). For simpler molecules (e.g. CO_2 and

NCO radical) Eggers and Crawford [29] and Dixon [30] have found that the values of Fermi coupling coefficients calculated independently from the known anharmonic constants show only a slight mismatch with those calculated from the approximate equation (1.12). However, for complex molecules this cannot be checked as anharmonic constants are not usually known.

1.3.2 Three Levels Fermi Resonance

Dellepiane et al. [31] have extended the theoretical examination of Fermi resonance to a special case of three levels : two fundamentals and one overtone in solid N-methyl acetamide. The unperturbed positions of the fundamentals and the overtone were known in this case at room temperature. For Fermi resonance in a three levels system the secular equation, in general, will be

$$\begin{vmatrix} E_1^0 - \lambda & H'_{12} & H'_{13} \\ H'_{21} & E_2^0 - \lambda & H'_{23} \\ H'_{31} & H'_{32} & E_3^0 - \lambda \end{vmatrix} = 0 \quad (1.19)$$

This equation is not solvable even for the case of one fundamental and two overtones under the assumption that the intrinsic intensities of overtones are very small (i.e. $I_2^0 \simeq 0$ and $I_3^0 \simeq 0$), as it still involves six unknown coefficients, whereas the observed transitions provide only five data. For Fermi resonance among more than three levels

the situation would be even worse.

1.3.3 Methods of Identifying Fermi Resonance

Fermi resonance is not the only origin of an anomalous doublet. It may also arise from association, solvation, conformational isomerism, hot bands etc. [28]. The presence of Fermi resonance can be established by the following methods:

(i) The method of isotopic substitution

Appropriate isotopic substitution may alter one of the transitions to remove the accidental degeneracy. The absence of perturbation in the substituted compound confirms that the presence of anomalous doublet in the parent compound was due to Fermi resonance.

(ii) The method of solvent variation

It consists in studying the observed doublet in solutions of the compound in a wide series of solvents. One can write a set of n equations of the types

$$R_i = F(\delta_i, R_{0i}, |H'_{12}|_i) \quad (1.20)$$

for n different solvents. A plot of R vs. δ contains all the information of the system of n equations. The positions of the related transitions may vary from solvent to solvent. Therefore, the magnitude of Fermi interaction would also vary accordingly. It can be recognized as a change in the ratio of intensities of the doublet from one solvent to the

other [28,32,33]. A smooth R vs. δ curve, thus confirms the presence of Fermi resonance.

1.4 ISOTOPE EFFECT

The vibrational investigation of isotopes of polyatomic molecule is helpful in force constant calculations, assignments of vibrational modes and structural determinations. To quite a good approximation the isotopic molecules have the same electronic structure and the potential function as the parent molecule.

1.4.1 The Teller-Redlich Product Rule

In order to overcome the tedious calculations in determining the isotopic shifts in the frequencies of a particular species for large molecules Teller and Redlich [3] have given a simple product rule : For two isotopic molecules the product of the ν^s/ν values for all vibrations of a given symmetry type is independent of the potential constants and depends only on the masses of the atoms and the geometrical structure of the molecule . The formula for any molecule is

$$\frac{\nu_1^s \nu_2^s \cdots \nu_f^s}{\nu_1 \nu_2 \cdots \nu_f} = \left[\left(\frac{m_1}{m_1^s} \right)^\alpha \left(\frac{m_2}{m_2^s} \right)^\beta \cdots \cdots \cdots \right. \\ \left. \left(\frac{M}{M^s} \right)^t \left(\frac{I_x^s}{I_x} \right)^{\delta x} \left(\frac{I_y^s}{I_y} \right)^{\delta y} \left(\frac{I_z^s}{I_z} \right)^{\delta z} \right]^{1/2} \quad (1.21)$$

Here the superscript s stands for isotopic substituted quantities, $\nu_1, \nu_2 \dots \nu_f$ are the frequencies of f genuine vibrations of the symmetry type considered, $m_1, m_2 \dots$ masses of the representative atoms of the various sets of equivalent atoms, α, β, \dots are the number of vibrations (inclusive of non-genuine vibrations) each set contributes to the symmetry type considered, M is the total mass of the molecule, t is the number of transitions of symmetry type considered, I_x, I_y, I_z are the moments of inertia about the x, y and z axes through the centre of mass, $\delta_x, \delta_y, \delta_z$ are 1 or 0 depending on whether or not the rotation about the x, y, z axis is a non-genuine vibration of the symmetry type considered. Both on the left and right hand side (in α, β, \dots t, $\delta_x, \delta_y, \delta_z$) a degenerate vibration is counted only once.

Let us consider the case of $(\text{CH}_3)_4\text{N}^+$ ion under point group symmetry T_d . The distribution of vibrations of any T_d symmetric molecule under the point group T_d are given in Table 1.1 [3]. Here there are no nuclei in general position ($m = 0$). Nitrogen atom is on all elements of symmetry ($m_0 = 1$). One set of nuclei (H atoms) are on the planes σ_d but on no other element of symmetry ($m_d = 1$), one set of nuclei (C-atoms) lie on the three-fold axes ($m_3 = 1$), no atom lies on two-fold axes ($m_2 = 0$). Then the general equation for $(\text{CH}_3)_4\text{N}^+$ ion becomes as given below [34]

$$\prod_{i=1}^3 \left(\frac{\nu_i^D}{\nu_i^H} \right) = \sqrt{\left(\frac{m^H}{m^D} \right)^2} = 0.500 \text{ (A}_1\text{-modes)}$$

$$\frac{\nu_4^D}{\nu_4^H} = \sqrt{\frac{m^H}{m^D}} = 0.707 \quad (A_2\text{-modes})$$

$$\prod_{i=5}^8 \left(\frac{\nu_i^D}{\nu_i^H} \right) = \sqrt{\left(\frac{m^H}{m^D} \right)^3} = 0.354 \quad (E\text{-modes})$$

$$\prod_{i=9}^{12} \left(\frac{\nu_i^D}{\nu_i^H} \right) = \sqrt{\left(\frac{m^H}{m^D} \right)^4 \left(\frac{I_z^D}{I_z^H} \right)^1} \quad (F_1\text{-modes})$$

$$\prod_{i=12}^{19} \left(\frac{\nu_i^D}{\nu_i^H} \right) = \sqrt{\left(\frac{m^H}{m^D} \right)^5 \left(\frac{m^D}{m^H} \right)} = 0.221 \quad (F_2\text{-modes}) \quad (1.22)$$

If the symmetry of an isotopic molecule is lower than that of the ordinary molecules, it is necessary for applying the product rule to know the symmetry species of point group of lower symmetry.

1.5 STRUCTURAL PHASE TRANSITIONS

Structural phase transitions occur when a material changes its crystallographic structure as a result of variation in temperature, pressure or any other parameter like an applied electric or magnetic field [35]. Both microscopic and macroscopic properties of the system change with such phase transitions. Their studies are of importance for various applications of the materials, like use of ferroelectrics as piezoelectric components and pyroelectric detectors, computer core storage in magnetized ferrite rings, liquid crystal displays, etc. [35-38]. Various experimental techniques such

as X-ray diffraction, neutron diffraction, Hall coefficient, specific heat measurement, heat capacity measurement, elastic constant measurement, susceptibility measurement, ultrasonic wave propagation, Raman and infrared spectroscopic studies, etc. [39] have been used to investigate such phase transitions. Raman scattering studies of structural phase transitions have been reviewed by Fleury [40], Scott [41], Steigmeier [42] and Nakamura [43]. These are important because at least one component of the soft mode of a continuous structural phase transition is always Raman active below the phase transition temperature [36]. A further advantage of Raman technique is that it can provide information about the specific molecular motions involved in triggering the phase transition [44].

1.5.1 Classification of Phase Transitions

Different types of phase transitions cannot be rigorously classified. For instance, although phase transitions are classified as those of the first order or the second order, there are numerous cases exhibiting features of both [37]. Moreover, there are many different criteria too for classification of phase transitions. However, some broad classifications are given below.

(i) Reversible and irreversible phase transitions

A phase transition in which the system returns to its initial phase on withdrawal of the agency or parameter which caused the phase transition is known as a reversible

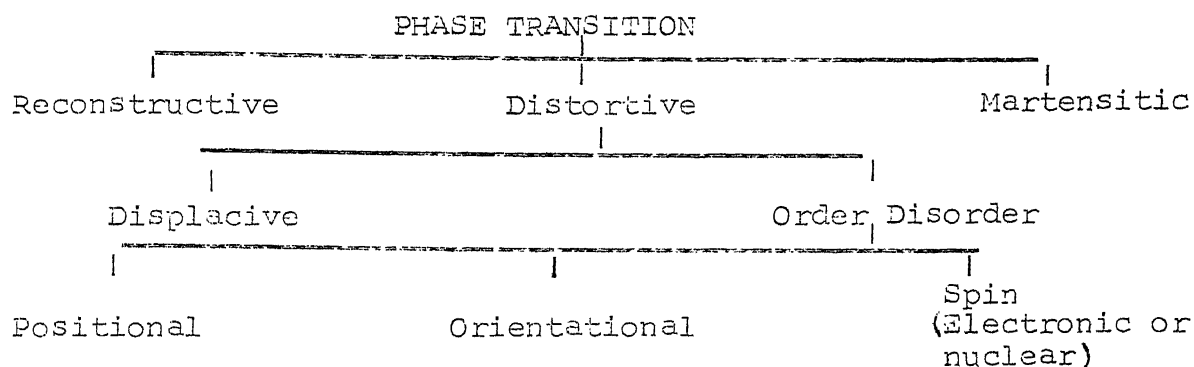
phase transition. But if the system does not do so, the transition is known as an irreversible phase transition. The change of graphite to diamond is an outstanding example of an irreversible phase transition.

(ii) The first order (or discontinuous) and second order (or continuous) phase transitions

A first order transition involves a sharp and discrete change in internal and free energies at the transition point. Therefore the system shows a discontinuity in almost all the physical and chemical properties at the transition point. In contrast the second order phase transitions occur over a wide range of the variable parameter. With temperature as the variable parameter these transitions are generally associated with increase of disorder and internal energy with rise in temperature, [45]. During a second order phase transition, the entropy and volume of the system remain continuous while the heat capacity and thermal expansivity undergo a discontinuous change [46]. The λ -transition is a particular case of second order transition in which the heat capacity tends towards infinity [37].

(iii) The Buerger classification

Buerger classifies the phase transitions according to the changes in crystal structure at the transition point [37,47]. That is as follows :



In a reconstructive phase transition the original linkages of the net are disrupted and the atoms or molecules of the solid reconstruct a new lattice. Some typical transitions of the reconstructive type are : graphite to diamond [48], transformation of CsCl at 479°C [49] and of NH_4Cl at 180°C [37].

In a distortive phase transition the linkages of the net are not disrupted, but the regular lattice gets slightly distorted. This distortion may involve small displacements in the lattice positions of molecular units or may involve changes in the ordering of atoms or molecules among various equivalent positions (without altering the lattice type). Accordingly, the distortive phase transition is called a displacive or order-disorder type.

The various equivalent positions in the case of an order-disorder transition may refer to positions of atoms in the lattice or to angular orientations of molecules or ions or to spin of electrons or protons. Accordingly the order-disorder transition is called positional, orientational or

spin (electronic/nuclear) order-disorder type. Positional disorder has been observed in various inorganic compounds such as AgI [50], RbAg_4I_5 [51] and Fe_3O_4 [52]. Orientational disorder has been observed in KCN [53], NaNO_2 [54] and NH_4Cl [55].

A distinction between the displacive and order-disorder type transitions is possible on the basis of atomic single cell potential [36]. This is schematically shown in Fig. 1.1 for one spatial coordinate Q . The anharmonic potential used is $V(Q) = aQ^2 + bQ^4$, with $a < 0$ and $b > 0$. This is a double well potential in which the height of the hump between the two minima is given by $\Delta E = \frac{a^2}{4b}$. For the case $\Delta E \gg kT_c$ the transition occurs due to ordering between $Q_0 + \sqrt{\frac{-a}{2b}}$ and $Q_0 - \sqrt{\frac{-a}{2b}}$. On the other hand, if we have $\Delta E \ll kT_c$ a continuous cooperative displacement of atoms along Q is found as a function of temperature around T_c .

(iv) Incommensurate-commensurate phase transitions

The recent discovery of incommensurably distorted structures has important implications for the study of structural phase transitions [56]. In a few years numerous examples have become known of compounds having in certain temperature interval a structure without any space group symmetry, whereas outside that interval the structure is crystalline. The non-crystalline structure is not amorphous but is well ordered and may be described as a periodic distortion not fitting with the crystal periodicity. The study

of the behaviour of incommensurate phase is now a subject of utmost interest theoretically as well as experimentally [56-63]. Pynn [56] has suggested a model to explain the incommensurate phase as shown in Fig. 1.2.

Consider a uniform chain of atoms, equally spaced by a (Fig. 1.2A), is modulated by sinusoidal displacement whose wavelength is $4a$ (Fig. 1.2B). Then every fourth atom is displaced by the same amount. The distorted structure (Fig. 1.2C) can thus be described in terms of a unit cell which is four times larger and contains four times as many atoms as the original one. Most previous reports on structural transitions described systems in which the unit cell size either remained the same or was changed by a simple multiple at the transition. However, it is certainly not a priori necessary for a lattice modulation to have a periodicity which is rational multiple of a unit cell size. An example of a modulation which does not satisfy this simple criterion and which is thus incommensurable with the undistorted lattice is shown in Fig. 1.2D. The atomic arrangement in the incommensurable phase is depicted in Fig. 1.2E. This phase has the remarkable property that no two atoms are displaced by the same distance from their positions in the undistorted phase. It is thus impossible to find any lattice translation which maps the crystal into itself.

The incommensurable phase has been observed both in metallic and insulating materials. The physical effects which

drive the transitions are somewhat different in the two cases. For the insulators it is often found that competing, short-range interatomic forces of different ranges and similar magnitudes give rise to an incommensurable modulated phase. To have an idea how this may arise, consider the monoatomic chain in Fig. 1.2A and suppose that only elastic forces between first and second neighbour atoms contribute to the energy. The latter may then be written as

$$U = \sum_{n=1}^N [A_1 \sum_{i=\pm 1} (U_n - U_{n+i})^2 + A_2 \sum_{i=\pm 2} (U_n - U_{n+i})^2] \dots (1.23)$$

where U_n is the longitudinal displacement of the n^{th} atom from its lattice site and A_1 and A_2 are the first and second neighbour harmonic force constants, respectively.

Expanding the displacement as a Fourier series

$$U_n = \sum_q U_q \cos(qna) \quad (1.24)$$

and substituting in equation (1.23) one finds that the energy is given by

$$\begin{aligned} U &= 4 \sum_q U_q^2 [A_1 (1 - \cos qa) + A_2 (1 - \cos 2qa)] \\ &= 4 \sum_q U_q^2 A_q \end{aligned} \quad (1.25)$$

A sinusoidal modulation structure will be stable if A_q in equation (1.25) has a minimum value for a non zero wave vector q_0 . Necessary conditions for this to occur are that

$$\frac{\partial A}{\partial q} = 0 ; \quad \frac{\partial^2 A}{\partial q^2} > 0 \quad (1.26)$$

at the wave vector q_0 . These conditions imply that a modulation of wave vector q_0 given by

$$\cos(q_0 a) = -A_1/4A_2 \quad (1.27)$$

will be stable provided $A_1 < 4|A_2|$ and $A_2 \leq 0$.

For conducting materials, interesting incommensurable transitions result from the interaction between conduction electrons and the atomic lattice. These interactions give rise to effective long-range interatomic forces.

1.6 EARLIER STUDIES ON TETRAMETHYL AMMONIUM HALLIDES

Tetramethyl ammonium halides (abbreviated as TMACl, TMABr and TMAI for chloride, bromide and iodide, respectively) have been extensively studied for their vibrational dynamics [34,64-84] and phase transitions [85-91]. The vibrational assignments of the modes of TMA ion are, however, not the same. The intensity pattern of the bands in the methyl stretching region in Raman spectra of TMA halides in aqueous solutions is quite complex. Anhouse and Tobin [70], Berg [34] and Kabisch and Klose [77] have all attributed this complexity due to Fermi resonance interactions, although their conclusions as regarding assignments of the bands are not identical. To explain the abnormally high intensities of the combination/overtone bands in this region Kabisch and

Klose [77] have also invoked the effect of ion association occurring in concentrated solutions. Recently, Kabisch and Mobius studied the methyl deformation [79] and Stretching [80] regions of selectively deuterated TMA ion (TMA-d_n^+ ; $n = 0, 1, 3, 9, 10, 11$ and 12) in aqueous solutions. They explained the non-appearance of polarized CH_3 symmetric bending mode $\nu_2(\text{A}_1)$ in TMA-d_0 to the overlapping of the wavefunctions of C_4N^+ skeleton and methyl groups, and the usual complexity in the intensity pattern of the bands in methyl stretching region to Fermi resonance interactions.

Aimone and Cachet [81] have studied the far-infrared (FIR) spectra of TMA halides and proposed a model for inter-ionic potential energy calculation. Ratcliffe and Waddington [82] have used inelastic neutron scattering to determine the positions of the modes of TMA ions which are forbidden in vibrational spectra (Raman and IR) such as CH_3 torsion modes $\nu_4(\text{A}_2)$ and $\nu_{12}(\text{F}_1)$ etc. Some IR absorption data at high pressure [83] and ^{15}N substituted halides [84] are also available.

As regarding phase transitions, Chang and Westrum [85] measured the heat capacities of these halides between 5 and 300 K, and found a first order phase transition at 75.8 K and a λ -transition at 184.9 K in the chloride. Stammlier [87] found a third phase transition at 536 K in the chloride by

* n denotes the number of H atoms replaced by D-atoms in $(\text{CH}_3)_4\text{N}^+$.

differential thermal analysis. He suggested that the compounds are free from hydrogen bonding. Gibson and Raab [89] found one phase transition at ~ 415 K by proton magnetic resonance. They have also shown that methyl group reorientation occurs without noticeable tunneling, followed by pseudoisotropic reorientation of the cations at slightly higher temperatures. Ionic diffusion occurs only in phase I, and phase II is piezoelectric [89]. Pistorius and Gibson [81] have suggested the space groups C_{3v}^5 ($Z = 1$) and O_h^5 ($Z = 4$) for TMACl in phases II and I, respectively.

However, the vibrational study of these compounds offers fertile field in view of the following :

- (i) the vibrational assignments still need more insight, especially for the methyl modes.
- (ii) the three halides are isostructural, but only TMACl-d_0 is known to undergo four successive phase transitions between 4 and 540 K.
- (iii) the nature and mechanism of these phase transitions are not yet clear.

1.7 EARLIER STUDIES ON TETRAMETHYL AMMONIUM TETRAHALO METALLATES

Tetramethyl ammonium tetrahalo metallates $[(\text{TMA})_2\text{MX}_4]$; $\text{TMA} = (\text{CH}_3)_4\text{N}$, $\text{M} = \text{Zn, Mn, Ni, Cu, Co, Fe}$ and $\text{X} = \text{Cl, Br}$ are of special interest from the following points of view [92]. First of all, the occurrence of one or more phase

transitions below room temperature, which are commonly related to organic group motion, is known. Secondly, the sequence of phase transitions near room temperature occurs together with the existence of an incommensurate phase. This transition sequence is similar to that found in inorganic compounds of the same family, although in this case the set of transitions is located in wider and generally different temperature ranges. Finally, the A_2BX_4 compounds are also interesting for a ferroelectric phase which remains down to very low temperatures in inorganic crystals but only for a few degrees when $(CH_3)_4N$ groups are present. The sequences of successive phase transitions in tetramethyl ammonium tetrahalo metallates have been characterized by methods such as differential thermal analysis [93-95], inelastic neutron scattering [96-99], X-ray diffraction [100-106], specific heat measurement [95,107,108], thermal expansion measurement [92], dielectric measurement [109-115], electron paramagnetic resonance [116,117], nuclear magnetic resonance [118,119], ultrasonic wave propagation [120] etc. The details of the phases and transition temperatures are compiled in Table 1.2.

REFERENCES

1. J G Grasselli, M K Snavely and B J Bulkin, Phys. Rep. 65, 231 (1980).
2. E B Wilson, J C Decius and P C Cross, "Molecular Vibrations - The theory of infrared and Raman vibrational spectra", McGraw-Hill Book Co. Inc., New York (1955).
3. G Herzberg, "Molecular Spectra and Molecular Structure", Vol. 2, D. Von Nostrand Co. Inc., New York (1945).
4. F A Cotton, "Chemical Applications of Group Theory", Interscience Publishers, New York (1963).
5. N B Colthup, L H Daly and S E Wiberley, "Introduction to Infrared and Raman Spectroscopy", 2nd edn., Academic Press, New York (1975).
6. S Krim, in "Infrared Spectroscopy and Molecular Structure", M. Davies (ed.) Elsevier, Amsterdam (1963).
7. V P Tayal, B K Srivastava, D P Khandelwal and H D Bist, Appl. Spectros. Rev. 16, 43 (1980).
8. S Bhagavantam, Proc. Ind. Acad. Sci. A13, 543 (1941).
9. S Bhagavantam and T Venkatarayudu, "Theory of Groups and Its Application to Physical Problems", Academic Press, New York (1969).
10. R S Halford, J. Chem. Phys. 14, 8 (1946).
11. D F Hornig, J. Chem. Phys. 16, 1063 (1948).
12. L Vegard and K Sollenas, Phil. Mag. 4, 985 (1927).
13. R W G Wyckoff, Z. Krist. 67, 61 (1928).
14. R W G Wyckoff, "Crystal Structure", Vol. 1, 2nd edn., Interscience Publishers, New York, p107 (1948).
15. H Winston and R S Halford, J. Chem. Phys. 17, 607 (1949).

15. M Born and T Von Karman, Z. Phys. 13, 297 (1912) cited in Handbuch der Phys. 7, 325 (1955).
17. W G Fatelay, F R Dollish, N T McDevitt and F F Bentlay, "Infrared and Raman Selection Rules for Molecular and Lattice Vibrations : The correlation method", Wiley Interscience, New York (1972).
18. J R Ferraro and J S Ziomek, "Introductory Group Theory and It's Application to Molecular Structure", 2nd edn., Plenum Press, New York (1975).
19. S Bhagavantam, "Scattering of Light and the Raman Effect", Chemical Publication Co., New York (1942).
20. S S Mitra, in "Optical Properties of Solids", S Nudelman and S S Mitra (eds.), Plenum Press, New York (1969).
21. G Turrell, "Infrared and Raman Spectra of Crystals", Academic Press, London (1972).
22. J C Decius and R M Hexter, "Molecular Vibrations in Crystals" McGraw-Hill International Co., New York (1977).
23. Y S Jain, Ph.D. Thesis, Indian Institute of Technology, Kanpur, India (1974).
24. P Gans, "Vibrating Molecules", Chapman and Hall Ltd., London (1971).
25. A Foldes and C Sandorfy, J. Mol. Spectrosc. 20, 262 (1966).
26. R C Herman and K E Shuler, J. Chem. Phys. 22, 481 (1954).
27. E Fermi, Z. Physik, 71, 250 (1931).
28. J F Bertran, L Ballester, L Dobrihalova, N Sanchez and R Arrieta, Spectrochim. Acta 24A, 1765 (1968).
29. D F Eggers Jr. and B L Crawford Jr., J. Chem. Phys. 19, 1554 (1951).
30. R N Dixon, J. Chem. Phys. 31, 258 (1959)

31. G Dellepiane, S Abbate, P Bosi and G Zerbi, J. Chem. Phys. 73, 1040 (1980).
32. H Fritzsche, Spectrochim. Acta 22, 1139 (1966).
33. P V Huong and J Lascombe, J. Chim. Phys. 59, 719 (1962).
34. R W Berg, Spectrochim. Acta 34A, 655 (1978).
35. A D Bruce and R A Cowley, "Structural Phase Transitions", Taylor and Francis Ltd., London (1981).
36. K A Muller and H Thomas (eds.), "Structural Phase Transitions", Vol. 1, Springer-Verlag, Berlin (1981).
37. C N R Rao and K J Rao, "Phase Transitions in Solids", McGraw-Hill Inc., New York (1978).
38. Frank J Owens, Charles P Poole Jr. and Horacio A Farach, "Magnetic Resonance of Phase Transitions", Academic Press, New York (1979).
39. M B Patel, Ph.D. Thesis, Indian Institute of Technology, Kanpur, India (1982).
40. P A Fleury (Ed. by M Balkanski, R C C Leite and S P S Porto) Proceedings of the 3rd International Conference on Light Scattering in Solids, Flammasion, Paris (1976).
41. J F Scott, Rev. Mod. Phys. 46, 83 (1974).
42. E F Steigmier, Ferroelectrics 7, 65 (1974).
43. T Nakamura, Ferroelectrics 9, 159 (1975).
44. M Schlaak, M Couzi and P V Huong, Berichte der Bunsen-Gesellschaft fur Physikalische Chemie (fruker Zeitschrift fur Electrochemie), 880 (1975).
45. C N R Rao and K J Rao, in "Progress in Solid State Chemistry", H Reiss (ed.) Vol. 4, Pergamon Press, Oxford (1967).
46. L D Landau and E M Lifshitz, "Statistical Physics", T B Sykes and M J Kearsley (Translators), Vol. 5, 3rd edn., Pergamon Press, Oxford (1969).

47. M J Buerger, in "Phase Transitions in Solids", R Smoluchowski, J E Mayer and W A Weyl (eds.), John Wiley, New York (1951).
48. H P Bovenkerk, F P Bundy, H T Hall, H M Strong and R H Wentorf Jr., Nature 184, 1094 (1959).
49. K J Rao, G V S Rao and C N R Rao, Trans. Faraday Soc. 63, 1013 (1967).
50. W Van Gool, in "Fast Ion Transport in Solids", W Van Gool (ed.), North-Holland, Amsterdam (1973).
51. M A Krivoglaz and A A Smirnov, "The Theory of Order-Disorder in Alloys", H Warlimont (ed.), Springer-Verlag, Berlin (1974).
52. K Kamigaki, M Ohalshi and T Kaneklo, in "Ferrites", Y Hoshino, S Iida and M Sugimoto (eds.), University Park Press, Baltimore (1971).
53. M Atoji, J. Chem. Phys. 54, 3514 (1971).
54. Y Yamada, I Shibuya and S Hoshino, J. Phys. Soc. Jpn. 18, 1594 (1963).
55. H A Levy and S W Peterson, Phys. Rev. 86, 766 (1982).
56. R Pynn, Nature 281, 433 (1979).
57. M Iizumi, J D Axe, G Shirane and K Shimaoka, Phys. Rev. B15, 4392 (1977).
58. V Dvorak and J Petzelt, J. Phys. C11, 4827 (1978).
59. H Poulet and R M Pick, J. Phys. C14, 2675 (1981).
60. M S Haque and J R Hardy, Phys. Rev. B21, 245 (1980).
61. W L McMillan, Phys. Rev. B12, 1187 (1976).
62. T Janssen and J A Tjon, J. Phys. C16, 4789 (1983).
63. M Iizumi, XIIth Congress of International Union of Crystallography, Canada (1981).
64. J T Edsall, J. Chem. Phys. 5, 225 (1937).

65. C W Young, J S Koehler and D S McKinney, J. Am. Chem. Soc. 69, 1410 (1947).
66. R A Heacock and L Marion, Can. J. Chem. 34, 1782 (1956).
67. E A V Ebsworth and N Sheppard, Spectrochim. Acta 13, 261 (1959).
68. N Krishnamurthy, Proc. Indian Acad. Sci. A61, 164 (1965).
69. G L Bottger and A L Geddes, Spectrochim. Acta 21, 1701 (1965).
70. S A Anhouse and M C Tobin, Spectrochim. Acta A28, 2141 (1972).
71. K M Harmon, I Gennick and S L Maderia, J. Phys. Chem. 78, 2585 (1974).
72. W von der Ohe, J. Chem. Phys. 62, 3933 (1975).
73. W von der Ohe, J. Chem. Phys. 63, 2949 (1975).
74. R W Berg, F W Poulsen and N J Bjerrum, J. Chem. Phys. 67, 1829 (1977).
75. R W Berg, J. Chem. Phys. 69, 1325 (1978).
76. R W Berg, J. Chem. Phys. 71, 2531 (1979).
77. G Kabisch and M Klose, J. Raman Spectrosc. 7, 311 (1978).
78. G Kabisch, J. Raman Spectrosc. 9, 279 (1980).
79. G Kabisch and G Mobius, Spectrochim. Acta 38A, 1189 (1982).
80. G Kabisch and G Mobius, Spectrochim. Acta 38A, 1195 (1982).
81. L Aimone and H Cachet, Infrared Physics 18, 867 (1978).
82. C I Ratcliffe and T C Waddington, J. Chem. Soc. Faraday Trans. II 72, 1935 (1976).
83. S D Hamann, High Temp. High Press. 7, 177 (1975).
84. K G Van Senden, Red. Trav. Chim. Pays-Bas Belg. 84, 1459 (1965).
85. S S Chang and E F Westrum Jr., J. Chem. Phys. 36, 2420 (1962).
86. A J Tench, J. Chem. Phys. 38, 593 (1963).

87. M Stammier, J. Inorg. Nucl. Chem. 29, 2203 (1967).
88. J Dufourcq, Y Haget-Bouillaud, N B Chanh and B Lemanceau, Acta Cryst. B28, 1305 (1972).
89. A A V Gibson and R E Raab, J. Chem. Phys. 57, 4688 (1972).
90. S Albert, H S Gutowsky and J A Ripmeester, J. Chem. Phys. 56, 3672 (1972).
91. C W F T Pistorius and A A V Gibson, J. Solid State Chem. 8, 126 (1973).
92. A G Cuevas, M J Tello, J Fernandez, A L Echarri, J Herreros and M Couzi, J. Phys. C16, 473 (1983).
93. S Sawada, Y Shiroishi, A Yamamoto, M Takashige and M Matsuo, J. Phys. Soc. Jpn. 44, 687 (1978).
94. S Sawada, Y Shiroishi, A Yamamoto, M Takashige and M Matsuo, Phys. Lett. 67A, 56 (1978).
95. H Shimizu, N Abe, N Yasuda, S Fujimoto, S Sawada and Y Shiroishi, Japanese J. Appl. Phys. 18, 857 (1979).
96. G Marion, R Almairac, J Lefebvre and M Ribet, J. Phys. C14, 3177 (1981).
97. M Iizumi, J D Axe, G Shirane and K Shimaoka, Phys. Rev. B15, 4392 (1977).
98. K Gesi and M Iizumi, J. Phys. Soc. Jpn. 48, 337 (1980).
99. K Gesi and M Iizumi, J. Phys. Soc. Jpn. 48, 1775 (1980).
100. H Mashiyama, S Tanisaki and K Hamano, J. Phys. Soc. Jpn. 51, 2538 (1982).
101. H Mashiyama and S Tanisaki, Phys. Lett. 76A, 347 (1980).
102. S Tanisaki and H Mashiyama, J. Phys. Soc. Jpn. 48, 339 (1980).
103. R Almairac, M Ribet, J L Ribet and M Bziouet, J. Physique Lett. 41, L315 (1980).

104. H Mashiyama, S Tanisaki and K Gesi, J. Phys. Soc. Jpn. 50, 1415 (1981).
105. H Mashiyama, K Hasebe and S Tanisaki, J. Phys. Soc. Jpn. (Suppl. B) 49, 92 (1980).
106. H Mashiyama and S Tanisaki, J. Phys. Soc. Jpn. 50, 1413 (1981).
107. I R Larrea, A Lapez-Echarri and M J Tello, J. Phys. C14, 3171 (1981).
108. A G Cuevas, A L Echarri, M J Tello and P Vidaurrezaga, Ferroelectrics 36, 339 (1981).
109. S Sawada, T Yamaguchi and N Shibayama, J. Phys. Soc. Jpn. 48, 1397 (1980).
110. M Wada, M Suzuki, A Sawada, Y Ishibashi and K Gesi, J. Phys. Soc. Jpn. 50, 1813 (1981).
111. K Hamano, T Hishinuma, K Ema, J. Phys. Soc. Jpn. 50, 2666 (1981).
112. K Hamano, K Ema and S Hirotsu, Ferroelectrics 36, 343 (1981).
113. M Wada, A Sawada and Y Ishibashi, J. Phys. Soc. Jpn. 50, 531 (1981).
114. H Shimizu, N Abe, N Kokubo, N Yasuda, S Fujimoto, M Yamaguchi and S Sawada, Solid State Commun. 34, 363 (1980).
115. K Gesi, J. Phys. Soc. Jpn. 51, 203 (1982).
116. I Suzuki, K Tsuchida, M Fukui and R Abe, Japanese J. Appl. Phys. 20, L84 (1981).
117. J Chandrasekhar, M Chandra Kumar and S Subramaniam, J. Magnetic Resonance 18, 129 (1975).
118. R Blinc, M Burgar, J Slak, V Rutar and F Milia, Phys. Stat. Sol. A56, K65 (1979).

119. B W Mangum and D B Utton, Phys. Rev. B6, 2790 (1972).
120. H Hoshizaki, A Sawada and Y Ishibashi, J. Phys. Soc. Jpn. 47, 341 (1979).

Table 1.1 : Number of vibrations of each species for the point group $T_d [3]$.

Point group, total number of atoms	Species of vibration	Number of vibrations*	
		Non genuine	
		T	R
T_d ($N=24m+12m_d$ $+6m_2+4m_3+m_o$)	A_1		$3m+2m_d+m_2+m_3$
	A_2		$3m+m_d$
	E		$6m+3m_d+m_2+m_3$
	F_1	1	$9m+4m_d+2m_2+m_3-1$
	F_2	1	$9m+5m_d+3m_2+2m_3+m_o-1$

* m is the number of sets of nuclei not on any element of symmetry, m_o is the number of sets of nuclei on all elements of symmetry, m_2 , m_3 are the number of sets of nuclei on a two fold and three fold axis but not on any other element of symmetry that does not wholly coincide with that axis, m_d are the number of sets of nuclei on plane σ_d but not on any other element of symmetry.

Table 1.2 : Summary of observed phase transitions sequence in $(\text{TMA})_2\text{MX}_4$ compounds.*

MX_4	$\text{ZnCl}_4\text{-d}_0$	$\text{CoCl}_4\text{-d}_0$	$\text{FeCl}_4\text{-d}_0$	$\text{MnCl}_4\text{-d}_0$	$\text{CuCl}_4\text{-d}_0$	$\text{ZnCl}_4\text{-d}_{12}$	$\text{ZnBr}_4\text{-d}_0$	$\text{CoBr}_4\text{-d}_0$	$\text{CuBr}_4\text{-d}_0$
Phase									
I (normal)	23.6	20.6	6.9	19.3	27	27.5	24.7	13.5	13.8
II (Incom)									-1
III (Com: Ferro- Ele.)	7.0	8.0	-6.9	18.7	22	2	14.0		-31
II' (Incom)	2.3	6.3							-36
IV (Com. Elas.)		4.5							
II'' (Incom)							10.5		
V	-10.5	-8.1	-3.2	-6.3	-11	4.5	4.9		
	-118	-151				-1.4	0.6		

*All transition temperatures are in $^{\circ}\text{C}$.

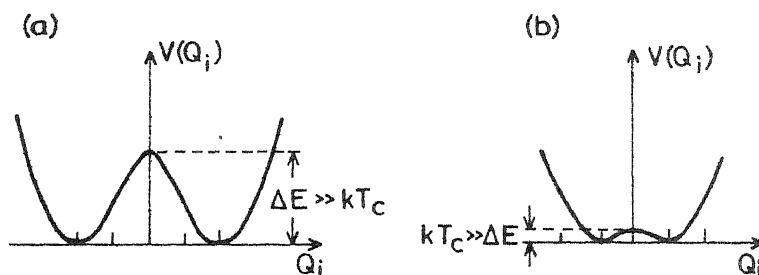


Fig.1.1 Single cell potentials in (a) order-disorder, (b) displacive structural phase transition system [36].

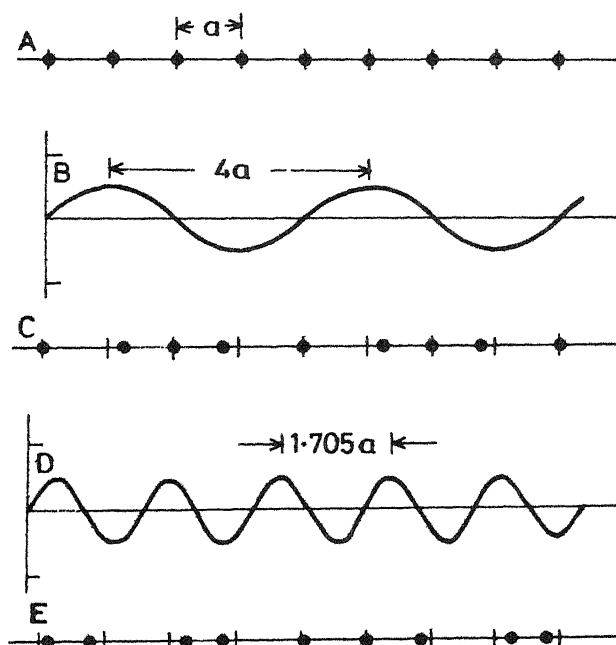


Fig. 1.2 A, a uniform chain of atoms; B, a commensurable modulation; C, distorted chain which results when the modulation of B is imposed on the chain in A; D, an incommensurable modulation; E, distorted chain which results when the modulation of D is imposed on chain in A. In rows A, C and E the tick marks represent the position of the undisplaced atoms [56].

2. EXPERIMENTAL

This chapter briefly describes the main techniques used to record the Raman and infrared spectra at ambient, lower and higher temperatures. Emphasis is given on the techniques employed rather than on the description of the instruments used. The method used to resolve an observed contour of overlapping bands is also outlined.

2.1 SAMPLE PREPARATION

Commercially available AR-grade tetramethyl ammonium halides were used to record the spectra. Normal tetramethyl ammonium halides were obtained from SISCO, Bombay. Perdeuterated tetramethyl ammonium chloride was obtained from MSD, Canada. Selectively deuterated tetramethyl ammonium iodides (TMAI-d_n; n = 1, 3, 9, 10, 11 and 12) were obtained from Isocommerz GmbH, German Democratic Republic. Tetramethyl ammonium chlorides (normal and perdeuterated) are highly hygroscopic. So they were dried under vacuum at least for 8 hours at room temperature before use.

Single crystals of normal tetramethyl ammonium tetrachlorozincate were grown by slow evaporation at room temperature from an aqueous solution containing stoichiometric proportions of TMACl-d₀ and ZnCl₂ [1]. The crystals were properly cut and polished with morphology suggested by Wada et al. [2]. The steps are shown in Fig. 2.1.

2.2 RAMAN SPECTRA

The Raman data were obtained with a Spex model 1403 Ramalog spectrophotometer, using a 5 watt Spectra Physics model 165-09 argon ion laser as exciting source. A block diagram of the experimental set up is shown in Fig. 2.2.

To obtain stabilized three phase 203 volts for the laser power supply the three phase mains voltage is first stabilized to 400 volts by a 20 KVA voltage stabilizer and then converted to 203 volts by a 12.6 KVA power transformer. The laser head and its power supply are cooled by distilled water circulated in a closed loop and maintained at a temperature of 20 °C by the HX-500 chilling plant obtained from Neslab. The heat of the chilling plant is dissipated through tap water.

The optical diagram of the set up for Raman studies is shown in Fig. 2.3. The 514.5 nm Ar⁺ laser beam in light control mode is used for excitation of the samples. The laser beam passes through the lasemate which filters out the plasma lines. Then it enters the UVISIR illuminator, where a low focal length fused silica condenser lens focusses the laser beam of 1.5 mm diameter to a spot of 10 μ m diameter on the sample. An elliptical mirror collects the scattered radiations and focusses it on the entrance slit of the monochromator. The outcoming radiation falls onto a thermoelectrically cooled C-31034 photomultiplier tube used as the detector. The signal is analysed by the Spex photon counting system DPC-2 and the spectrum is recorded on a linear chart recorder.

To study the polarization of Raman bands a polarizer (analyser) is placed before the elliptical mirror and a scrambler is placed before the entrance slit which converts the plane polarized light to circularly polarized light. The plane of polarization of the laser beam can be rotated by 90° , keeping a polarization rotator before the lasermate.

2.2.1 Spectra at Room Temperature

The following principal methods were used to obtain the Raman spectra :

(i) For solutions

The solution was taken in a cylindrical quartz cell with a flat bottom. The laser beam entered from the bottom and the scattered light was collected from the curved sides of the cell.

(ii) For polycrystalline samples

(a) Capillary method

The finely ground sample was filled in a quartz capillary, which was mounted on a stand in the sample compartment. It is the most widely used technique for colourless samples and requires a very small quantity of the sample.

(b) Rotating sample method

Some compounds (mostly coloured ones) strongly absorb the incident laser beam and get decomposed/dehydrated due to

localized heating. In such cases a pellet of the pure sample was mounted on a rotating sample holder. The rotation gives relative motion between the sample and laser beam, and avoids local heating.

(iii) For single crystals

A properly cut and polished crystal was mounted on a goniometer and the Raman scattering was observed in 90° geometry. A component of the scattering tensor, say α_{xy} , is determined experimentally by arranging the crystal geometry such that the incident light is polarized in X-direction and the Y-component of the scattered light is allowed to enter the monochromator. The polarizability character of a particular spectrum and the geometry in which it was recorded can be represented by notations like Z(XZ)Y [3,4] (see Fig. 2.4), where the symbols Z and Y outside the parenthesis denote the direction of propagation of the incident and scattered beams, respectively, while the symbols X and Z inside the parenthesis indicate the polarization characters of the incident and the scattered light, respectively.

2.2.2 Spectra at Low Temperature

For low temperature Raman studies a cell shown in Fig. 2.5 has been fabricated. Typical sample holders used for different samples are also shown. Essentially the cell is a cylindrical glass dewar with the bottom parts modified. The inner jacket bottom carries a rectangular brass attachment

for the sample holder joined to the dewar with the help of a Kovar seal. The outer jacket bottom has two quartz windows, one at the bottom for the incident laser beam and the other on the cylindrical surface for the outcoming scattered radiation. Liquid nitrogen cools the brass block and hence the sample. In order to reach temperatures below the normal nitrogen boiling point, an arrangement was made for evaporation of liquid nitrogen under reduced pressure. A T-joint was attached to the inner jacket of the cell with the help of male-female joint and was driven by two rotory pumps. This system provided temperatures down to 63 K. The temperature was controlled with a 25 watts heater attached with the sample holder. A copper-constantan thermocouple, whose junction was kept in contact with the sample, was used to measure the temperature. The temperature could be controlled within ± 2 K, and measured within ± 1 K.

2.2.3 Spectra at High Temperature

The Raman spectra at temperatures above the ambient temperature were recorded with a locally fabricated cell shown in Fig. 2.6. It consists of three parts : (i) the heating block, (ii) the sample holders and (iii) the temperature controller.

The heating block ($18 \times 18 \times 38 \text{ mm}^3$) with a 8 mm diameter hole drilled to a depth of 28 mm (to insert the sample holder) is made of brass. This is heated from three sides by 25 watts

heaters fitted into properly created grooves. On the bottom and the fourth side two conical holes are drilled to admit the exciting radiation and collect the scattered radiation, respectively. The whole system is mounted on a spex three-way motion platform to permit alignment of the sample. Different types of sample holders for studying liquid, polycrystalline (even hygroscopic) and single crystal samples are shown in Fig. 2.6, and need no description.

A Cu-constantan thermocouple kept in contact with the sample measures the temperature. Another Cu-constantan thermocouple is connected to a relay for controlling the temperature; junction of this thermocouple is attached to the heating block in order to provide quicker response due to its higher heat capacity and conductivity. Temperatures upto 600 K, controllable upto ± 1 K, could be achieved with this system.

2.3 INFRARED SPECTRA

The infrared spectra were recorded on Perkin Elmer-580 spectrophotometer with dry air purging system and covering the range $4000-100\text{ cm}^{-1}$. Its details are well described elsewhere [5]. The spectrum of polystyrene was used for calibration of the frequency scale.

For solution state spectra a drop of the aqueous solution was pressed between two AgBr windows, thus giving a thin absorbing layer. The infrared spectra of polycrystalline

sample were recorded in KBr pellets and nujol mulls. For temperature dependence studies the samples were kept in a Specac variable temperature cell (Fig. 2.7). The temperature of the sample could be stabilized to within ± 2 K in the range 77 to 523 K.

2.4 RESOLUTION OF THE OVERLAPPING BANDS

There are many instances in which two or more neighbouring bands overlap considerably to give a contour. Although unique resolution in such contours is fraught with many uncertainties, it is useful to extract some information by resolving such a contour by geometrical drawing. The component bands in an experimental band contour are expected to be Voigt like combinations of Lorentzian and Gaussian curves [6]. However, if the actual band width of each component is substantially larger than the instrumental slit width, the Lorentzian shape alone gives a reasonably good fit, especially when one does not look far into the tails of the components. Further, in the condensed phase theoretical considerations also justify the use of Lorentzian shapes for the bands in the contour [7]. Therefore we have assumed Lorentzian shapes to resolve the overlapping bands geometrically. A Lorentzian contour $I(\nu)$ around a band centre ν_0 is given as

$$I(\nu) = I(\nu_0) \frac{b^2}{b^2 + (\nu - \nu_0)^2} \quad (2.1)$$

where $2b$ is the full band width at half the maximum intensity, designated as $\Delta\nu_{1/2}$.

Selection of a proper base line is the first step for the analysis of an overlapping band. This we did by considering the general base well beyond the band, and allowing for the contribution of the tails. Having chosen the base line, a linear absorbance plot was drawn for the observed contour. It was then resolved into the minimum number of Lorentzian components as justified by the peaks, shoulders and distinct bulges in the contour. Some initial $I(\nu_0)$ and $\Delta\nu_{1/2}$ parameters were chosen for the different components and the corresponding absorbance curves obtained from eq. 2.1 were plotted and added together. From the deviation between this and the observed contour new $I(\nu_0)$ and $\Delta\nu_{1/2}$ parameters were estimated and the process was repeated. The best fit obtained after a few iterations was used as the final result. Minor residues or deviations were ignored, since the Lorentzian shape is only an approximation. In case more than one alternative analysis gave equally good fit, that which maintained the peak positions nearer the observed humps was preferred. A component not indicated in the contour by a hump or a shoulder was introduced only in those cases where repeated Lorentzian trials otherwise failed by wide margins and there were spectral evidences too for such a component.

The inaccuracies of the derived parameters vary from one situation to another. Band positions are accurate to within $\pm 2 \text{ cm}^{-1}$ for sharp peaks, $\pm 5 \text{ cm}^{-1}$ for broad but distinct bands and shoulders, and $\pm 10 \text{ cm}^{-1}$ for bulges and very weak evidences. For intensities the error level may be upto 10% in the case of envelopes with weak overlappings and upto 30% in the case of envelopes with strong overlapping.

REFERENCES

1. B Morosin and E C Lingafelter, J. Phys. Soc. Jpn. 43, 2099 (1977).
2. N Wada, M Suzuki, A Sawada, Y Ishibashi and K Gesi, J. Phys. Soc. Jpn. 50, 1813 (1981).
3. T C Daman, S P S Porto and B Tell, Phys. Rev. 142, 570 (1960).
4. T C Daman, S P S Porto and B Tell, Phys. Rev. 144, 771 (1966).
5. M B Patel, Ph.D. thesis, Indian Institute of Technology, Kanpur (1982).
6. W Voigt, Munch. Berg. 603 (1912).
7. H A Lorentz, Koninkl. Ned. Akad. Welenschap. Proc. 8, 591 (1960).

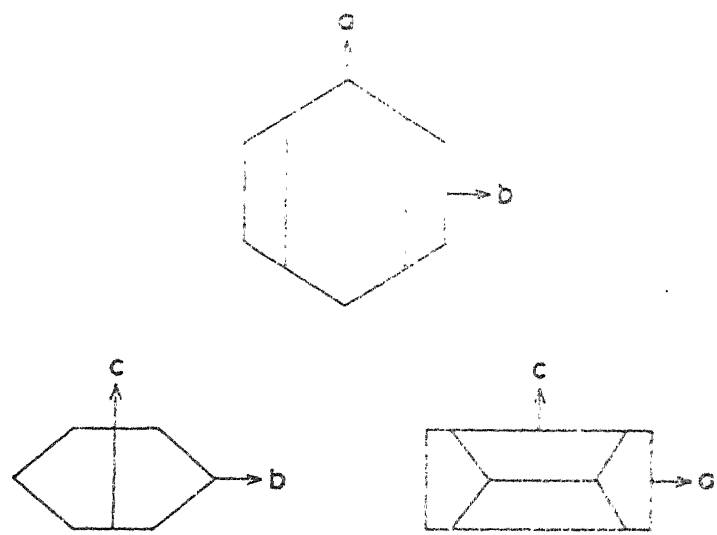


Fig. 2-1 Form of typical as grown $[N(CH_3)_4]_2ZnCl_4$ crystal [2].

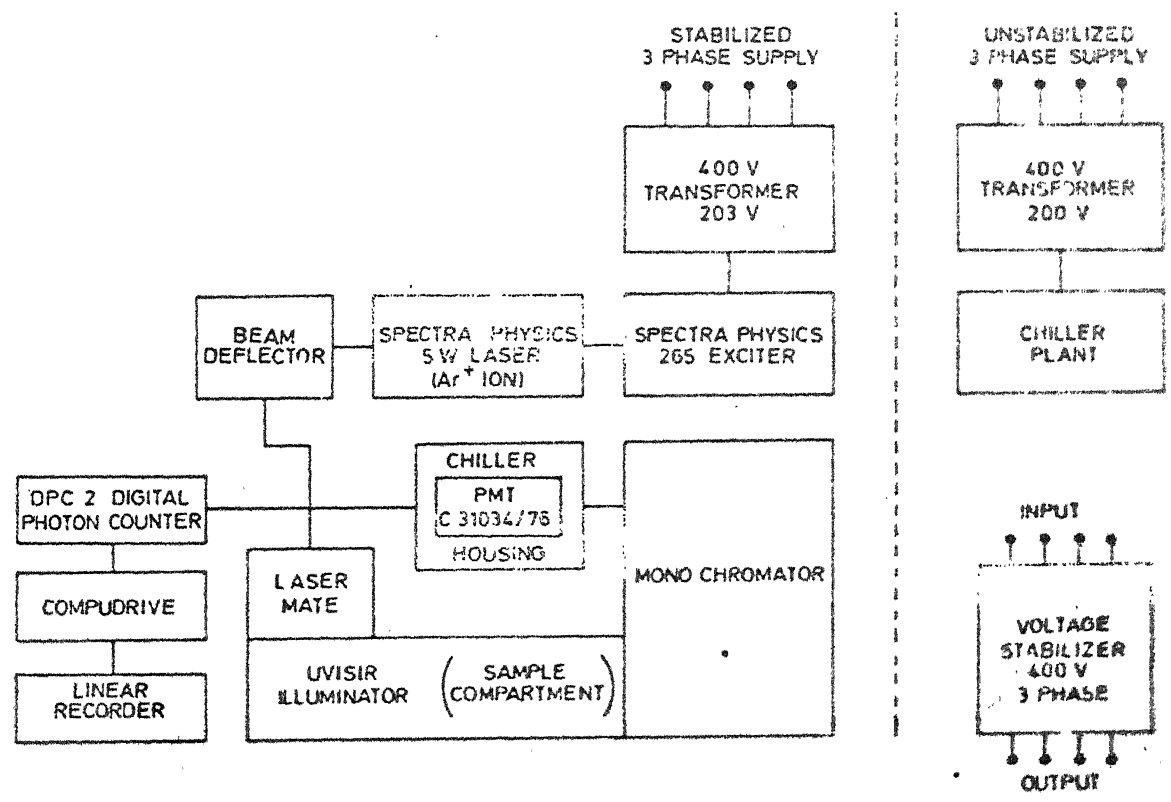
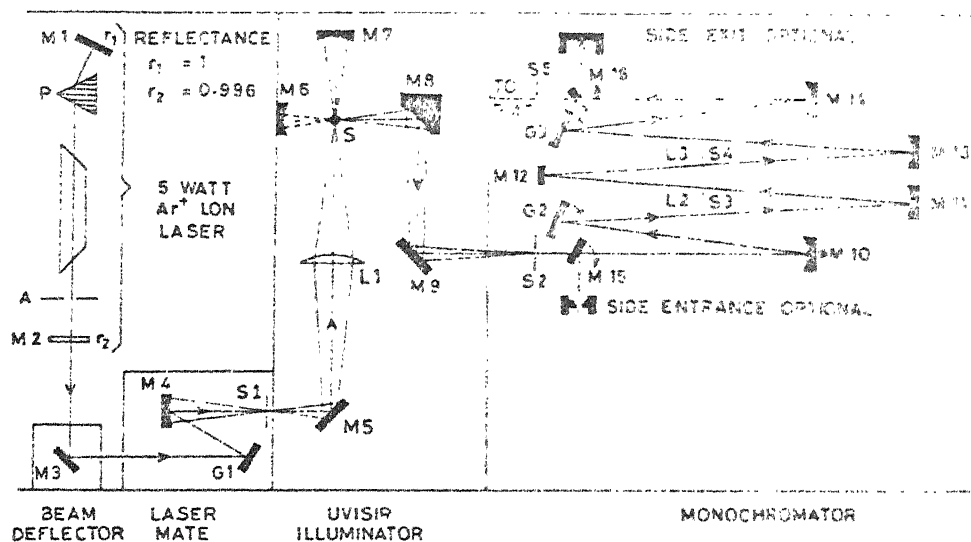


Fig. 2-2 Laser Raman spectrometer (Block diagram).



P, Prism; A, Aperture; M1-M3, M5, M9, M15, M16, Plane mirrors; M4, M6, M7, M10-M14, Concave mirrors; M8, Elliptical collector mirror; S1-S5, Slits; G1-G3, Gratings; L1, Fused silica condenser lens; S, Sample; L2, L3, Optical filter; PMT, Photomultiplier tube.

Fig.2-3 Optical diagram of spectra physics laser and Ramalog 1403 spectrometer.

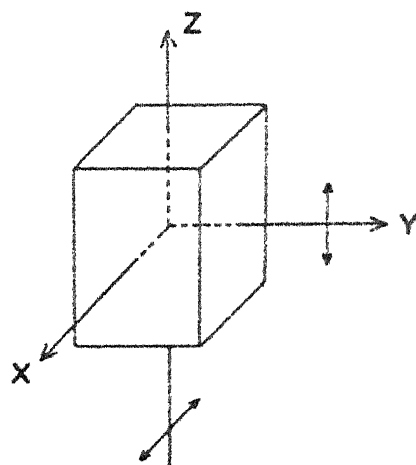


Fig.2-4 Excitation geometry, Z (XZ) Y.

Fig. 2.5 The design of a high temperature cell with different types of sample holders for Raman Studies.

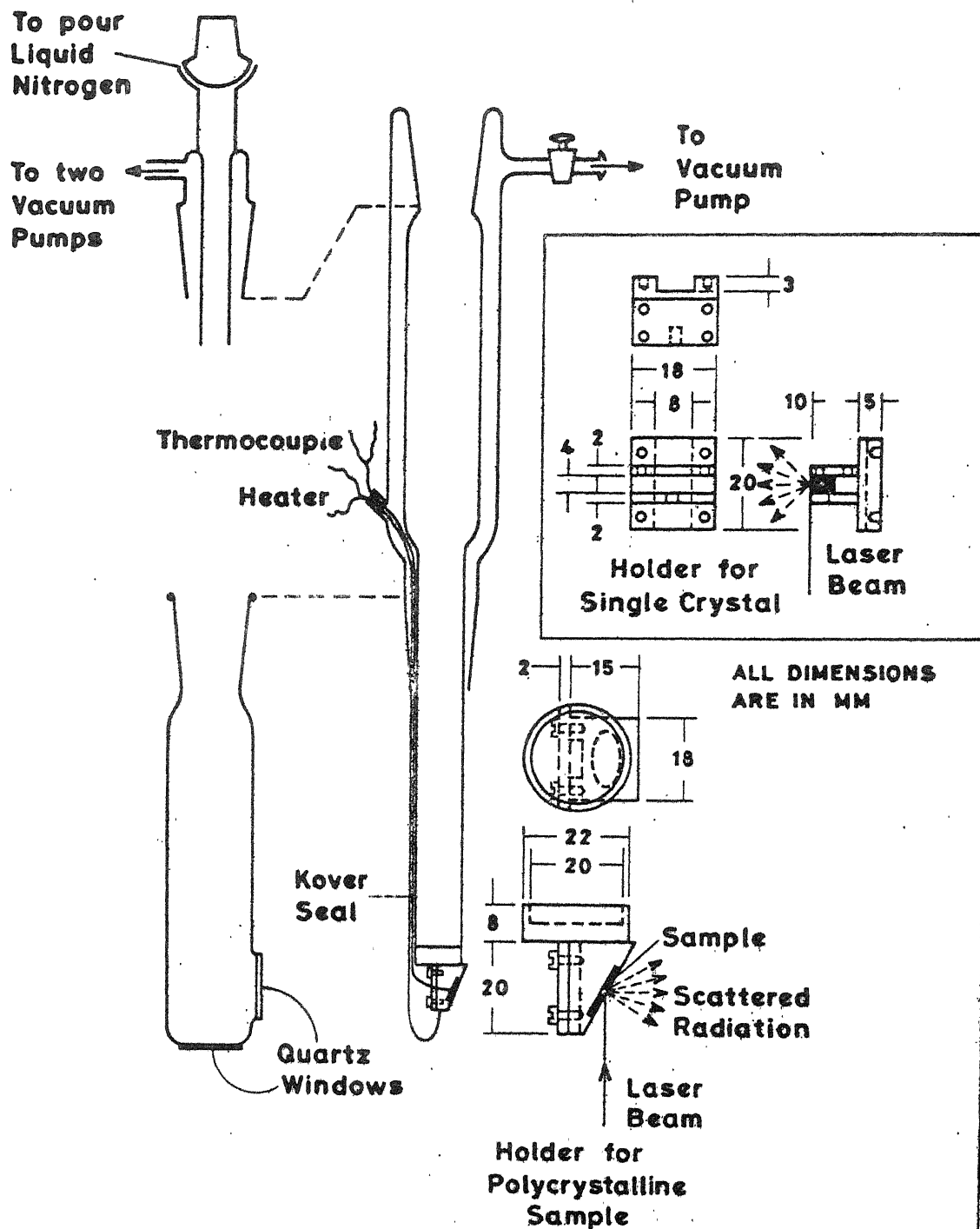


Fig.2-6 Low Temperature Cell for Raman Studies (300-63K)

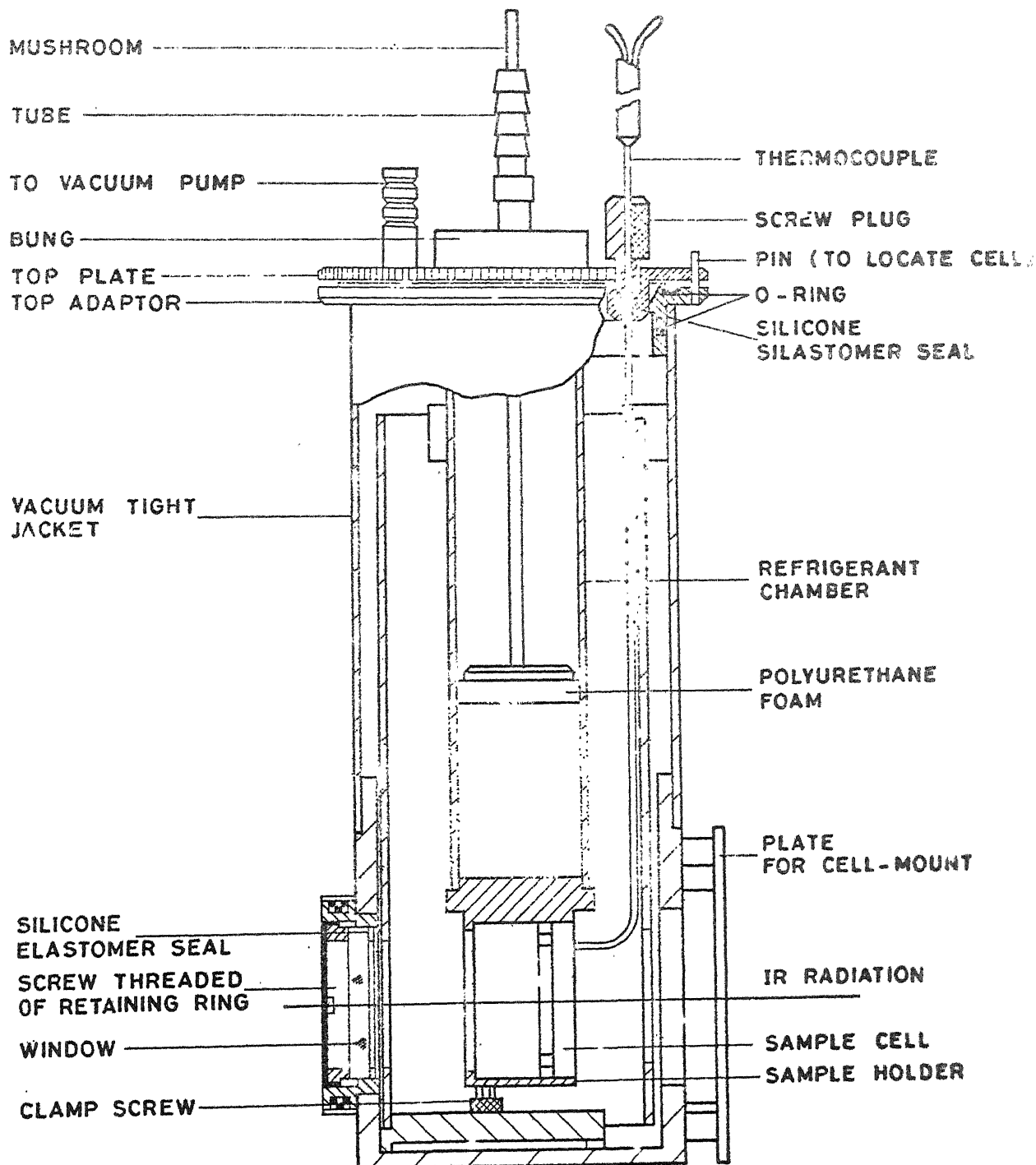


Fig. 2.7 SPECAC VARIABLE TEMPERATURE CELL

87525

3. VIBRATIONAL STUDIES AND PHASE TRANSITIONS IN NORMAL (d_0) AND PERDEUTERATED (d_{12}) TETRAMETHYL AMMONIUM CHLORIDES

In this chapter we present our vibrational studies (Raman and infrared) of TMACl-d_0 and TMACl-d_{12} . We attempt to explain the three abnormally high intensity bands in the CH_3 stretching region in TMACl-d_0 by proposing a model in which the T_d symmetry of TMA-d_0 ion dynamically distorts to C_{3v} [1]. We have characterized three phase transitions above liquid nitrogen temperature in TMACl-d_0 and one phase transition above room temperature in TMACl-d_{12} [2,3].

3.1 CRYSTAL STRUCTURE

The TMA halides (chloride, bromide and iodide) are isostructural at room temperature as determined by X-ray diffraction studies [4-6]. They belong to the tetragonal system with space group D_{4h}^7 ($Z = 2$). A two dimensional view of the structure in XY plane is given in Fig. 3.1.

Vegard and Sollesnes [4] assigned the carbon atoms to the site $C_s(8)$ of D_{4h}^7 , which yields the same antiparallel arrangement of tetrahedra as in the tetragonal phase of ND_4Br [7,8]. Also the space group D_{4h}^7 requires the 24 hydrogen atoms in the unit cell to be divided either into three groups of 8 equivalent hydrogen atoms each or into two groups, one

of 8 and the other of 16. Only the latter arrangement is structurally acceptable to the cation at any temperature [8]. Powder patterns of TMACl-d_0 in phase II have been reported by Dufourcq et al. [9] and Pistorius and Gibson [8]. Since TMACl-d_0 in phase II is known to be piezoelectric [10], it must have a non-centrosymmetric space group. The structure is shown to be rhombohedral with one formula unit per unit cell [9]. Pistorius and Gibson [8] have suggested a space group C_{3v}^5 ($Z = 1$) using X-ray diffraction powder pattern in phase II and calculation of configurational entropy in phases III and II. In this structure the anion is located at the C_3 axis of the site C_{3v} . The nitrogen atom and one carbon atom are also on the three fold axis in the C_{3v} site. The other three carbon atoms of the tetrahedron cation occupy C_1 site.

In phase I the structure of TMACl-d_0 has been shown to be face-centred cubic with four formula units per unit cell [9]. Pistorius and Gibson [8] have found the space group to be O_h^5 ($Z = 4$) with $a_0 = 9.11 \text{ \AA}$ using configurational entropy calculation and X-ray powder pattern. There are a number of possible arrangements in this space group, but in the absence of sufficiently accurate diffraction intensities it is not possible to make a definite choice [8]. Regarding phase IV Tench [11] reports that the structure is the same (tetragonal) as for the room temperature phase, i.e., phase III, the unit cell dimensions also being only marginally different.

3.2 GROUP THEORETICAL ANALYSIS

The TMA group retains its identity over a wide range of environmental conditions. It is, therefore, appropriate to take TMA as a distinct group in any group theoretical analysis under the site symmetry approach. In phase II (C_{3v}^5 , $Z = 1$) the total number of modes, 54, for a unit cell could be distributed as six translatory phonons (including three acoustic phonons), three rotatory modes and forty five internal vibrations of the TMA ion. Two types of configurations, eclipsed and staggered [12,13], are possible for the TMA under the point group symmetry T_d . But the distributions of vibrational modes of TMA ion are the same for both the configurations. This is given in Table 3.2 :

$$\Gamma_{\text{vib}}^{\text{TMA}} = 3A_1 + A_2 + 4E + 4F_1 + 7F_2 \quad (3.1)$$

Young et al. [14] have pointed out that it is somewhat arbitrary to define one observed frequency as carbon-hydrogen frequency and another as that of C_4N , because in TMA ion the central atom (N) and the methyl carbon atoms are strongly bonded. Yet we present an approximate description of the observed modes in terms of vibrations of methyl group and the C_4N skeleton as given in Table 3.3. We have adopted the standard Herzberg's notations to denote the vibrations [15].

In other phases the distribution of total number of modes can be obtained from that of phase II ($Z = 1$) by multiplying it with the number of formula units per unit

cell (Z) in the desired phase ($Z = 4$ for phase I and $Z = 2$ for phase III). Table 3.4 illustrates the correlations of the species of factor groups C_{3v} and D_{4h} for phases II and III, respectively, through the species of their respective sites. The internal modes of TMA ion in phase II (45 in total) and phase III (90 in total) are distributed as follows

$$\Gamma_{\text{vib}}^{\text{II}} = 10A_1(\text{R, IR}) + 5A_2 + 15E(\text{R, IR}) \quad (3.2)$$

$$\begin{aligned} \Gamma_{\text{vib}}^{\text{III}} = & 7A_{1g}(\text{R}) + 4A_{2g} + 7B_{1g}(\text{R}) + 5B_{2g}(\text{R}) + 11E_g(\text{R}) \\ & + 5A_{1u} + 7A_{2u}(\text{IR}) + 4B_{1u} + 7B_{2u} + 11E_u(\text{IR}) \end{aligned} \quad (3.3)$$

For phase IV and V no structural data are available. The space group for phase I has been suggested to be O_h^5 ($Z = 4$) [8], but no possible site symmetry corresponding to $Z = 4$ is available [16]. Therefore a group theoretical analysis for these phases could not be carried out.

3.3 VIBRATIONAL SPECTRA OF TMACl-d₀ IN AQUEOUS SOLUTIONS

The observed Raman spectra of an aqueous solution of TMACl-d₀ (7 M) for both parallel and perpendicular polarizations are shown in Fig. 3.2. The normal Raman spectra with variation of concentration are shown in Fig. 3.3. The IR spectrum of an aqueous solution of TMACl-d₀ is given in Fig. 3.4. The observed band positions with half widths and relative integrated intensities are given in Table 3.5. IR

and Raman data of Berg [17] for TMACl-d₁₂ are also given in Table 3.5 for comparison and completeness.

The modes of C₄N skeleton have been assigned without controversy with the help of polarization data and exclusion principle [18] in Raman and IR spectra. A weak shoulder at 736 cm⁻¹ in the Raman spectrum (0.5 M) towards the lower frequency side of the intense band $\nu_3(A_1)$ is assigned as the overtone of $\nu_{19}(F_2)$. The band at 920 cm⁻¹ in the spectrum is assigned as the overtone of $\nu_{18}(F_2)$.

The CH₃ symmetric bending mode $\nu_2(A_1)$ has not been ascertained experimentally in the Raman spectra of the compounds containing TMA-d₀. A polarized band in the Raman spectra of TMACl-d₁₂ at 1144 cm⁻¹ is observed in the region free from the other bands [17]. The position of $\nu_2(A_1)$ in TMACl-d₀ is estimated to be ~1450 cm⁻¹ on the basis of isotopic shift calculations. But it could neither be detected by extracting the pure isotopic scattering intensity from the difference $I_{||} - \frac{4}{3} I_{\perp}$ nor from a plot between depolarization ratio versus wavenumber which should give a dip at the position of $\nu_2(A_1)$ mode [19]. Thus for TMACl-d₀ the in-phase bending mode $\nu_2(A_1)$ must be of negligible intensity, whereas it appears as a sharp band of appreciable intensity in the spectrum of TMACl-d₁₂. Kabisch and Mobius [19] have shown theoretically that $\nu_2(A_1)$ in TMACl-d₁₂ gets intensity due to mixing of wavefunctions of C₄N and CD₃ groups, whereas in TMACl-d₀ its intensity is very low. Taylor et al. [20] have calculated with the help of bond

polarizability theory that the intensities of $\nu_2(A_1)$ in the normal and deuterated tetramethyl methanes are in ratio 0.7:1.2. Young et al. [14] have pointed out that the methyl group deformation and rocking modes of F_2 species $\nu_{15}(F_2)$, $\nu_{16}(F_2)$ and $\nu_{17}(F_2)$ resonate with the C_4N asymmetric stretch, $\nu_{18}(F_2)$ and get pushed up. Accordingly, one may expect resonance between CD_3 symmetric deformation $\nu_2(A_1)$ and C_4N symmetric stretch $\nu_3(A_1)$ in $TMACl-d_{12}$ which are more close in $TMACl-d_{12}$ than in $TMACl-d_0$. Thus $\nu_2(A_1)$ mode would appear more intense in $TMACl-d_{12}$ than in $TMACl-d_0$.

The methyl symmetric stretching mode, $\nu_1(A_1)$ is quite difficult to assign due to appearance of a number of intense polarized bands observed in the stretching region. The assignments are based on two alternative considerations: (i) Fermi resonance and anharmonicity and (ii) dynamic distortion of the C_4N skeleton. It is noted that the calculated mechanical anharmonicities vary marginally on going from the dilute to the concentrated solution while the relative intensities change drastically.

3.3.1 Fermi-resonance and Anharmonicity

Our assignments, shown in column 8 of Table 3.5 are analogous to those proposed by Kabisch and Klose [21]. The moderate intense band at 2826 cm^{-1} (in 0.5 M solution) shows the largest mechanical anharmonicity and its intensity is about an order of magnitude smaller than that of the other

strong polarized bands. This band has been attributed to an overtone of the $\nu_{16}(F_2)$ mode. Similarly the other very weak bands at 2880 and 2905 cm^{-1} (in 0.5 M solution), with less anharmonicities, are assigned to a combination and an overtone respectively. The depolarized band at 3043 cm^{-1} and the polarized band at 2991 cm^{-1} can safely be assigned to the CH_3 asymmetric and the CH_3 symmetric stretching modes respectively. The polarized band at 2966 cm^{-1} can also be justified as the allowed A_1 component of the overtone of $\nu_{15}(F_2)$ mode. The other polarized band at 2933 cm^{-1} cannot be assigned as the combination of the $\nu_6(E)$ and the $\nu_{15}(F_2)$ modes.

In general, due to Fermi-resonance, the resonating band which is nearer to the fundamental gains more intensity than the band farther from it. Neither the Fermi-resonance nor the electrical anharmonicity consideration can alone explain the observed intensity distribution in this region and its variation with concentration. The Fermi-resonance combined with the electrical anharmonicity (coupled with mechanical anharmonicity) may explain the observed abnormal intensity distribution. One may argue that the band at 2933 cm^{-1} may have more electrical anharmonicity (as would be expected on the basis of higher mechanical anharmonicity) than the band at 2966 cm^{-1} , making it (2933 cm^{-1} band) more intense under Fermi-resonance than the band at 2966 cm^{-1} which is closer to the fundamental at 2991 cm^{-1} . However, this argument is untenable for the following reasons :

- (i) The fundamental requirement for Fermi-resonance is that the levels involved must have the same symmetry [15]. The selection rules show that the combination of $\nu_6(E)$ and $\nu_{15}(F_2)$ produces levels of symmetry species F_1 and F_2 which cannot resonate with CH_3 symmetric stretching mode of symmetry species A_1 .
- (ii) The intensity of the resonating band(s) can never exceed the intensity of the fundamental band, unless electrical anharmonicity is a dominating factor, which is seldom observed in Raman spectra.
- (iii) It is observed that on varying the concentration, the intensities of the resonating bands change drastically whereas the band positions remain almost unchanged. This ~~is~~ also not observed in Fermi-resonance especially when the positions of fundamental bands remain unchanged.

Thus the intense and the polarized band at 2933 cm^{-1} cannot unambiguously be assigned to the combination of the $\nu_6(E)$ and the $\nu_{15}(F_2)$ modes. Therefore an alternative explanation of the three strong polarized and intense bands may be searched in the dynamic distortion of the C_4N skeleton.

3.3.2 Dynamic Distortion of the C_4N Skeleton

The totally symmetric CH_3 stretching motions of the four CH_3 groups in TMA ion could result in three specific configurations consistent with the internal vibrations of

C_4N skeleton as shown in Fig. 3.5. In the first configuration (Fig. 3.5a) all the C-atoms vibrate in-phase along C-N bonds. In this case the T_d symmetry of the C_4N skeleton is maintained even dynamically. This situation corresponds to ν_1 mode of species A_1 for the skeleton and yields one totally symmetric polarized CH_3 stretching vibration (A_1).

In the second configuration, three C-atoms vibrate in-phase and one out-of-phase and vice versa along C-N bonds as shown in Fig. 3.5b. In this case the T_d symmetry of C_4N skeleton is distorted to C_{3v} dynamically corresponding to $\nu_3(F_2)$ mode for the skeleton (T_d) and yields under C_{3v} one totally symmetric polarized CH_3 stretching mode (A_1) and another asymmetric depolarized CH_3 stretching mode (E).

In the third configuration, three C-atoms vibrate in-phase perpendicular to C-N bonds and one along the C-N bond as shown in Fig. 3.5c. In this case, too, the T_d symmetry of C_4N skeleton is distorted to C_{3v} dynamically and the situation, corresponding to $\nu_4(F_2)$ mode for the skeleton (T_d), yields one totally symmetric polarized CH_3 stretching mode (A_1) and another asymmetric depolarized CH_3 stretching mode (E).

There are two more possible configurations with two asymmetric depolarized CH_3 stretching modes corresponding to the vibrations of the C_4N skeleton of species E and F_1 . It can, therefore, be concluded that three totally symmetric polarized C-H stretching bands must arise from dynamic distortion of C_4N skeleton and coupling between the four CH_3

groups. That would explain the three observed A_1 modes in CH_3 stretching region.

The four CH_3 asymmetric stretches may appear at the same frequency giving thereby a single depolarized band at 3043 cm^{-1} (in 0.5 M solution). The larger half-width of this band and its shift with concentration may also corroborate the presence of more than one unresolved bands under the combined envelope.

A correlation of isolated CH_3 stretching vibrations (C_{3v} point groups) with those of TMA under T_d and C_{3v} point groups is given in Table 3.6. Under the group T_d in TMA the C-H symmetric stretching (A_1) vibrations of four isolated CH_3 groups produce a totally symmetric species A_1 and a triply degenerate species F_2 . Likewise, the four isolated CH_3 asymmetric stretching modes (E) under C_{3v} produce a doubly degenerate E species and two triply degenerate species F_1 and F_2 under T_d point group as shown in the second column of Table 3.6. As a result under the point group T_d one expects in the CH_3 stretching region four Raman active bands out of which only one should exhibit totally symmetric and polarized (A_1) character.

If the C_4N group of TMA acquires a C_{3v} symmetry even dynamically (e.g., this could be the case during its ν_3 vibration as discussed later and shown in Fig. 3.5) the situation gets changed as illustrated in the third column of Table 3.6. It is evident that one would expect a maximum of three totally

symmetric polarized (A_1) CH_3 stretching bands along with four doubly degenerate (E) depolarized C-H stretching modes. This situation will be applicable to the solutions where the crystalline field effects would be missing.

To get rid of the difficulty in assigning the band at 2933 cm^{-1} as combination of $\nu_6(E)$ and $\nu_{15}(F_2)$ Kabisch and Mobius [22] have pointed out that in the CH_3 stretching region a number of overtones of $\nu_2(A_1)$, $\nu_7(E)$, $\nu_{11}(F_1)$, $\nu_{16}(F_2)$ and $\nu_{17}(F_2)$ are falling, which may resonate with $\nu_1(A_1)$. The appearance of only one strong band in CH_3 symmetric stretching region in Raman spectra of polycrystalline TMA halides can also not be explained on the basis of dynamic distortion of C_4N skeleton.

3.4 CHARACTERISTIC RAMAN SPECTRA OF $TMACl-d_0$ IN THE FOUR PHASES ABOVE LIQUID NITROGEN TEMPERATURE AND THEIR ASSIGNMENTS

The relevant portions of the observed Raman spectra of $TMACl-d_0$ in phases I (at 540 K), II (at 393 K and 300 K on cooling under vacuum), III (at 300 K) and IV (at 90 K) are depicted in Fig. 3.6. The observed band positions with half widths and relative integrated intensities are given in Table 3.7. The vibrational assignments of the observed bands are suggested under the undistorted point group symmetry T_d of tetramethyl ammonium ion and without taking into account the splitting due to lowering of symmetry on account of the crystal field.

3.4.1 Phase I

For TMACl-d_0 , Pistorius and Gibson [8] have suggested the space group for the phase I to be O_h^5 ($Z = 4$). The possible site symmetries for space group O_h^5 are $2O_h(1)$, $T_d(2)$, $D_{2h}(6)$, $C_{4v}(6)$, $C_{3v}(8)$, $3C_{2v}(12)$, $2C_s(24)$ and $C_1(48)$ [16]. So there is no possible site symmetry in this space group that can contain four symmetry points. According to Dufourcq et al. [9] the cations are at two T_d sites. If it is true, the Raman spectra of TMACl-d_0 in phase I must closely resemble with the aqueous solution spectra as observed by Kabisch [22] in $[(\text{CH}_3)_4\text{N}]_2\text{SnCl}_6$. But in phase I the intensities of all the bands reduce to nearly zero. So it seems that either TMACl-d_0 does not have space group O_h^5 ($Z = 4$) in phase I or due to some other effects intensities of the bands are suddenly reduced to zero. Amongst possible reasons suggested are very low activation energy for CH_3 librations [8] and occurrence of ionic diffusion in this phase [10].

3.4.2 Phase II

The Raman spectrum of TMACl-d_0 in this phase at 393 K below 1300 cm^{-1} is similar to the aqueous solution spectrum except for the occurrence of some additional details. The asymmetric stretching mode of C_4N , $\nu_{18}(\text{F}_2)$ appears as a doublet in phase II which is clearly resolved on cooling the sample to room temperature in the same phase as shown in Fig. 3.6. It is consistent with the group theoretical

splitting. A band at 1068 cm^{-1} , appearing in phase II, gains intensity on cooling the sample to room temperature in the same phase. The band is assigned to CH_3 rocking, $\nu_{11}(\text{F}_1)$. Kabisch [22] observed a very weak band at 1081 cm^{-1} in phase III and assigned it to this mode.

In the Raman spectra of TMACl-d_0 above 1300 cm^{-1} we get two strong bands at 1403 and 1462 cm^{-1} in CH_3 deformation region and two strong bands at 2946 and 3017 cm^{-1} in the CH_3 stretching region. The band at 3017 cm^{-1} again splits into two components at 3014 and 3028 cm^{-1} on cooling the sample in the same phase.

Table 3.8 is an illustration and extension of Table 3.4 for the CH_3 modes. For isolated CH_3 group having C_{3v} symmetry, group theoretically the stretching (or deformation) modes produce one vibration each of species A_1 and E as shown in column 1 of Table 3.8. The four symmetric stretches (or deformations) of species A_1 for the four CH_3 groups in TMA ion under molecular symmetry T_d produce the species $\text{A}_1 + \text{F}_2$, and the corresponding modes are denoted as ν_1 and ν_{14} for stretches (ν_2 and ν_{16} for deformation). Likewise the asymmetric stretches (or deformations) of species E are distributed as $\text{E} + \text{F}_1 + \text{F}_2$, and the corresponding modes are denoted as ν_5, ν_9 and ν_{13} for stretches (ν_6, ν_{10} and ν_{15} for deformations) as given in Table 3.8. As given in column 5 of Table 3.8, the four symmetric (A_1) and four asymmetric (E) stretches (or deformations) are further split as the bands of species $2\text{A}_1 + \text{E}$ and $\text{A}_1 + \text{A}_2 + 3\text{E}$ under the factor group C_{3v} (through the site C_{3v}). Thus all the CH_3

stretches (or deformations) may split into seven ($3A_1+4E$) Raman active components in phase II as given in last row of Table 3.8. A_2 being inactive both in IR and R. Experimentally two strong bands in the deformation (or stretching) region are observed in the Raman spectra in phase II which are identical to the Raman spectra of isolated CH_3 group. So it is appropriate to assign the bands at 1403 and 1462 cm^{-1} as CH_3 symmetric deformation and CH_3 asymmetric deformation, respectively. Similarly in the CH_3 stretching region the bands at 2946 and 3017 cm^{-1} are assigned as CH_3 symmetric stretch and CH_3 asymmetric stretch, respectively. The splitting of 3017 cm^{-1} may be due to correlation field as expected.

3.4.3 Phase III (RT phase)

The assignments of all the fundamentals of TMA ions for the room temperature phase III below 1300 cm^{-1} are identical to those made by Kabisch [22]. In the CH_3 deformation region, $1350-1500\text{ cm}^{-1}$, as already explained and given in Table 3.8, five bands $\nu_2(A_1)$, $\nu_{16}(F_2)$, $\nu_6(E)$, $\nu_{10}(F_1)$ and $\nu_{15}(F_2)$ are group theoretically expected under the point group symmetry T_d for free TMA ion. The splittings of the bands in phase III under the factor group D_{4h} through the site D_{2d} are given in the last column of Table 3.8. In the Raman spectra of $TMACl-d_0$ we get five bands at 1398 , 1402 , 1454 , 1477 and 1483 cm^{-1} . The doublet with components at 1398 and 1402 cm^{-1} (which splits into triplet with components at 1392 , 1399 and 1407 cm^{-1} in phase

IV) is assigned as $\nu_{16}(F_2)$, consistent with group theoretical analysis. The bands of species F_2 are expected to split into two Raman active (B_{1g} and E_g) components for room temperature phase III. It is observed that most of the bands of species F_2 in phase IV split into three components. Thus the bands at 1477 and 1483 cm^{-1} , assigned as $\nu_{15}(F_2)$ in phase III, also split into three components (1474, 1479 and 1486 cm^{-1}) in phase IV. The band at 1454 cm^{-1} could be assigned either to $\nu_2(A_1)$ or to $\nu_6(E)$. However, it has been observed that in CH_3 and C_4N stretching regions of TMA ion the intensities of the bands corresponding to symmetric species A_1 are diminished with respect to the corresponding asymmetric bands in going from solution to polycrystalline state and $\nu_2(A_1)$ could not be observed in Raman spectra of aqueous solution of TMACl-d_0 . Therefore the band at 1454 cm^{-1} has been assigned to $\nu_6(E)$. This band can, however, have some minor contribution due to $\nu_2(A_1)$ as expected by spectra of deuterated TMA ion [17]. The band of species F_1 under T_d is Raman inactive, so the band of species E_g arising from $\nu_9(F_1)$ may be too weak to identify in polycrystalline TMACl-d_0 in phase III.

3.4.4 Phase IV

Pistorius and Gibson [8] have suggested that the lattice in this phase is tetragonal with lattice constants close to those of the room temperature phase III. No structural data are available for this phase. As mentioned

earlier, it is observed that most of the bands of species F_2 split into three components in the Raman spectra of TMACl-d_0 in this phase.

It can be expected that on lowering the temperature (III \rightarrow IV) the inversion symmetry in phase III is lost and therefore the lattice goes to a space group lower than D_{4h}^7 . The most probable tetragonal space groups having four fold symmetry without inversion would be anyone from D_4^1 , D_4^2 , D_4^3 D_4^{10} . However D_4^1 and D_4^9 are the only space groups which do not possess screw symmetry, thus resembling the D_{4h}^7 group as far as screw symmetry is concerned. If one assumes that the primitive cell is preserved on lowering the temperature, the space group for phase IV will be D_4^1 ($Z = 2$). Under this situation the bands of species F_2 are expected to split into three Raman active components, which is actually observed in phase IV.

3.5 INFRARED SPECTRA OF TMACl-d_0

The IR spectra of TMACl-d_0 in an aqueous solution kept between AgCl windows and in the polycrystalline form in KBr pellet at 300 and 90 K are shown in Fig. 3.4. The vibrational assignments are given in Table 3.5 and Table 3.7 for aqueous solution spectra and for polycrystalline spectra, respectively. The assignments are similar to those proposed by Bottger and Geddes [23] except for some details. The IR data of TMACl-d_{12}

are also given in the tables for comparison and completeness.

The CH_3 asymmetric stretching mode $\nu_{13}(\text{F}_2)$ shows only one component at 3020 cm^{-1} in IR spectra of polycrystalline TMAcI-d_0 at 300 K. On cooling the sample to liquid nitrogen temperature (90 K), it splits into components at 3017 and 3023 cm^{-1} . The splitting may be due to correlation field as expected from group theoretical analysis.

In the C_4N -asymmetric stretching region three bands are observed at 920, 948 and 958 cm^{-1} in the IR spectra at 300 K. The bands at 948 and 958 cm^{-1} are assigned to the components of C_4N -asymmetric stretching mode $\nu_{18}(\text{F}_2)$ and the band at 920 cm^{-1} to an overtone of $\nu_{19}(\text{F}_2)$. In the IR spectra at 90 K, one more band at 938 cm^{-1} is observed as a shoulder of the band at 948 cm^{-1} . The three bands at 938, 948 and 958 cm^{-1} cannot be assigned as the components of $\nu_{18}(\text{F}_2)$ since TMAcI-d_0 has space group D_{4h}^7 ($Z = 2$) at room temperature and according to group theoretical analysis the modes of species F_2 can have only two $\text{A}_{2u} + \text{E}_u$ IR active components. The band at 938 cm^{-1} could be arising due to phase transition but the same splitting is also observed in the cases of TMAbR-d_0 and TMAI-d_0 which do not show any phase transitions in this temperature range. An alternative assignment, which looks more logical, is that the bands at 920 and 938 cm^{-1} are the components of overtone of $\nu_{19}(\text{F}_2)$. According to group theoretical analysis a mode of species F_2 splits into $\text{A}_{2u} + \text{E}_u$ IR active components whereas an overtone of modes of species F_2 may split into

$A_{2u} + 2E_u$ IR active components under the space group D_{4h}^7 through the site symmetry D_{2d} as shown in Table 3.4. Thus a number of components of overtone of $\nu_{19}(F_2)$ may resonate with the components of $\nu_{18}(F_2)$.

3.6 RAMAN SPECTRA OF $TMACl-d_{12}$ IN PHASES III AND II

The relevant portions of the observed Raman spectra of $TMACl-d_{12}$ in phase III (at 300 K) and in phase II (at 448 and 300 K - on cooling under vacuum) are depicted in Fig. 3.7. The Raman spectrum at 90 K are also shown in the Fig. 3.7; but it is similar to the spectrum in phase III. The observed band positions with peak intensities, half-widths and relative integrated intensities and their assignments are given in Table 3.7.

The modes of C_4N in $TMACl-d_{12}$ in both the phases have been assigned by correlating the Raman spectra of $TMACl-d_{12}$ in aqueous solution [8], Raman spectra of $TMACl-d_0$ in the two phases [2] and isotopic shift calculations [8]. Two bands at 808 and 813 cm^{-1} are observed in phase III which shift to 809 and 816 cm^{-1} in phase II. When the sample in phase II is cooled to room temperature the band at 809 cm^{-1} further splits into two components at 806 and 810 cm^{-1} . These split bands cannot be attributed to the C_4N asymmetric stretch, $\nu_{18}(F_2)$ as group theoretically the mode of F_2 species under point group symmetry T_d may split into only two Raman active components of species $A_1 + E$ under the space group C_{3v}^5 through

the site symmetry C_{3v} in phase II [2]. Thus the triplet may be due to either structural change, distortion in symmetry of TMA ion or appearance of some overtone/combination of the lower frequency bands. Another alternative assignment is that the band at 813 cm^{-1} in phase III is a component of CD_3 rocking, $\nu_{11}(F_1)$. The isotopic shift ratio (ν^D/ν^H) for this band then turns out to be 0.761 which is quite close to the theoretically calculated value (0.774) [17]. The reason for the appearance of so strong a component of $\nu_{11}(F_1)$ at 813 cm^{-1} is that each of the modes $\nu_{11}(F_1)$ and $\nu_{18}(F_2)$ has at least one component of the same species in both the phases as shown in Table 3.9 and both $\nu_{11}(F_1)$ and $\nu_{18}(F_2)$ in $TMACl-d_{12}$ fall very close. Therefore the CD_3 rocking mode, $\nu_{11}(F_1)$ gets intensity from C_4N asymmetric stretch, $\nu_{18}(F_2)$ due to resonance interaction.

The bands in the region $1040-1100\text{ cm}^{-1}$ in $TMACl-d_{12}$ show temperature dependent behaviour similar to that of $\nu_6(E)$ and $\nu_{15}(F_2)$ in $TMACl-d_0$. Therefore the band at 1052 cm^{-1} is assigned to $\nu_6(E)$ and the bands at 1066 and 1076 cm^{-1} are assigned to $\nu_{15}(F_2)$ in the room temperature phase III. This assignment is in accordance with Berg's assignment in the Raman spectra of $TMACl-d_{12}$ in aqueous solution [17].

The band at 1191 cm^{-1} in polycrystalline $TMACl-d_{12}$ can be assigned to either $\nu_{16}(F_2)$ or $\nu_{17}(F_2)$. Kabisch et al. [19] have shown that the CD_3 symmetric deformation, $\nu_{16}(F_2)$ has very small intensity in the Raman spectra of deuterated (d_{12}) tetramethyl ammonium iodide. In the Raman spectra of $TMACl-d_{12}$

in aqueous solution a band at 1192 cm^{-1} is assigned as CD_3 rocking mode, $\nu_{17}(\text{F}_2)$ with the help of Teller Redlich product rule [17]. This gives an isotopic shift ($\nu^{\text{D}}/\nu^{\text{H}}$) of 0.922 for $\nu_{17}(\text{F}_2)$ whereas the calculated isotopic shift for this mode is 0.744. So the interpretation of band at 1191 cm^{-1} as $\nu_{17}(\text{F}_2)$ in TMACl-d_{12} still needs a theoretical verification.

Methyl symmetric stretch, $\nu_1(\text{A}_1)$ is quite difficult to assign due to appearance of a number of intense polarized bands in this region. Kabisch et al. [24] have calculated the value of unperturbed methyl symmetric stretch, $\nu_1(\text{A}_1)$ as 2947.5 cm^{-1} for TMACl-d_0 and 2142 cm^{-1} for TMACl-d_{12} in the Raman spectra of aqueous solutions, but the calculation of unperturbed $\nu_1(\text{A}_1)$ contributed nothing significant to the assignment. The sharp band at 2077 cm^{-1} in the Raman spectrum of TMACl-d_{12} in phase III is tentatively assigned to $\nu_1(\text{A}_1)$ since it does not show any splitting even at liquid nitrogen temperature as expected from group theoretical consideration [2].

The bands at 2255 and 2273 cm^{-1} are assigned to methyl asymmetric stretches, $\nu_5(\text{E})$ and $\nu_{13}(\text{F}_2)$, respectively. Other bands in the methyl stretching region are also assigned tentatively as overtones/combinations of lower frequency bands as given in Table 3.7.

3.7 PHASE TRANSITIONS

Tetramethyl ammonium chloride (TMACl-d₀) undergoes four successive phase transitions detected by differential thermal analysis [8,9,25,26], nuclear magnetic resonance [10], proton spin-lattice relaxation [27] and electron paramagnetic resonance [11] studies. The details of phases and transitions are compiled in Table 3.10.

The phase transition temperatures are determined with the temperature dependence of $\nu_6(E)$ and $\nu_{15}(F_2)$ modes for transitions III \rightarrow II \rightarrow I as shown in Figs. 3.8 (without vacuum) and 3.9 (under continuous vacuum). The transition III \rightarrow IV is followed by monitoring the temperature dependence of $\nu_{16}(F_2)$ as shown in Fig. 3.10. It is observed from Fig. 3.8 that in transition III \rightarrow II the bands at 1454, 1477 and 1483 cm⁻¹ start to diminish at 412 K and a new band starts to appear at 1462 cm⁻¹, the latter band gaining intensity with increase in temperature. At ~430 K the bands at 1454, 1477 and 1483 cm⁻¹ completely disappear and the band at 1462 cm⁻¹ shifts to 1466 cm⁻¹ and becomes fairly strong. So it is seen here that the phase transition III \rightarrow II is a second order transition taking place over a temperature range of 18 K. Pistorius and Gibson [8] have suggested that III \rightarrow II transition has a thermal hysteresis of 18-24 K. We have observed that the transition temperature depends on the initial moisture content and the rate of heating. On very slow heating it is found to be ~20 K higher than the

reported one. But in the presence of much moisture and fast heating it is found to occur around 390 K. We have further observed that the phase transition $\text{III} \rightarrow \text{II}$ in TMACl-d_0 occurs at 367 ± 2 K on keeping the sample under continuous vacuum during the investigation (Fig. 3.9). The variations of peak intensities of $\nu_6(\text{E})$ (1454 cm^{-1}) and $\nu_{15}(\text{F}_2)$ (1477 and 1483 cm^{-1}) with temperature are shown in Fig. 3.11. On cooling the sample under vacuum to room temperature from 400 K the band at 1466 cm^{-1} gains in intensity and shifts to 1468 cm^{-1} . Thus the phase transition $\text{III} \rightarrow \text{II}$ is irreversible and phase II is metastable below 367 K. As soon as we release the water vapour to the sample in phase II at room temperature, it transforms to phase III. The arrangement for transferring water vapour to the sample under vacuum is shown in Fig. 3.12. Thus phase III is stable only in presence of a small amount of moisture. Pistorius and Gibson [8] have shown that only 0.5% water is sufficient for the stability of phase III.

In the transition $\text{II} \rightarrow \text{I}$ the band at 1466 cm^{-1} disappears in an hour when the sample is kept at constant temperature at 540 K just above the reported transition temperature (Fig. 3.8). Other bands also disappear in phase I except for the bands of C_4N skeleton which are found to be very weak.

On lowering the temperature in phase transition $\text{III} \rightarrow \text{IV}$ the band at 1402 cm^{-1} having slight asymmetry on the lower frequency side at 1398 cm^{-1} , first suddenly splits into two components near the transition temperature and finally into

three components at 1392, 1399 and 1407 cm^{-1} within a temperature interval of ~ 10 K (Fig. 3.10). The sudden splitting of band at 1402 cm^{-1} into three components at 185 K indicates that the transition III \rightarrow IV is first order. On heating back we observed reversal of the same pattern, indicating that the transition III \rightarrow IV is reversible without hysteresis.

The temperature dependence of CD_3 asymmetric deformation $\nu_6(\text{E})$ and $\nu_{15}(\text{F}_2)$ in the Raman spectra of TMACl-d_{12} is shown in Fig. 3.13. The variations of peak intensities of the components of $\nu_{15}(\text{F}_2)$ (at 1066 and 1076 cm^{-1}) with temperature is shown in Fig. 3.14; $\nu_6(\text{E})$ at 1052 cm^{-1} is too weak to monitor its variation with temperature. A new band at 1058 cm^{-1} appears at 407 K which gains intensity upto 430 K. A component of $\nu_{15}(\text{F}_2)$ at 1076 cm^{-1} completely disappears around 430 K. Thus the phase transition III \rightarrow II in TMACl-d_{12} starts at 407 ± 5 K and completes around 430 K. The transition III \rightarrow II in TMACl-d_{12} is also found to be irreversible in the absence of moisture.

On cooling the sample to liquid nitrogen temperature we do not get any sudden changes in the spectra. So the phase transition III \rightarrow IV does not occur in TMACl-d_{12} in this temperature range.

3.8 CONCLUSION

For distinguishing the bands of different species in all the phases, single-crystal Raman spectra in different orientations are required. With the splitting of the bands of

species F_2 in $TMA-d_0$ ion under molecular symmetry T_d into three, the space group for phase IV is suggested to be D_4^1 ($Z = 2$), it needs verification by X-ray data which still seek to be determined for this phase as well as phase V.

It is clear from the above studies that the traces of water present in $TMACl-d_0$ and $TMACl-d_{12}$ play a major role in $III \rightarrow II$ phase transition. But the change in $III \rightarrow II$ transition temperature on deuteration and the non-existence of lower temperature phase in $TMACl-d_{12}$ similar to those in $TMACl-d_0$ suggest that the traces of water are not the only responsible entities for phase transitions in the tetramethyl ammonium chlorides. Among the normal (d_0) tetramethyl ammonium halides (i.e. chloride, bromide and iodide), which are isostructural [4-6], only $TMACl-d_0$ undergoes four successive phase transitions. Pistorius and Gibson [8] have pointed out that the occurrence of phase transitions in $TMACl-d_0$ only may be found in the generalized phase diagram of ammonium halides. The generalized phase diagram of ammonium halides [7] is shown in Fig. 3.15. Our observations would lead to conclude that $TMACl-d_{12}$ lies in between $TMACl-d_0$ and tetramethyl ammonium bromide in the generalized phase diagram of tetramethyl ammonium halides.

For phase I the earlier suggested space group O_h^5 ($Z = 4$) is inherently inconsistent and has to be reinvestigated crystallographically.

REFERENCES

1. H D Bist, Mahendra Pal, G S Raghuvanshi and V N Sarin, Proc. Ind. Acad. Sci. 91, 185 (1982).
2. Mahendra Pal, G S Raghuvanshi and H D Bist, Chem. Phys. Lett. 92, 85 (1982).
3. Mahendra Pal, A Agarwal, M B Patel and H D Bist, J. Raman Spectrosc. 00, 000 (1984).
4. L Vegard and K Sollesnes, Phil. Mag. 4, 985 (1927).
5. R W G Wyckoff, Z. Krist. 67, 61 (1928).
6. R W G Wyckoff, "Crystal Structure", Vol. 1, 2nd edn. Interscience Publishers, New York, p107 (1948).
7. R Stevenson, J. Chem. Phys. 34, 1757 (1961).
8. C W F T Pistorius and A A V Gibson, J. Solid State Chem. 8, 126 (1973).
9. J Dufourcq, Y H Bouilland, N B Chanh and B Lemanceau, Acta Crystal. B28, 1305 (1972).
10. A A V Gibson and R E Raab, J. Chem. Phys. 57, 4688 (1972).
11. A J Tench, J. Chem. Phys. 38, 593 (1963).
12. S Silver, J. Chem. Phys. 8, 919 (1940).
13. W von der Ohe, J. Chem. Phys. 62, 3933 (1975).
14. C W Young, J S Koehler and D S McKinney, J. Am. Chem. Soc. 69, 1410 (1947).
15. G Herzberg, "Infrared and Raman Spectra of Polyatomic Molecules", Vol. 2, D. Van Nostrand Co. Inc., New York (1945).
16. W G Fatelay, F R Dollish, N T McDevitt and F F Bentley, "Infrared and Raman Selection rules of Molecular and Lattice Vibrations : The correlation method" , Wiley Interscience, New York, p179 (1972).

17. R W Berg, Spectrochim. Acta 34A, 655 (1978).
18. S Bhagvantam and T Ventarayudu, "Theory of Groups and Its Application to Physical Problems", Academic Press, New York (1969).
19. G Kabisch and G Mobius, Spectrochim. Acta 38A, 1189 (1982).
20. K A Tayler and L A Woodward, Proc. Roy. Soc. London 264A, 558 (1961).
21. G Kabisch and M Klose, J. Raman Spectrosc. 7, 311 (1978).
22. G Kabisch, J. Raman Spectrosc. 9, 279 (1980).
23. G L Bottger and A L Geddes, Spectrochim. Acta 21, 1701 (1965).
24. G Kabisch and G Mobius, Spectrochim. Acta 38A, 1195 (1982).
25. S S Chang, E F Westrum Jr., J. Chem. Phys. 36, 2420 (1962).
26. M Stammli, J. Inorg. Nucl. Chem. 29, 2203 (1967).
27. S Albert, H S Gutowsky and J A Ripmeester, J. Chem. Phys. 56, 3672 (1972).

Table 3.1 : Values of various parameters used to determine the positions of various atoms in crystal structure (see Fig. 3.1) and unit cell dimensions for tetramethyl ammonium halides [4].

	$(\text{CH}_3)_4\text{NCl}$	$(\text{CH}_3)_4\text{NBr}$	$(\text{CH}_3)_4\text{NI}$
p	0.361	0.375	0.394
s	0.339	0.339	0.347
r	0.156	0.153	0.164
C-H bond length	1.62 Å	1.63 Å	1.64 Å
N-C bond length	1.48 Å	1.49 Å	1.51 Å
Unit cell parameters	$\left\{ \begin{array}{l} \text{a} \\ \text{c} \end{array} \right.$	$\left\{ \begin{array}{l} 6.118 \text{ Å} \\ 4.366 \text{ Å} \end{array} \right.$	$\left\{ \begin{array}{l} 6.023 \text{ Å} \\ 4.265 \text{ Å} \end{array} \right.$

Table 3.2 : Classification of the modes of $(\text{CH}_3)_4\text{N}^+$ ion under the point group T_d
(same for both eclipsed and staggered configurations).

T_d	E	$8C_3$	$3C_2$	$6C_2$	$6C_4$	N_1	Activity*	
							Raman	IR
A_1	1	1	1	1	1	3	a	ia
A_2	1	1	1	-1	-1	1	ia	ia
E	2	-1	2	0	0	4	a	ia
F_1	3	0	-1	-1	1	4	ia	ia
F_2	3	0	-1	1	-1	7	a	a
ϕ	0	120	180	0	90			
ω_R	17	2	1	5	1			
$X_T(R)$	45	0	1	5	-1			
$X_\alpha(R)$	6	0	2	2	0			
$X_M(R)$	3	0	-1	1	-1			

ϕ - Angle of rotation.

ω_R - Number of atoms remains invariant under the operation.

$X_T(R)$ - Character for internal vibrational modes.

$$X_T(R) = (\omega_R - 2) (1 + 2 \cos \phi)$$

for proper rotations

$$= \omega_R (-1 + 2 \cos \phi)$$

for improper rotations

$X_\alpha(R)$ - Character for polarizability tensor.

$$X_\alpha(R) = 2 + 2 \cos \phi + 2 \cos(2\phi)$$

+ for proper rotations

- for improper rotations

$\chi_M(R)$ - Character for dipole moment
 $\chi_M(R) = +1 + 2 \cos \phi$ + for proper rotations
 - for improper rotations.

Number of fundamental of species i $N_i = \frac{1}{N_G} \sum n_e \chi_T(R) \chi_i(R)$

The modes of species i are Raman active $N_i^R = \frac{1}{N_G} \sum n_e \chi_a(R) \chi_i(R) \neq 0$

The modes of species i are IR active $N_i^{IR} = \frac{1}{N_G} \sum n_e \chi_M(R) \chi_i(R) \neq 0$

N_G - Number of elements of the group (= 24)

n_e - Number of elements in each class (e.g. for E, $n_E = 1$)

$\chi_i(R)$ - Character of species i in each class.

$$N_{A_1} = \frac{1}{24} [1x45x1 + 8x0x1 + 3x1x1 + 6x5x1 + 6x-1x1] = 3$$

$$N_{A_1}^R = \frac{1}{24} [1x6x1 + 8x0x1 + 3x2x1 + 6x2x1 + 6x0x1] = 1$$

$$N_{A_1}^{IR} = \frac{1}{24} [1x3x1 + 8x0x1 + 3x-1x1 + 6x1x1 + 6x-1x1] = 0$$

*a - active, ia - inactive.

For the analysis in detail, see refs. [4,5,18].

Table 3.3 : Nomenclature of the normal modes of $(\text{CH})_3\text{N}^+$ ion under the point group symmetry T_d [14].

Description	Symmetry class of point group T_d			
	A_1	A_2	E	F_2
CH_3 asy. str.	$\nu_5(\text{E})$	$\nu_{13}(\text{F}_2)$
CH_3 asy. str.	$\nu_1(\text{A}_1)$	$\nu_{14}(\text{F}_2)$
CH_3 asy. def.	$\nu_6(\text{E})$	$\nu_{15}(\text{F}_2)$
CH_3 sym. def.	$\nu_2(\text{A}_1)$	$\nu_{16}(\text{F}_2)$
CH_3 rock.	$\nu_7(\text{E})$	$\nu_{17}(\text{F}_2)$
C_4N asy. str.	$\nu_{18}(\text{F}_2)$
C_4N sym. str.	$\nu_3(\text{A}_1)$
C_4N asy. def.	$\nu_{19}(\text{F}_2)$
C_4N sym. def.	$\nu_8(\text{E})$
CH_3 torsion	$\nu_4(\text{A}_2)$
Activity*	R pol	ia	R dep	R dep, IR

*R - Raman, pol - polarized, dep - depolarized, IR - infrared, ia - inactive.

Table 3.4 : Correlation between the species of molecular point group and factor groups through the species of site symmetries for TMA ion in phases II and III.

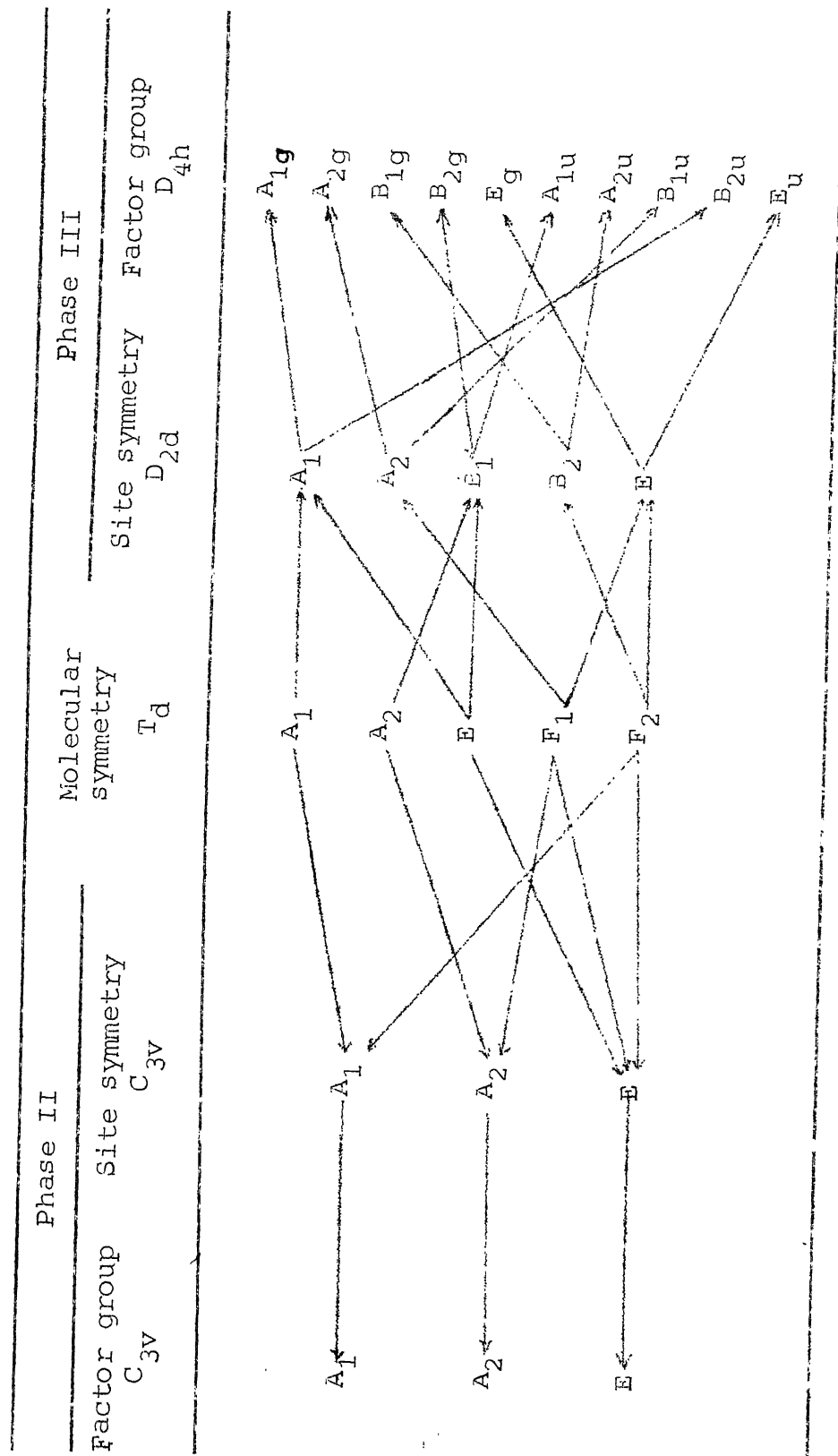


Table 3.5 : Band-positions (in cm^{-1}) of the observed bands in the Raman and IR spectra of normal (d_0) and perdeuterated (d_{12}) tetramethyl ammonium chloride in aqueous solutions and their assignments.

TMACl-d ₀				TMACl-d ₁₂ [*]			Assignments [†]	
Raman		IR	Raman	IR	Raman	IR		
Diluted solution (0.5 M)		Concentrated solution (6.0 M)						
1	2	3	4	5	6	7	8	9
370(18,7)dp		370(16,7)		316	$\nu_8(\text{E})$	
457(22,7)dp		457(16,9)		384	$\nu_{19}(\text{F}_2)$	
736(15,16)p		735(20,14)		$2\nu_8(\text{E})$	
755(9,38)p		754(9,54)		679	$\nu_1(\text{A}_1)$	
.....			920 m	$2\nu_{19}(\text{F}_2)$	
954(14,22)dp		953(13,31)		950vs	817	810	$\nu_{18}(\text{F}_2)$	
1178(16,4)dp		1174(16,5)		922	$\nu_7(\text{E})$	
1291(23,4)dp		1291(21,5)		1290m	1192	1187	$\nu_{17}(\text{F}_2)$	
1426(22,7)dp		1424(28,13)		1415s	$\nu_{16}(\text{F}_2)$	
.....		1144p	$\nu_2(\text{A}_1)$	
1454(14,23)dp		1456(16,44)		$\nu_6(\text{E})$	
.....			1485vs	1057dp	1062	$\nu_{15}(\text{F}_2)$	
.....			2364	
.....			2490	$\nu_{11}(\text{F}_1)+\nu_{16}(\text{F}_2)$	

1	2	3	4	5	6	7	8	9
.....			2520	$\nu_{11}(F_1) + \nu_{15}(F_2)$	
.....			2590	
.....			2618	
.....			2660	
.....			2770	$\nu_{15}(F_2) + \nu_{17}(F_2)$	
2826(15, 19)p	2852(26)	2823(17, 39)	2848(25)	2824	2107	$2\nu_{16}(F_2)$	
2880(22, 3)	2880(0)	2882(23, 8)	2880(-2)	$\nu_{16}(F_2) + \nu_6(E)$	
2905(20, 3)	2908(3)	2906(20, 6)	2912(6)	2119	$2\nu_6(E)$	
2933(13, 48)p	2939(6)	2925(17, 44)	2941(12)	2930	2139	2120	$\nu_6(E) + \nu_{15}(F_2)$	$\nu_s(A_1)$
2966(20, 66)p	2970(4)	2963(24, 123)	2970(7)	2960	2184	$2\nu_{15}(F_2)$	$\nu_s(A_1)$
2991(16, 100)p	2987(16, 100)	2083	$\nu_1(A_1)$	$\nu_s(A_1)$
3043(20, 50)dp	3033(25, 125)	3020	2283	$\nu_5(E)$ or $\nu_{15}(F_2)$	$\nu_s(A_1)$
.....			3980	$\nu_{13}(F_2) + \nu_{18}(F_2)$	$\nu_a(E)$

Columns 1, 3, 5, 6 and 7 indicate the observed wavenumbers (cm^{-1}). The figures in parentheses w each wavenumber in columns 1 and 3 denote the half-width and the relative integrated intensities respectively.

Columns 2 and 4 indicate the calculated values (cm^{-1}) of overtone/combination band in CH_3 stretching region as shown in column 8. The figures in parentheses in these columns represent the differences of the harmonic values (as expected from the assignments in column 8) and the actual observed wavenumbers shown in columns 1 and 3.

Columns 8 and 9 represent the assignments based on Fermi-resonance and anharmonicity and dynamical distortion of the C_4N - skeleton , respectively.

† The assignment of the bands not given in this column is identical to that of column 8.
 * Raman and IR data for TMACl-d₁₂ are taken from ref. [17].

V - very, s - strong, m - medium and w - weak.

Selection rules for overtones and combinations are

$$F_2xF_2 = A_1+E+F_1+F_2, \quad ExE = A_1+A_2+E, \quad ExF_2 = F_1+F_2$$

Table 3.6 : Correlation of the CH_3 stretching vibrations having point group C_{3v} with corresponding vibrations in TMA symmetries T_d or C_{3v} .

CH_3 stretching vibrations		
Isolated CH_3	CH_3 in TMA units	
C_{3v}	T_d	C_{3v}
Totally symmetric CH_3 stretching vibration, $\text{A}_1(\text{R})$	$\text{A}_1(\text{R})$ $\text{F}_2(\text{R}, \text{IR})$	$\text{A}_1(\text{R(p)}, \text{IR})$ $\text{A}_1(\text{R(p)}, \text{IR})$ $\text{E}(\text{R(dp)}, \text{IR})$
Asymmetric CH_3 stretching vibration, $\text{E}(\text{R}, \text{IR})$	$\text{E}(\text{R})$ F_1 $\text{F}_2(\text{R}, \text{IR})$	$\text{E}(\text{R(dp)}, \text{IR})$ $\text{E}(\text{R(dp)}, \text{IR})$ A_2 $\text{E}(\text{R(dp)}, \text{IR})$ $\text{A}_1(\text{R(p)}, \text{IR})$

The notations regarding species are discussed in the text. The activities in Raman (R) and infrared (IR) are given for ready reference.

p - polarized, dp - depolarized.

Table 3.7: Band-positions (cm^{-1}) with half-widths and relative integrated intensities in different phases of material (d_0) and perdeuterated (d_2) tetramethyl ammonium chloride (kept under continuous vacuum).

TMC L-d ₀													Assignment
IR													
RAPIN													
Phase I	Phase II		Phase III		Phase IV		Phase II		Phase III		IR		
540 K	393 K	300 K	300 K	90 K	300 K	448 K	300 K	300 K	300 K	90 K	300 K	300 K	
1	2	3	4	5	6	7	8	9	10	11	12	13	
....	368(12,3)	370(8,2)	376(5,1)	376(5,1)	355m	375m	316(15,6)	314(16,5)	319(9,4)	
....	388(6,4)	389(4,4)	331(8,9)	332(6,3)	
....	454(8,11)	456(8,10)	450m	456m	386(9,34)	388(6,26)	387(6,10)	382(5,10)	
450	460(7,26)	455(6,22)	459(6,8)	464(5,6)	468m	478m	392(6,12)	388(5,10)	
....	733(16,16)	734(14,9)	730(20,2)	736(16,2)	
752	764(6,39)	764(5,39)	760(10,39)	758(10,29)	677(6,86)	677(4,5,78)	686(5,85)	683(3,35)	
....	918(20,6)	917(20,5)	930(18,2)	887(17,2)	920m	920m	
....	928m	
....	947(10,26)	944(6,14)	940(3,1)	806(6,21)	
946	950(5,12)	950(7,20)	948(6,28)	946(5,5,30)	948m	948m	809(9,55)	810(6,16)	808(4,24)	805(4,26)	
....	958(2,1)	958m	958m	
....	1068(8,2)	1063(6,2)	1068m	1064m	816(7,11)	814(5,16)	813(7,13)	812(4,10)	
....	1188(7,3)	1184(4,6)	1180(5,2)	1183(4,3)	920(7,17)	921(4,13)	922(7,18)	926(6,11)	
....	1192(10,1)	1197(6,1)	928(10,9)	935(6,9)	
....	1202(11,3)	1206(5,9)	1291(5,10)	1182(20,29)	1186(14,26)	1194(14,26)	1194(20,75)	1188	
....	1293(16,9)	1296(5,9)	1296m	1300m	
....	1398(8,5)	1392(4,3)	1386	1390	
....	1482(6,8)	1397(4,4)	1403m	1400m	
....	1483(14,26)	1486(7,15)	1487(5,3)	
....	1138(13,11)	1132(16,15)	1131(11,16)	1132(7,14)	

1	2	3	4	5	6	7	8	9	10	11	12	13
....	1454 (6,10)	1452 (5,9)	1440vw	1443vw	1052 (6,1)	$\nu_6(E)$
....	1474 (3,3)	1058 (8,18)	1060 (7,16)
1466 (6,41)	1468 (4,32)	1477 (6,14)	1479 (4,14)	1063 (6,1)	1066 (4,12)	1066 (4,28)	1070 (3,17)	1066	$\nu_{15}(F_2)$
....	1483 (5,10)	1486 (5,15)	1485vw	1484vw	1076 (6,22)	1080 (4,16)
....	2330w	2340w
....	2466vw	2458vw	$\nu_{11}(F_1)+\nu_{16}(F_2)$
....	2570vw	2565vw	$\nu_{11}(F_1)+\nu_{15}(F_2)$
....	2770 (6,2)	2742vw	2740vw
2798 (25,28)	2792 (20,21)	2790 (18,13)	2792 (14,4)	2792 (14,4)	2760w	2762w	$2\nu_{16}(F_2)$
....	2800 (8,3)
2830 (26,13)	2858 (24,11)	2840 (20,4)	2834 (18,2)	2830w	2833w	$\nu_6(E)+\nu_{16}(F_2)$
2867 (27,27)	2874 (14,23)	2877 (20,27)	2872 (14,16)	$\nu_{15}(F_2)+\nu_{16}(F_2)$
2900 (28,32)	2898 (22,29)	2900 (20,10)	2900 (30,19)	$2\nu_6(E)$
....	2098 (17,33)
....	2922 (14,15)	2918 (12,22)	2920 (14,9)	2920w	2920w	2105 (36,81)	2105 (30,69)	2109 (20,34)	2098 (14,33)	$2\nu_{15}(F_2)$
....	2148 (20,16)	2128 (30,46)
2946 (18,100)	2946 (16,100)	2951 (24,100)	2950 (20,100)	2950 (20,100)	2075 (10,100)	2074 (7,100)	2077 (6,5,100)	2078 (4,100)	$\nu_1(A_1)$
2966 (31,74)	2960 (26,25)	2965 (28,20)	2966 (26,16)	2966 (26,16)	2964w	2965w
....	2155 (16,52)	$\nu_1(A_1)+\text{Lattice}$
....	2162 (19,109)	2167 (10,81)	2167 (22,131)	2167 (19,70)
....	3014 (6,28)	3019 (10,65)	3012 (6,21)	3012 (6,21)	2253 (12,58)	2255 (15,63)	2258 (18,163)	$\nu_5(E)$
....	3022 (5,80)	3022 (5,80)	3017s	$\nu_{13}(F_2)$
3017 (12,156)	3028 (7,66)	3027 (7,29)	3028 (4,16)	3028 (4,16)	3020s	3023s	2264 (12,5,168)	2267 (10,181)	2273 (13,164)	2274 (13,208)	2272
....	3033 (5,21)	3033 (5,21)
....	3080vw	3080w
....	3130w	3120w
....	3400w	3395w	$\nu_{13}(F_1)+\nu_{18}(E)$
....	3480vw	3480w	$\nu_{13}(F_1)+\nu_{19}(F_2)$
....	3970vw	3965w	$\nu_{13}(F_1)+\nu_{18}(F_2)$

The data on FeCl_4 are taken from ref. [17]. The figures in the parentheses with each wavenumber denote the half-widths (cm^{-1}) and relative integrated intensities, respectively.

v = very, s = strong, w = medium, v = weak, sh = shoulder.

Table 3.8 : The numbers and types of vibrations related to CH₃ stretching (or deformation) modes in phases II and III and TMA ions.

Isolated CH ₃ (C _{3v}) CH vibrations (stretch or deformation)	TMA(T _d)		Phase II(Z=1) C _{3v}		Phase III(Z = 2) D _{4h}
	Species	Notations for CH modes		C _{3v}	D _{4h}
		Str.	Def.		
A ₁ Sym.	A ₁ [*] F ₂ [*]	ν ₁ ν ₁₄	ν ₂ ν ₁₆	A ₁ [*] A ₁ [*] +E [*]	A _{1g} [*] +B _{2u} B _{1g} [*] +E _g [*] +A _{2u} +E _u
E	E [*]	ν ₅	ν ₆	E [*]	A _{1g} [*] +B _{2g} [*] +A _{1u} +B _{2u}
E Asym.	F ₁ F ₂ [*]	ν ₉ ν ₁₈	ν ₁₀ ν ₁₅	A ₂ +E [*] A ₁ +E [*]	A _{2g} +E _g [*] +B _{1u} +E _u B _{1g} [*] +E _g [*] +A _{2u} +E _u
Total number of bands expected				3A ₁ [*] +A ₂ +4E [*]	2A _{1g} [*] +2A _{2g} +2B _{1g} [*] +B _{2g} [*] + 3E _g [*] +A _{1u} +2A _{2u} +B _{1u} + 2B _{2u} +3E _u

*Denotes a Raman active species.

Table 3.9 : The factor group splittings of the modes of species F_1 and F_2 under the point group symmetry T_d for the TMA ion in phase III [$D_{4h}^7 (Z = 2)$] through the site D_{2d} and in phase II [$C_{3v}^5 (Z = 1)$] through the site C_{3v} .

Species	Phase III ($Z = 2$)	Phase II ($Z = 1$)
	D_{4h}	C_{3v}
F_1	$A_{2g} + E_g^* + B_{1u} + E_u$	$A_2 + E^*$
F_2	$B_{1g}^* + E_g^* + A_{2u} + E_u$	$A_1^* + E^*$

*Denotes a Raman active species.

Table 3.10 : The known phases and transition temperatures for normal (d_0) tetramethyl ammonium chloride.

Phase	Transition temperature	Type and nature	Space Group	Structure
I			$O_h^5 (Z = 4)$	fcc
	536 K	Reversible		
II			$C_{3v}^5 (Z = 1)$	Rhombohedral
	413 K*	Irreversible		
III			$D_{4h}^7 (Z = 2)$	Tetragonal
	1849 K	λ -transition		
IV			?	Tetragonal
	75.8 K	First order		
V			?	?

*Presently observed at 368 ± 2 K when the sample is kept in the cell under continuous evacuation.

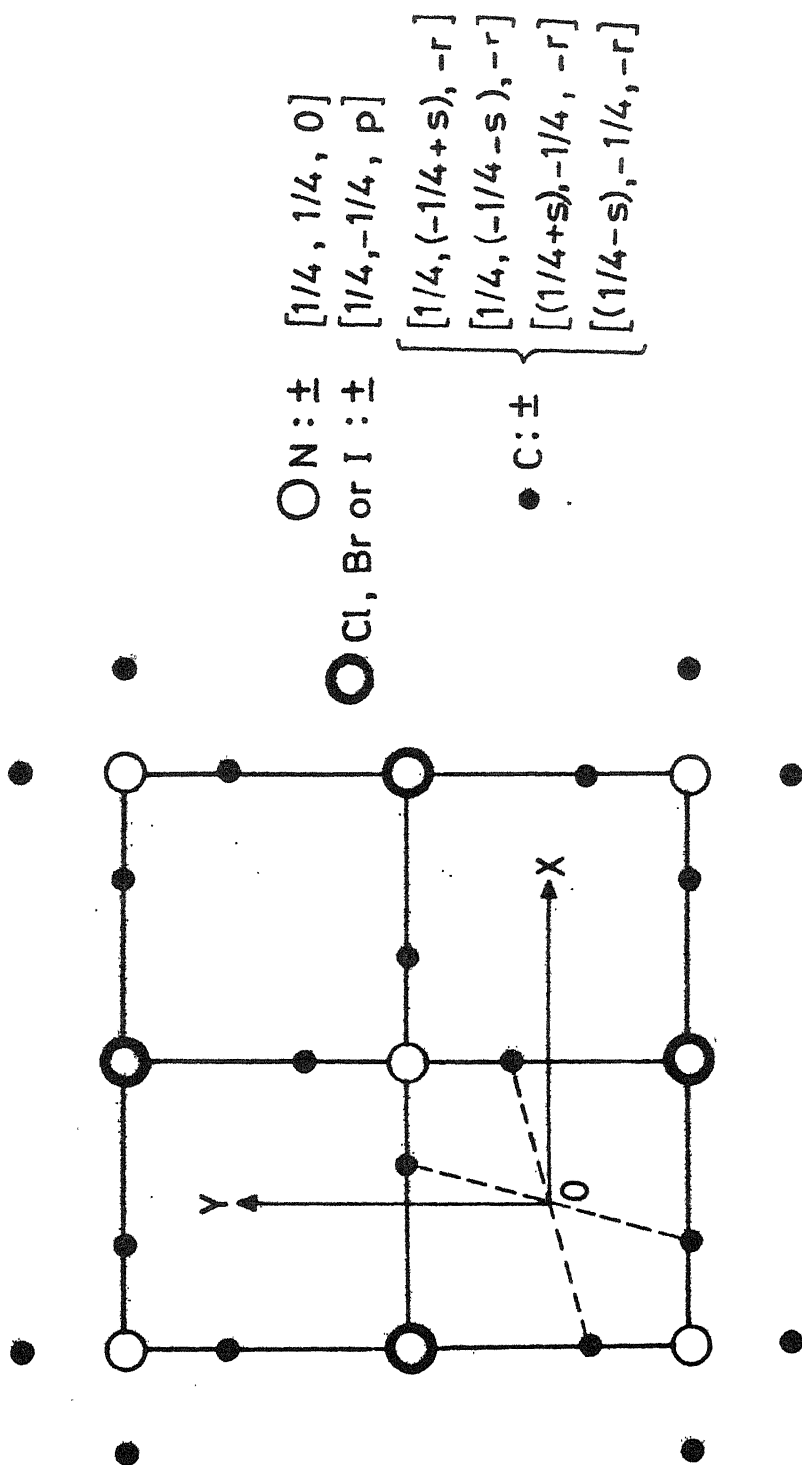


Fig.3.1 Crystal structure of tetramethyl ammonium halides: projection in XY-plane (after Vegard and Sollesnes [4]). Various parameters used to determine the positions of atoms are given in Table 3.1.

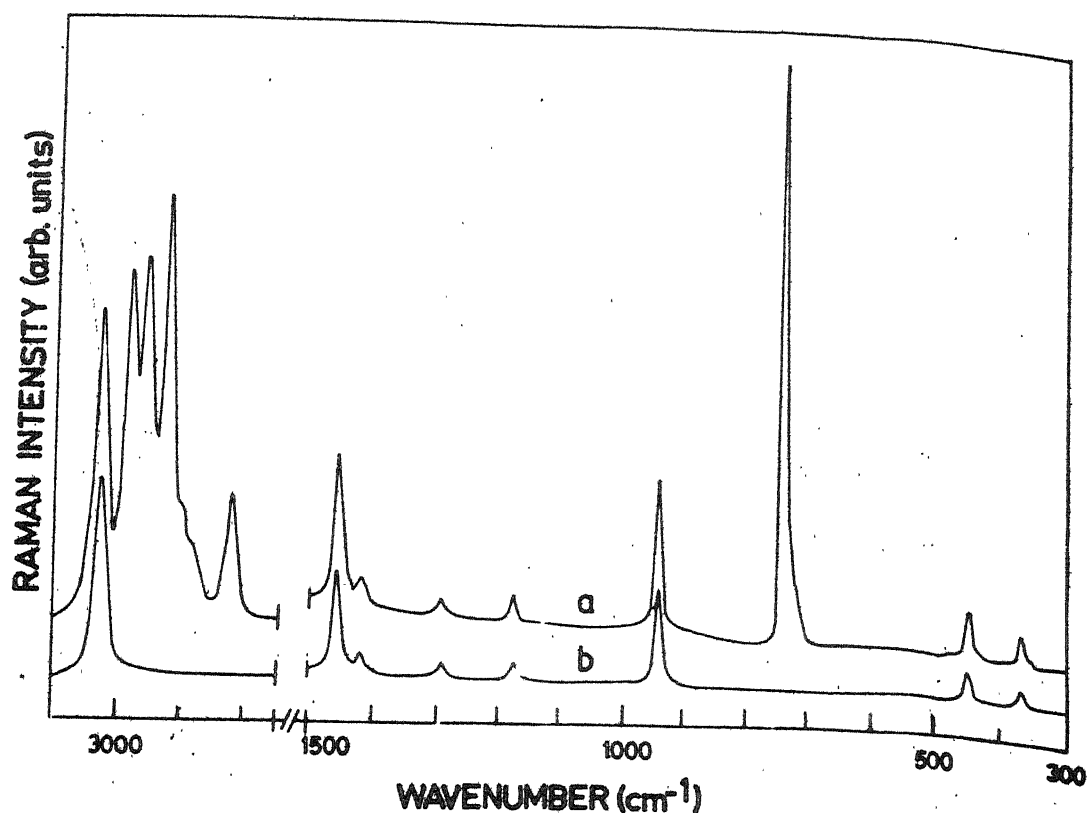


Fig. 3-2 Raman spectra of TMACl-d₀ in aqueous solution of 6.0 M:
(a) Parallel and (b) Perpendicular polarizations.

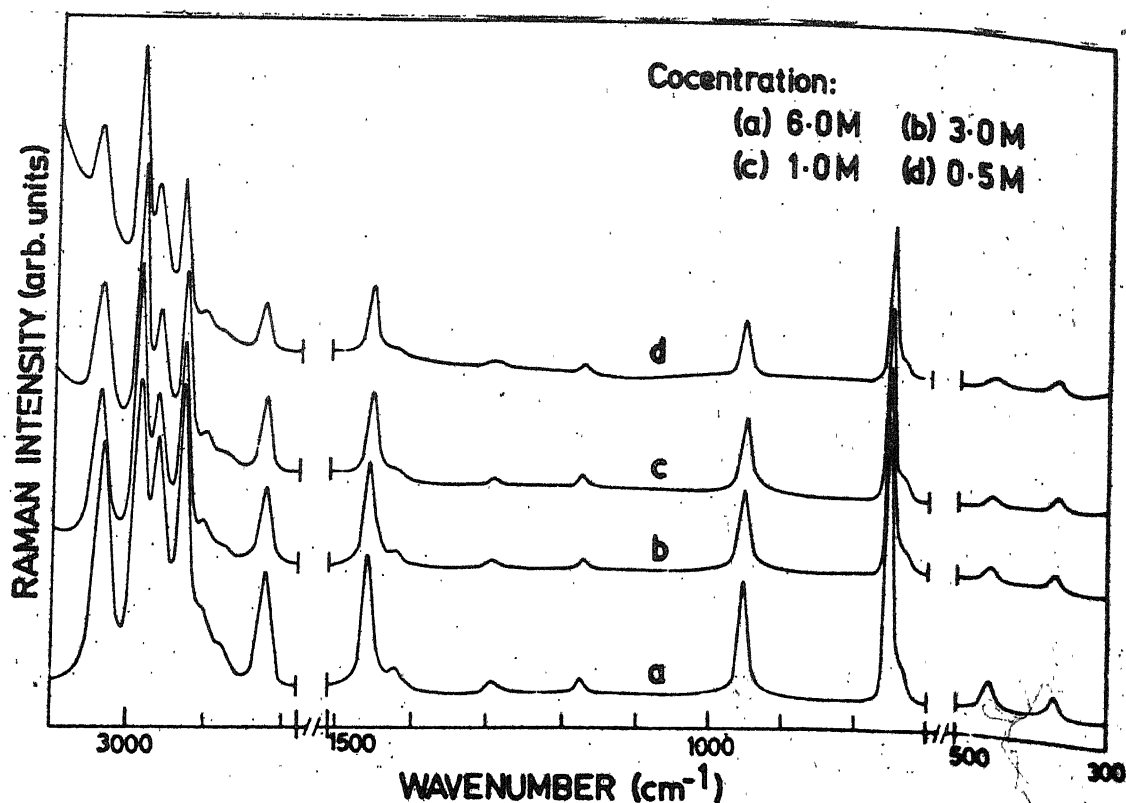


Fig. 3-3 Raman spectra of TMACl-d₀ in aqueous solutions with varying concentrations.

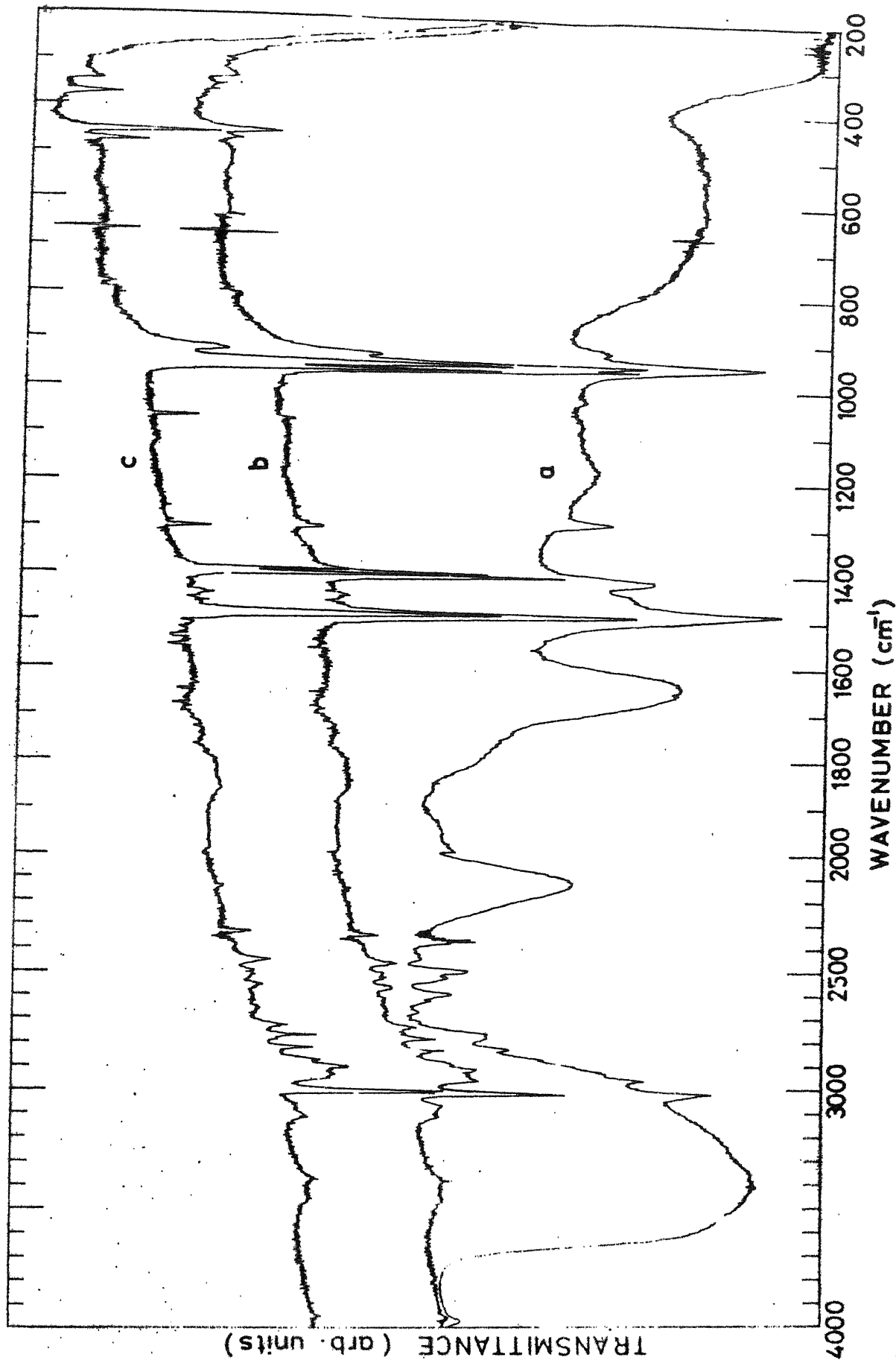


Fig. 3-4 Infrared spectra of TMACl-d_0 , (a) in aqueous solution kept between AgCl windows, (b) in KBr pellet at 300 K and (c) in KBr pellet at 90 K.

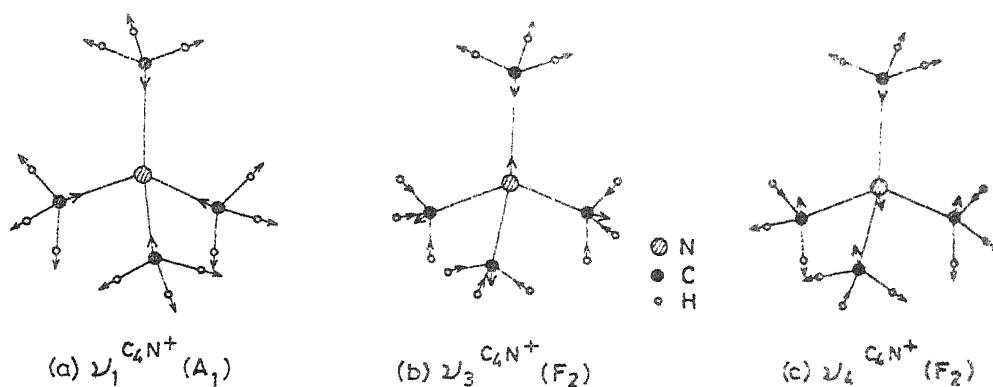


Fig. 3-5 Diagrammatic representation of three totally symmetric CH-stretching motions of CH_3 in tetramethyl ammonium ion. (a) The T_d symmetry is retained, (b) and (c) the symmetry will be dynamically distorted to C_{3v} (cf. column 3 in table 3-6)

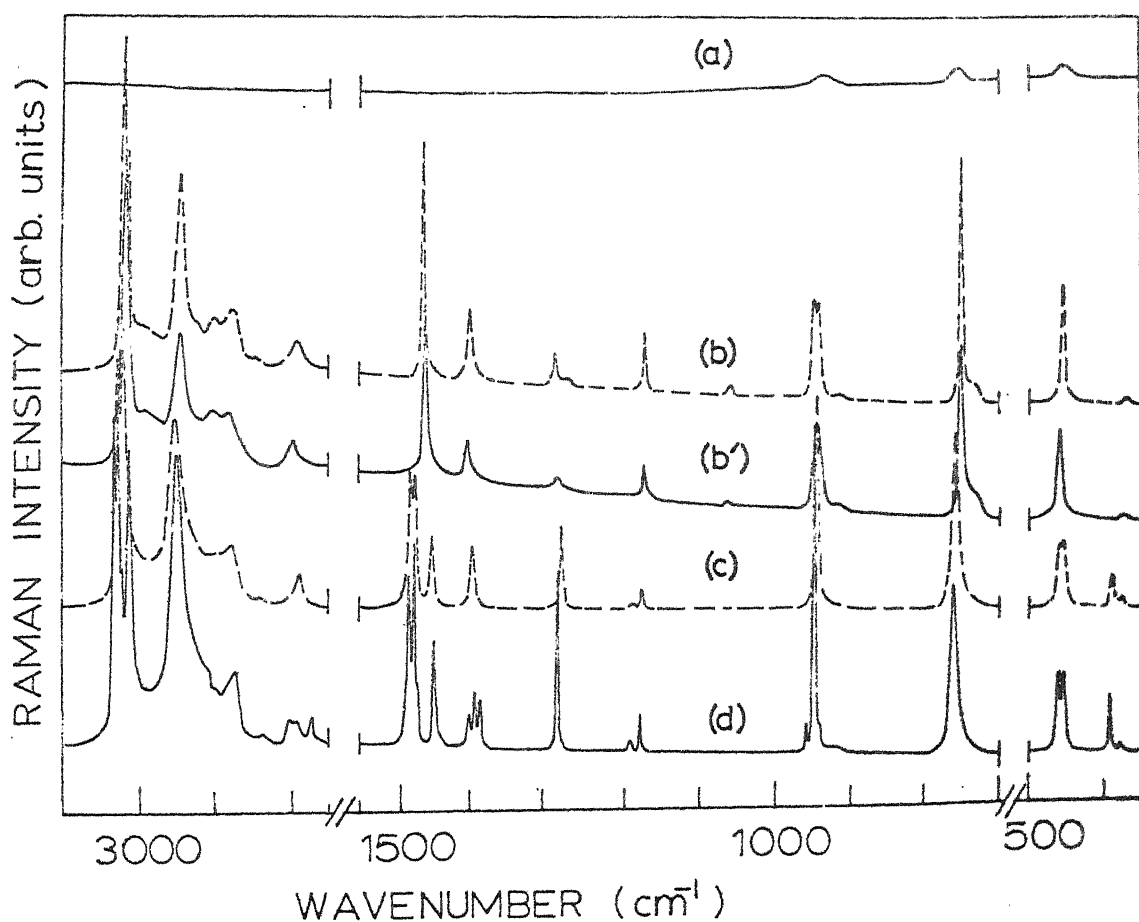


Fig. 3-6 Raman spectra of TMA Cl- d_0 in four phases: (a) in phase I at 540 K (b) in phase II at 393 K (b') in phase II at 300 K-after cooling under vacuum (c) in phase III at 300 K and (d) in phase IV at 90 K.

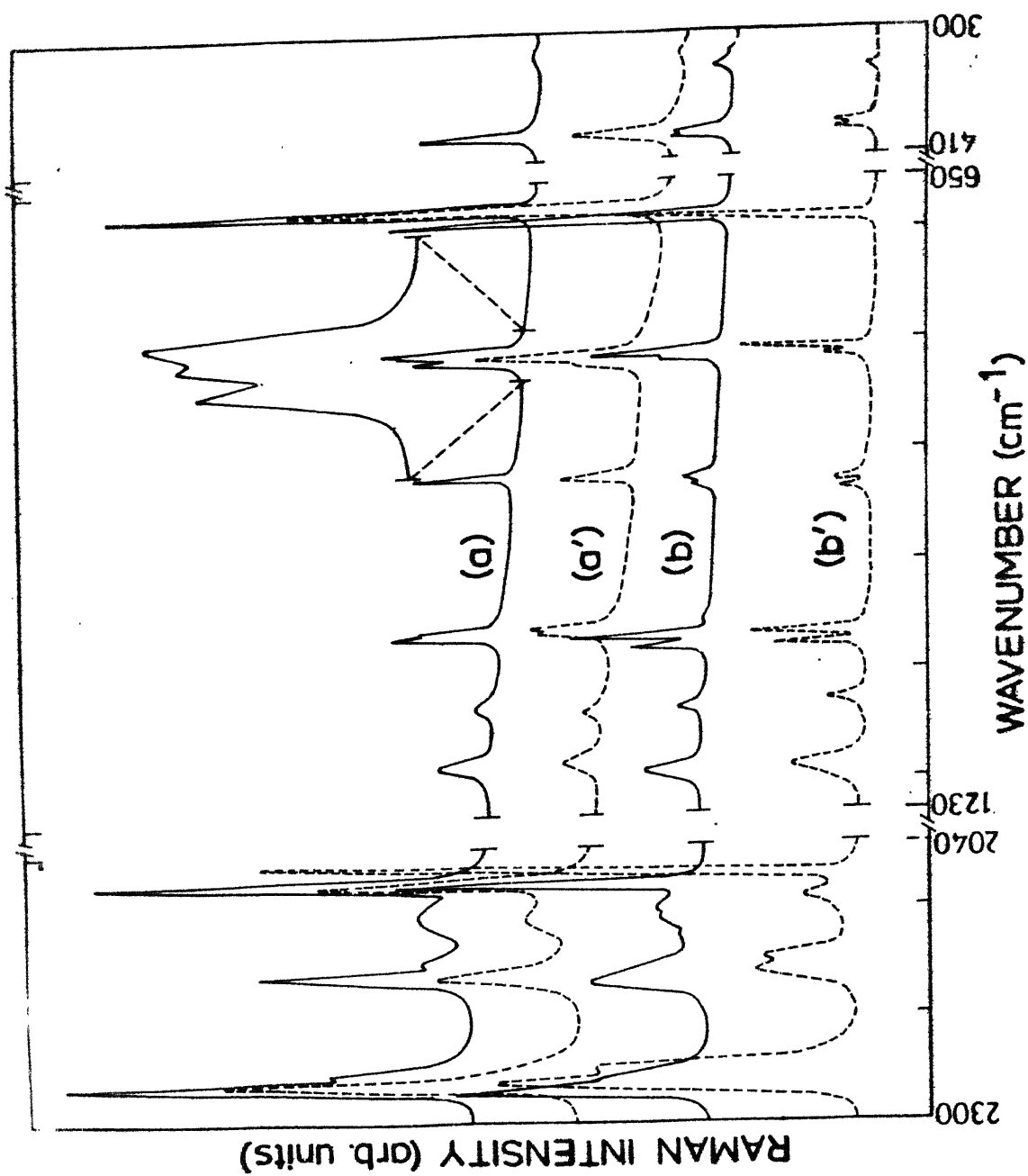
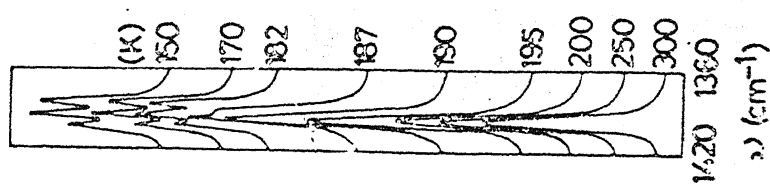
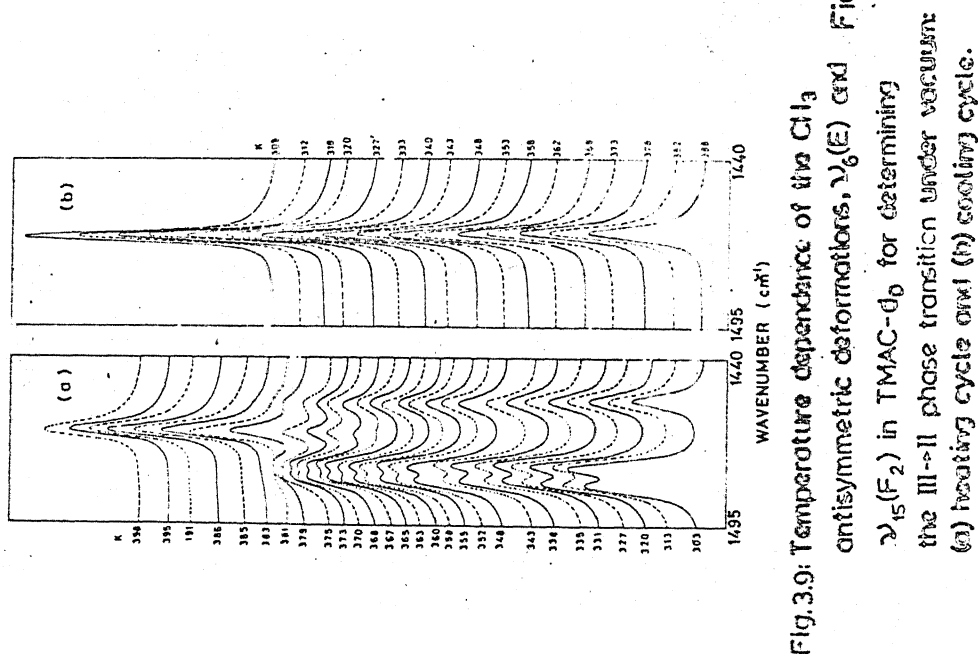
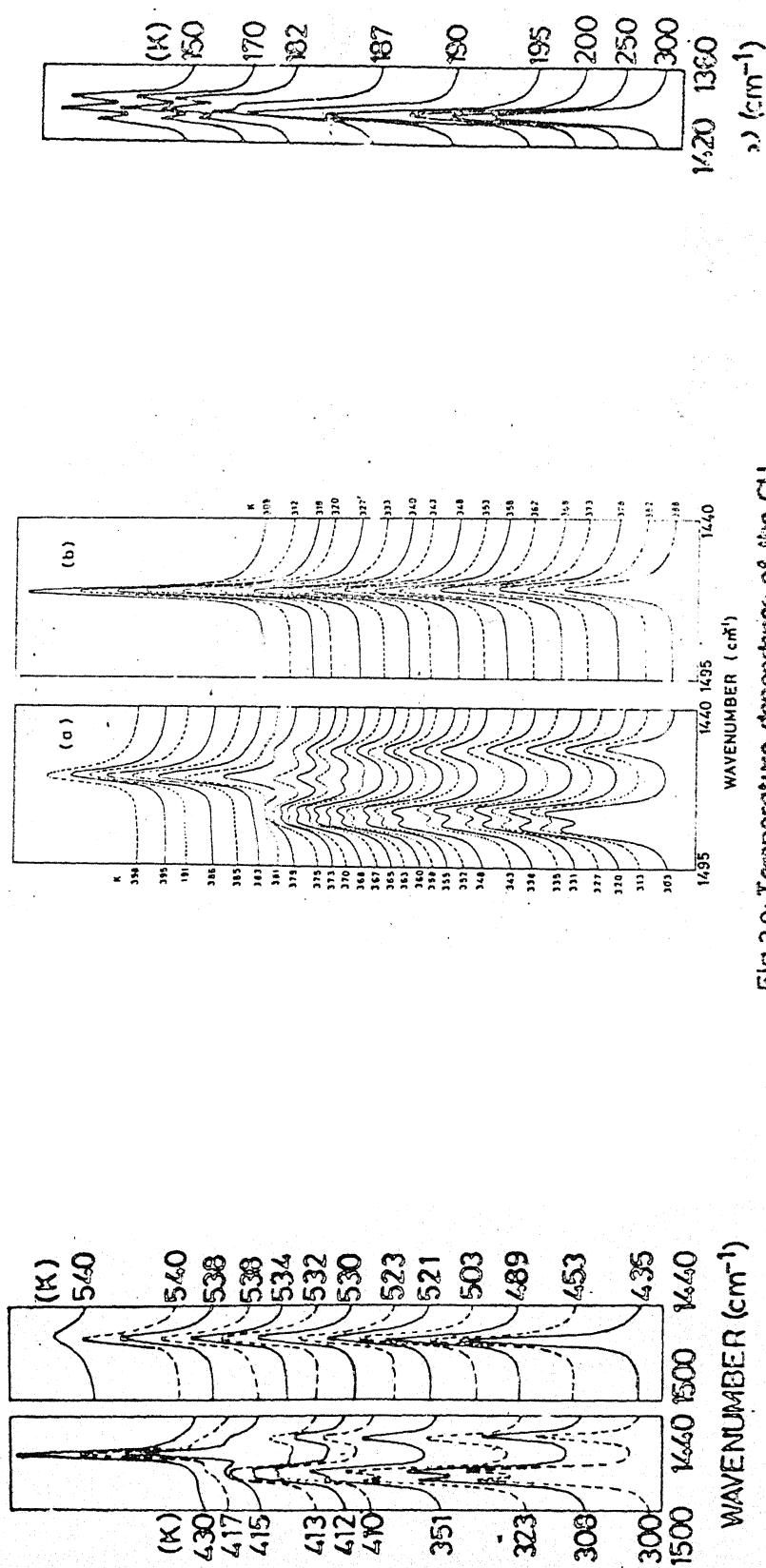


Fig. 3.7 Raman spectra of TMACl-d_{12} : (a) Phase II, at 433 K, (a') Phase II at 300 K - on cooling under vacuum, (b) Phase III at 300 K and (b') Phase III at 90 K.



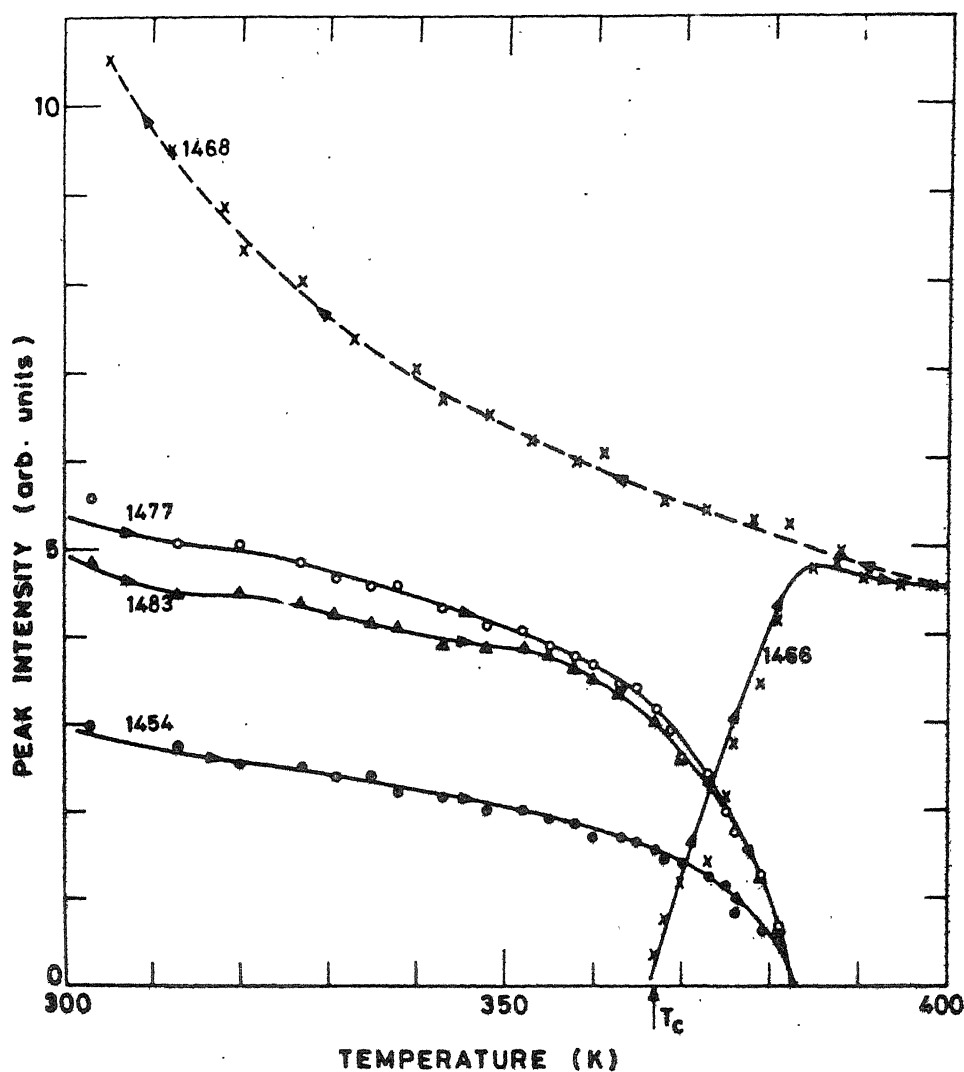


Fig. 3.11 The variation of peak intensities of $\nu_6(E)$ at 1454 cm^{-1} and $\nu_{15}(F_2)$ at 1477 and 1483 cm^{-1} in TMAC- d_0 with temperature. The phase transition $\text{III} \rightarrow \text{II}$ is characterized by the appearance of a new band at 1466 cm^{-1} . On cooling the sample from 400 K the band gains intensity.

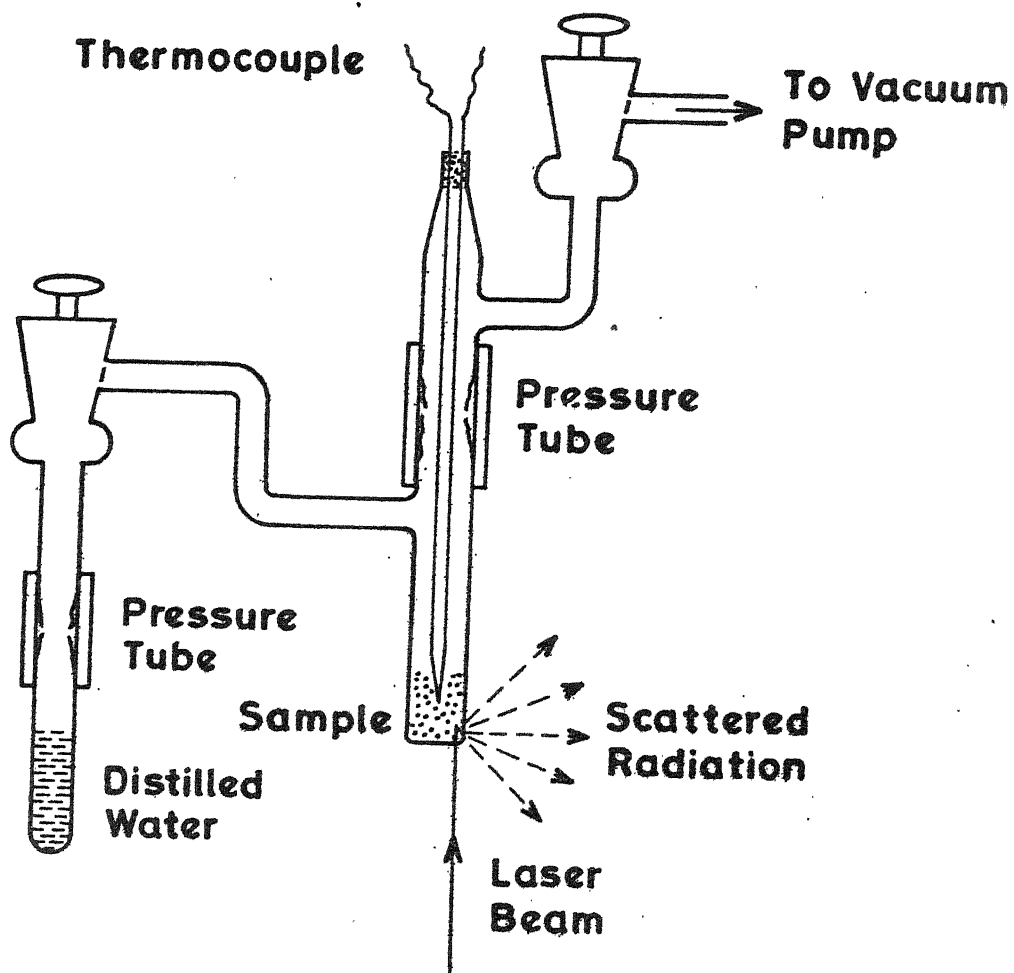


Fig.3.12 Sample Holder (for High Temperature Cell) having an Arrangement to Flow Water Vapour Over the Sample Under Vacuum.

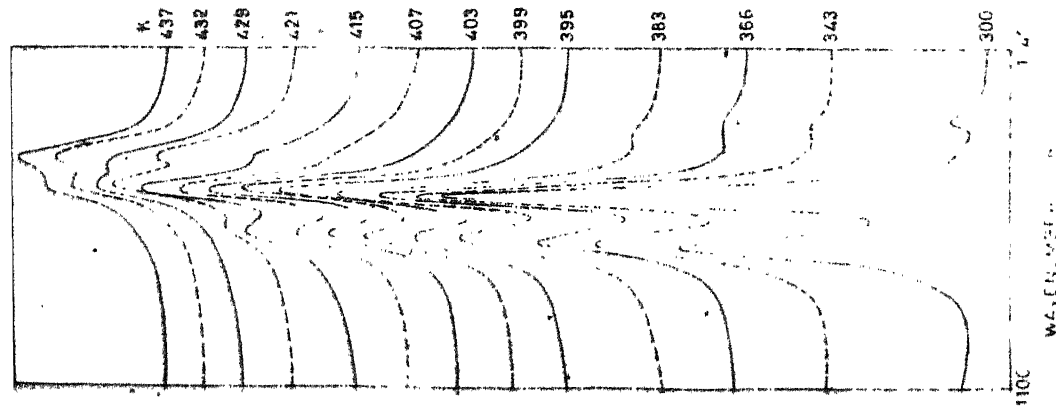


Fig.3.13 Temperature dependence of the CD_3 antisymmetric deformations, $\nu_g(\text{E})$ and $\nu_{15}(\text{F}_2)$ in TMAC- d_{12} for determining the phase transition III \rightarrow II (under vacuum).

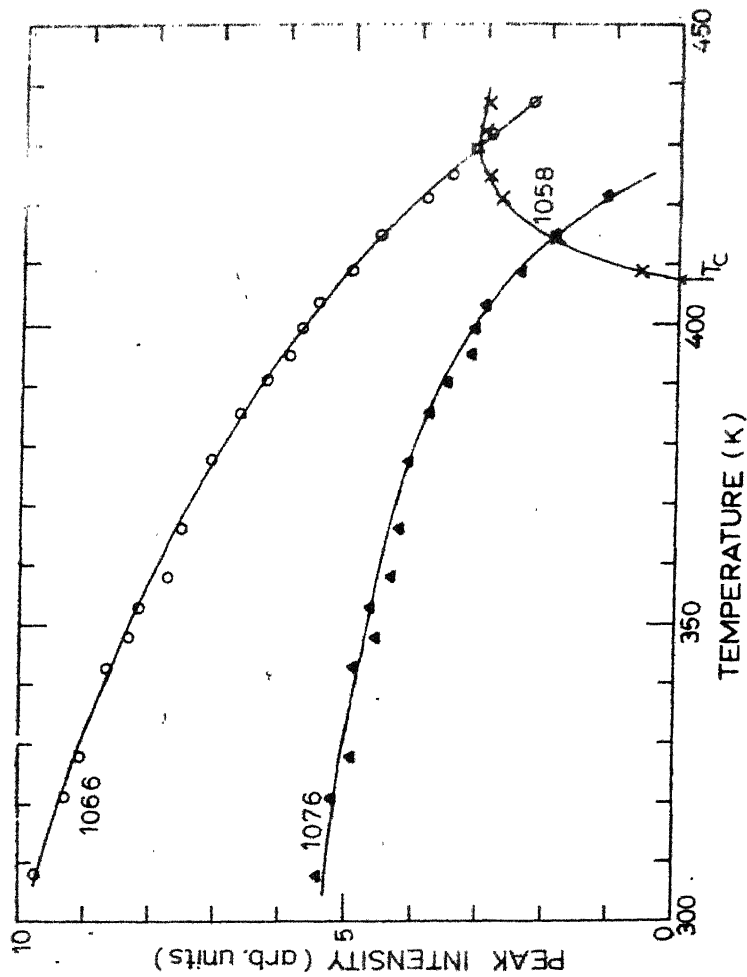


Fig.3.14 The variation of peak intensities of $\nu_g(\text{F}_2)$ at 1066 and 1076 cm^{-1} in TMAC- d_{12} with temperature. The phase transition III \rightarrow II is characterized by the appearance of a new band at 1058 cm^{-1} .

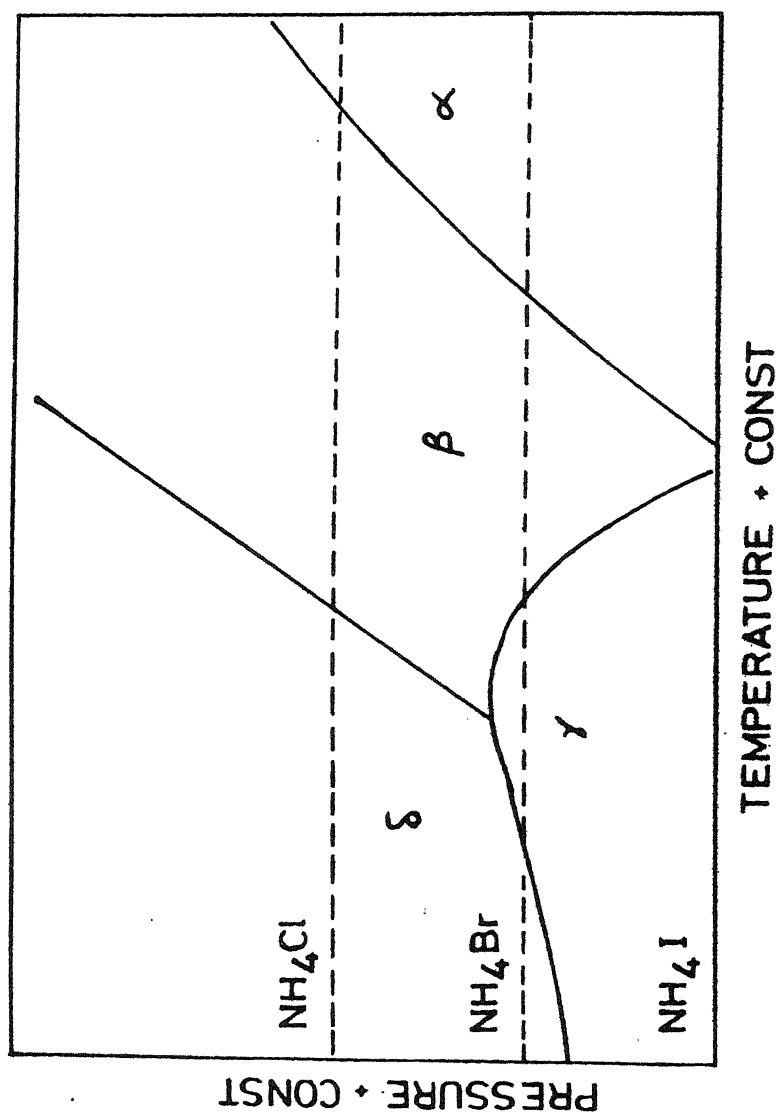


Fig. 3.15 Schematic generalized phase diagram of ammonium halides [7]

4. VIBRATIONAL STUDIES OF TETRAMETHYL AMMONIUM BROMIDE AND IODIDE

In this chapter we present the temperature dependent Raman studies of normal (d_0) tetramethyl ammonium bromide and iodide. These studies provide information about the specific molecular motions involved in the phase transitions [1]. For example, the C-N vibrational bands would be affected mainly by the reorientational motions of the whole TMA ion, the bands of CH_3 groups would change only if the motions of the methyl groups are affected, and a splitting of the totally symmetric stretching mode of C_4N skeleton [$\nu_3(A_1')$] will indicate orientational disorder of the TMA ion. Raman data for selectively deuterated tetramethyl ammonium iodide (TMAI- d_n ; $n = 0, 1, 3, 9, 10, 11$ and 12) at room temperature are also presented in this chapter.

4.1 CRYSTAL STRUCTURE AND GROUP THEORETICAL ANALYSIS

TMA halides at room temperature belong to the tetragonal system with space group D_{4h}^7 ($Z = 2$) [2,3]. It is useful to recall Ohe's proposal [4] of four types of structures for $(TMA)_2XCl_6$ ($X = U$ or Sn) which belong to the cubic system. The four structure arise from the 2×2 alternatives provided by

- (i) staggered and eclipsed configurations of the methyl groups of a TMA ion, and
- (ii) parallel and perpendicular orientations of TMA ion.

For a cubic system, viz. $(\text{TMA})_2\text{XCl}_6$, the two orientations are defined as N-C bonds pointing towards the corners of the cube occupied by the X atoms (parallel orientation) and the bonds pointing towards the vacant corners (perpendicular orientation) [4]. The parallel and perpendicular orientations for TMA halides are shown in Fig. 4.1. Since TMA halides belong to the tetragonal system, the equilibrium orientations for these will be somewhat different from the parallel and perpendicular orientations of a cubic system. Yet the terms may be used to give a close enough description of mutual orientation in the four possible structures.

The forty-five internal modes of TMA ion under point group T_d are distributed as $3A_1 + A_2 + 4E + 4F_1 + 7F_2$ and are represented as $\nu_1, \nu_2, \dots, \nu_{19}$ [see chap. 3]. The modes may further split due to correlation field under the known space group D_{4h}^7 ($Z = 2$) through site symmetry D_{2d} (in case both the TMA ions occupy the same site). Then

$$\begin{aligned}
 \text{TMA} \\
 \text{vib} &= 7A_{1g}(\text{R}) + 4A_{2g} + 7B_{1g}(\text{R}) + 5B_{2g}(\text{R}) + 11E_g(\text{R}) \\
 &+ 5A_{1u} + 7A_{2u}(\text{IR}) + 4B_{1u} + 7B_{2u} + 11E_u(\text{IR}) \quad (4.1)
 \end{aligned}$$

It is seen that each of the nineteen modes of isolated TMA produces at least one Raman active (g) species under the

space group D_{4h}^7 . Hence for a polycrystalline sample all these modes are expected to appear in the Raman spectrum.

4.2 CHARACTERISTIC RAMAN SPECTRA OF NORMAL (d_o) TMABr AND TMAI AT 300 AND 100 K

The relevant portions of the observed Raman spectra of normal (d_o) TMABr and TMAI in the region $200-4000\text{ cm}^{-1}$ are shown in Figs. 4.2 and 4.3, respectively. The peak positions of the observed bands and their assignments are given in Table 4.1. Positionwise, the observed spectra fit well into the assignment proposed earlier for TMACl (which are also given for comparison in Table 4.1). Hence the assignment aspect does not merit further discussion.

4.3 DYNAMIC DISORDER OF TMA ION IN NORMAL (d_o) TMA HALIDES

The temperature dependent Raman spectra in the C_{4N} symmetric stretching region ($735\text{ to }765\text{ cm}^{-1}$) of normal (d_o) TMAI are shown in Fig. 4.4. The room temperature spectrum shows two bands in this region at $748\text{ and }753\text{ cm}^{-1}$. On lowering the temperature the former band gains intensity and shifts to 746 cm^{-1} whereas the later does not show an appreciable change in intensity but shifts to 758 cm^{-1} . In case of TMACl and TMABr, too, two bands appear at $730\text{ and }760\text{ cm}^{-1}$ and at $724\text{ and }757\text{ cm}^{-1}$, respectively. Out of these the lower frequency member is very weak. The main band (at 760 cm^{-1} in TMACl and 757 cm^{-1} in TMABr) has been assigned

to the $\nu_3(A_1)$ mode while the weak one is assigned to the overtone of $\nu_8(E)$. In TMAI, the $\nu_8(E)$ mode has negligible intensity and its position could not be sorted out from the spectra; the overtone would be even weaker. The observed 748 cm^{-1} band has good intensity, particularly so at low temperatures. Therefore the 748 cm^{-1} band in TMAI cannot be an overtone of the $\nu_8(E)$ mode. If one considers the band at 753 cm^{-1} as an overtone of $\nu_8(E)$ assuming that its intensity is due to Fermi resonance with 748 cm^{-1} band, then the assignment becomes untenable due to the following reasons :

- (i) in the cases of TMACl and TMABr the overtone of $\nu_8(E)$ falls at 730 and 724 cm^{-1} , respectively,
- (ii) the increase in intensity of 748 cm^{-1} band on going to lower temperatures would then suggest a decrease in Fermi resonance interaction, while the observed opposite shifts of the two bands (to 746 and 758 cm^{-1} at 100 K) would suggest an enhancement in Fermi resonance interaction.

The above discussion leads to the idea that neither of the two bands in the stretching region of TMAI spectra can be an overtone of $\nu_8(E)$. The only other alternative is that these are the two components of $\nu_3(A_1)$. On the other hand, factor group analysis suggests that although a mode of species A_1 under the point group symmetry T_d may split into two components under the space group D_{4h}^7 through the site

symmetry D_{2d} , only one of them would be Raman active. In a vibrational spectrum some of the bands might be missing because of either lack of intensity or accidental degeneracy, but the appearance of extra bands contrary to the spectral model is unacceptable. The two observed Raman components of $\nu_3(A_1)$ in TMAI could therefore be explained only in terms of a model with two different sites for TMA ions in the lattice which could arise on account of parallel and perpendicular orientations of TMA ions (cf. Fig. 4.1). The model is discussed in section 4.3.1.

The CH_3 asymmetric deformation mode $\nu_{15}(F_2)$ (cf. Table 4.1) also needs attention. It shows only two components at room temperature in TMACl and TMABr, whereas it has three components in TMAI. The splitting of $\nu_{15}(F_2)$ into three components in TMAI is again contrary to the group theoretical prediction. On lowering the temperature, the $\nu_{15}(F_2)$ mode in TMABr also splits into three components at 182 K (Fig. 4.5). However, the temperature behaviour of the three components in TMABr and TMAI are not the same. It is thus obvious that the structure of TMAI at room temperature is different from that of TMABr and TMACl, although X-ray studies have not been able to record this difference and have shown that all the three salts are isostructural [2,3].

In TMACl the modes belonging to the CH_3 groups and C_4N skeleton are found to be thermosensitive [Chap. 3]. Since Tench [5] has shown from X-ray studies that phase IV

of TMACl (184.9 K to 75.8 K) has nearly the same structure (tetragonal) and dimensions as those in the room temperature phase III, the transition III \rightarrow IV is attributed to a change in reorientational freedom of the TMA ion [6]. Nuclear magnetic relaxation studies [6-10] have shown that CH_3 reorientation and tumbling of TMA ion occurs in TMA halides. Chang et al. [11] have suggested that the phase transition III \rightarrow IV in TMACl may involve motion of TMA ion in the free space available inside the lattice. If this holds then tumbling motion of TMA ion should depend directly on the free space available in the crystal lattice. The data of Table 4.2 clearly show that the free space available for TMA ion in the unit cell is larger in TMAI than that in TMABr and TMACl. Thus the TMA ion is relatively more free to tumble in TMAI. This explains why the C_4N skeleton bands show considerable thermosensitivity in TMAI.

4.3.1 Pseudo-double Well Potential Model

Let us assume a pseudo-double well potential [12,13] with different levels of their potential minima. The energy difference of the minima can be derived from the slope m of $\ln(I_1/I_2)$ versus $1000/T$ curve (Fig. 4.6) using Boltzmann statistics. Here I_1/I_2 is the intensity ratio of the two component bands and equals the occupation ratio of the two sites. This leads to

$$\frac{I_1}{I_2} = \frac{n_1}{n_2} = C \exp \left(- \frac{\Delta E}{RT} \right) \quad (4.2)$$

where C is a constant, ΔE is energy difference in molar units and R is the gas constant. The slope m of the dotted line in Fig. 4.6 gives

$$\Delta E = - 1000 \text{ mR} \quad (4.3)$$

The observed slope in the TMAI case leads to $\Delta E = 0.43$ KCal mol⁻¹. The deviation of the curve from straight line at the low temperature end may be due to the dominance of temperature dependent flip-flop relaxation [12]. Since the components are overlapping and the half-widths of the bands are of the order of the slit-width, the value of difference between the two potential minima can only be treated as a broad estimate.

4.4 RAMAN SPECTRA OF SELECTIVELY DEUTERATED TETRAMETHYL AMMONIUM IODIDE

The Raman spectra of the polycrystalline TMAI-d_n (n = 0, 1, 3, 9, 10, 11 and 12) at room temperature are shown in Fig. 4.7. The observed band-positions along with their vibrational assignment are given in Table 4.3. The assignment is done under the point group symmetry T_d for TMA ion, neglecting the possible distortion in this symmetry on isotopic substitution and correlation field splittings. The spectra of TMAI-d₀ and -d₁₂ differ from those of the corresponding Cl analogues only in the additional splittings of a few of the bands. The assignment of the bands for TMAI-d₀ has been

discussed earlier in sec. 4.2 and that for TMAI-d₁₂ conveniently follows from a comparison with the spectrum of TMACl-d₁₂ (cf. sec. 3.6). The assignment of bands in TMAI-d_n (n = 1, 3, 9, 10 and 11) is, however, not straight-forward. The details of the band assignments are discussed below.

4.4.1 Modes of C₄N Skeleton

The band-positions of the four internal modes of C₄N skeleton are well known. The symmetric stretching mode, $\nu_3(A_1)$ appears as a strong band at 748 cm⁻¹ in TMAI-d₀, with a weak shoulder at 753 cm⁻¹. In the deuterated samples, TMAI-d_n we find a single strong band in each sample, which shifts to 743, 737, 695, 688, 682 and 678 cm⁻¹ with n = 1, 3, 9, 10, 11 and 12, respectively in TMAI-d_n. The two-fold splitting of this band in d₀ salt has been ascribed to the dynamic disorder of TMA ion. The appearance of this band as a singlet in the deuterated salts may be due to two counts : (i) the D for H substitution causes a decrease in the splitting, and (ii) the TMA ion is less disordered in the deuterated salts. The asymmetric stretch, $\nu_{18}(F_2)$, which appears as a single strong band at 940 cm⁻¹ in d₀ sample, appears as a single band also in d₁₂ but at 806 cm⁻¹. This is as expected, because the symmetry is not changed, and mass effect would decrease ν . In the intermediate samples the band, however, shows a multiplet structure, three components being identified in each case. This is

expected because of different distributions of D's among the four methyl groups. We note that with increasing n the intensity weighted frequency shifts monotonously to lower values and that the intensity distribution varies among the components. The asymmetric deformation mode, $\nu_{19}(F_2)$ appears as a doublet for d_0 , d_3 , d_{11} and d_{12} salts, while as a triplet for d_1 , d_9 and d_{10} salts. The band-positions are as given in Table 4.3. The symmetric deformation mode, $\nu_8(E)$ could not be observed in any of these compounds. The intensity distribution among various component bands of the degenerate modes vary anomalously from one salt to the other. The appearance of the asymmetric bands as doublets for some of the partially deuterated salts may be due to very weak intensity of their third component or the two components falling together.

4.4.2 Deformation and Librational Modes of Methyl Group

The rocking mode of methyl group, $\nu_7(E)$ has been observed at 1172 and 923 cm^{-1} in TMAI- d_0 and TMAI- d_{12} , respectively, exhibiting a frequency shift ratio of 1.27. Thus frequency shift ratios of ~ 1.18 and ~ 1.09 are expected for the analogous rocking modes of CHD_2 and CH_2D groups, respectively. Therefore, the band at 958 cm^{-1} in TMAI- d_{11} is assigned to $\nu_7^{\text{CHD}_2}(E)$ and those at 1016 cm^{-1} in TMAI- d_{10} and 1000 cm^{-1} in TMAI- d_1 to $\nu_7^{\text{CH}_2\text{D}}(E)$. The band at

1000 cm^{-1} in TMAI-d₁, however, seems to have some additional contribution from a split component of $\nu_{18}(\text{F}_2)$. Another methyl rocking mode $\nu_{17}(\text{F}_2)$ shows a deuteration shift ratio of 1.28 (1282 cm^{-1} in TMAI-d₀ and 1184 cm^{-1} in TMAI-d₁₂), fixing the frequency of $\nu_{17}^{\text{CH}_2\text{D}}(\text{F}_2)$ to be around 1245 cm^{-1} which is indeed observed in TMAI-d₁ but there is no evidence of this band in TMAI-d₁₀. Therefore this band (1246 cm^{-1}) and two other bands (1260 and 1292 cm^{-1}) in TMAI-d₁ are assigned to the split components of $\nu_{17}^{\text{CH}_3}(\text{F}_2)$ due to the distortion of TMA ion from T_d symmetry on replacing one H by D. The asymmetric deformation of methyl group, $\nu_6(\text{E})$ and $\nu_{15}(\text{F}_2)$ are difficult to identify separately in the deuterated salts because of the strong mixing of these bands. Therefore, the four bands at 1058, 1066, 1072 and 1078 cm^{-1} in TMAI-d₁₂ are jointly assigned to $\nu_6(\text{E})$ and $\nu_{15}(\text{F}_2)$ of CD₃ group. Thus the frequency shift ratio for these bands on complete deuteration turns out to be ~ 1.37 which implies a frequency shift ratio of ~ 1.12 and ~ 1.24 for CH₂D and CHD₂ rock modes, respectively. Therefore, the bands at 1334 in TMAI-d₁, and at 1318 and 1328 cm^{-1} in TMAI-d₁₀ are easily assigned to asymmetric deformations of CH₂D group and the band at 1174 cm^{-1} in TMAI-d₁₁ to asymmetric deformation of CHD₂ group. In TMAI-d₀ the symmetric deformation mode $\nu_{16}(\text{F}_2)$ appears as a strong band at 1397 cm^{-1} but $\nu_2(\text{A}_1)$ does not appear at all. The case is inverted for TMAI-d₁₂ where $\nu_2(\text{A}_1)$ appears at 1132 cm^{-1} , though not very strong, but $\nu_{16}(\text{F}_2)$ does

not appear. The bands at 1405, 1402 and 1416 cm^{-1} in TMAI- d_1 , d_3 and d_9 , respectively, are assigned to the $\nu_{16}(\text{F}_2)$ mode of CH_3 group. The weak doublet at 1310, 1334 cm^{-1} in TMAI- d_{11} is tentatively assigned to a component of $\nu_{16}(\text{F}_2)$ due to CHD_2 group which needs verification, may be with the help of the spectrum of TMAI- d_2 . The bands at 1150, 1118 and 1108 and 1117 cm^{-1} in TMAI- d_3 , d_9 , d_{10} and d_{11} , respectively, are by analogy assigned to the $\nu_2(\text{A}_1)$ mode.

4.4.3 Methyl Stretching Region

There are a number of bands in the methyl stretching region including four fundamentals. The assignments in TMAI- d_0 and d_{12} conveniently follow from the comparison of spectra with those of TMAI- d_0 and d_{12} [cf. Chap. 3] and are shown in Tables 4.1 and 4.3. The bands in TMAI- d_1 , d_3 , d_9 , d_{10} and d_{11} having the band shapes similar to the bands in TMAI- d_0 and d_{12} in the respective regions (CH_3 or CD_3 as the case may be) are tentatively assigned to the same bands as in latter salts, though there might be minor variations in the positions of some of the bands. This minor frequency variation is expected due to a variation in the intramolecular coupling on account of different D substituents. A few bands in d_1 , d_{10} and d_{11} salts are differently assigned. In d_1 and d_{10} , there is one CH_2D group while the rest are either all CH_3 groups or all CD_3 groups. The CH_2D group would give rise to one uncoupled C-D stretch, and to one symmetric and one asymmetric stretching

modes of CH_2 . Therefore the bands at 2968 and 3010 cm^{-1} in TMAI- d_{10} are unambiguously assigned to $\nu_{\text{sym.}}^{\text{CH}_2\text{D}}$ and $\nu_{\text{asym.}}^{\text{CH}_2\text{D}}$ stretching modes, respectively. In TMAI- d_1 , the band at 2970 cm^{-1} is assigned to $\nu_{\text{sym.}}^{\text{CH}_2\text{D}}$ stretch whereas the $\nu_{\text{asym.}}^{\text{CH}_2\text{D}}$ stretch could not be observed separately because of overlapping bands of $\nu_5(\text{E})$ and $\nu_{13}(\text{F}_2)$ modes of CH_3 group. In the CD_3 stretching region for TMAI- d_1 , only one band that due to uncoupled C-D stretch is expected. However, we observe two bands at 2194 and 2223 cm^{-1} . The doublet may arise due to the reasons: (i) the bond lengths of C-H bonds in CH_3 may be nonequivalent, and (ii) one band is due to C-D stretch while the other is some combination or overtone. The solution spectrum supports the later possibility where two bands in this region are observed. Therefore the band at 2223 cm^{-1} is assigned to $\nu(\text{C-D})$ whereas the other could be some two-phonon band and is left unassigned. Similarly, in TMAI- d_{10} the band at 2220 cm^{-1} is assigned to $\nu(\text{C-D})$. TMAI- d_{11} has one CHD_2 group and the rest CD_3 groups. We, therefore, expect an uncoupled C-H stretching band in the CH_3 -region and two bands in the CD_3 region (one symmetric stretch and one asymmetric stretch of CD_2) of CHD_2 group apart from the modes of CD_3 group. The single band at 2984 cm^{-1} in the CH_3 stretching region is unambiguously assigned to $\nu(\text{C-H})$. The band at 2174 cm^{-1} is conveniently assigned to $\nu_{\text{sym.}}^{\text{CHD}_2}$ whereas the $\nu_{\text{asym.}}^{\text{CH}_2\text{D}}$ band is overlapped by the $\nu_5(\text{E})$ (or $\nu_{13}(\text{F}_2)$) mode of CD_3 . In TMAI- d_9 , we observed some unexpected additional weak bands having positions very near to the ones in TMAI- d_1 .

It is, therefore, suspected that small traces of TMAI-d₁ were present in TMAI-d₉ as impurity.

4.5 CONCLUSION

The spectral evidence shows that TMACl-d₀ and TMABr-d₀ are isostructural while TMAI-d₀ seems to possess a different structure at room temperature. This needs to be verified by the direct and conventional methods such as X-ray diffraction, inelastic neutron scattering etc. The free space available to TMA-d₀ ion in the unit cell is larger in the case of TMAI-d₀ than in TMACl-d₀ and TMABr-d₀ and the electronegativity of halide ion is less for TMAI-d₀. These facts put together allows the TMA-d₀ ion in TMAI-d₀ to tumble more freely in two inequivalent orientational positions (parallel and perpendicular) leading to the splitting of the totally symmetric mode of C₄N skeleton, $\nu_3(A_1)$. A tentative assignment of the vibrational modes of selectively deuterated TMA iodides is proposed on the basis of their room temperature Raman spectra. The distribution of intensity among various bands vary anomalously in the differently deuterated salts (TMAI-d_n, n = 0, 1, 3, 9, 10, 11 and 12). The separation between methyl symmetric and asymmetric stretching modes also show anomalous behaviour being less in TMAI-d₀ than in TMAI-d₁₂.

REFERENCES

1. Mahendra Pal, A Agarwal, D P Khandelwal and H D Bist, J. Mol. Structr. 112, 309 (1984).
2. L Vegard and K Sollesnes, Phil. Mag. 4, 985 (1927).
3. R W G Wyckoff, Z. Kristallogr. 67, 61 (1928).
4. W von der Ghe, J. Chem. Phys. 62, 3933 (1975).
5. A J Tench, J. Chem. Phys. 38, 593 (1963).
6. S Albert, H S Gutowsky and J A Ripmeester, J. Chem. Phys. 56, 3672 (1972).
7. A A V Gibson and R E Raab, J. Chem. Phys. 57, 4688 (1972).
8. J Dufourcq and B Lemanceau, J. Chim. Phys. 67, 9 (1970).
9. D J Blears, S S Danyluk and E Dock, J. Phys. Chem. 72, 2269 (1968).
10. S B W Rodder and D C Douglass, J. Chem. Phys. 52, 5525 (1970).
11. S S Chang and E P Westrum Jr., J. Chem. Phys. 36, 2420 (1962).
12. A K Sood, A K Arora, S Dattagupta and G Venkataraman, J. Phys. C 14, 5215 (1981).
13. H H Eysel and G Schumacher, Chem. Phys. Lett. 47, 168 (1977).

Table 4.1 : Raman band-positions (cm^{-1}) of tetramethyl ammonium halides (chloride, bromide and iodide) at room temperature and low temperature with their proposed assignments under point group symmetry T_d for $(\text{CH}_3)_4\text{N}^+$ ion.

TMACl-d ₀ ^a		TMABr-d ₀		TMAI-d ₀		Assignment
300 K	90 K	300 K	100 K	300 K	100 K	
376	376	$\nu_8(\text{E})$
388	389	384w, b	392w	
454	456	450s	454s	449s	451s	$\nu_{19}(\text{F}_2)$
459	464	460m	466m	460m	464m	
730 ^b	736 ^b	724 ^b vw	726 ^b vw	$2\nu_8(\text{E})$
760	758	757s	757s	748s	746s	$\nu_3(\text{A}_1)$
...	753m	758m	
...	887 ^b	916 ^b vw	924 ^b vw	916 ^b vw	920 ^b vw	$2\nu_{19}(\text{F}_2)$
930 ^b	940	938vw	$\nu_{18}(\text{F}_2)$
948	946	945vs	946vs	940vs	942vs	
...	958	
1182	1183	1180w, b	1183w	1172w, b	1176w, b	$\nu_7(\text{E})$
1192	1197	
...	1278vw	1280w	$\nu_{17}(\text{F}_2)$
1286	1291	1284s	1286s	1282s	1285s	
1398	1392	1394sh	1393sh	$\nu_{16}(\text{F}_2)$
1402	1397	1399s	1396s	1397vs	1395vs	
...	1407	
1454	1452	1451m	1449m	1448m	1447m	$\nu_6(\text{E})$
...	1474	1468w	1465m	1466m	
1477	1479	1472s	1474s	1468s	1469s	$\nu_{15}(\text{F}_2)$
1483	1486	1477m	1480m	1471m	1471s	

Table 4.1 Contd.....

TMACl-d _o ^a		TMABr-d _o		TMAI-d _o		Assignment
300 K	90 K	300 K	100 K	300 K	100 K	
...	2770	
2790	2792	2786m	2780m	2783m	2776m	$2\nu_{16}(\text{F}_2)$
...	2800	2780w	
2840	2834	2840vw	2834vw	2834vw	2828vw	$\nu_6(\text{E}) + \nu_{16}(\text{F}_2)$
2877	2872	2872m, b	2868m, b	2868m	2864m	$\nu_{15}(\text{F}_2) + \nu_{16}(\text{F}_2)$
2900 ^b	2900 ^b	2893 ^b vw	2886 ^b vw	2892 ^b vw	2880 ^b vw	$2\nu_6(\text{E})$
2918 ^b	2920 ^b	2912 ^b vw	2912 ^b vw	2914 ^b vw	2912 ^b vw	$2\nu_{15}(\text{F}_2)$
2951	2950	2944vs	2944vs	2938vs	2938vs	$\nu_1(\text{A}_1)$
2985 ^b	2986 ^b	2973 ^b w, b	2980 ^b w, b	$\nu_{14}(\text{F}_2)$
3019	3012	3014vs	3016vs	3010s	3009vs	$\nu_5(\text{E})$
...	3022	
3027	3028	3020vs	3021vs	3015vs	3014vs	$\nu_{13}(\text{F}_2)$
...	3033	

^aFrom chap. 3.

^bThe bands are very weak and broad or overlapping a strong band, so their positions may be uncertain to $\pm 5 \text{ cm}^{-1}$.

v - very, s - strong, m - medium, w - weak, sh - shoulder, b - broad.

Table 4.2 : Calculation of free space available in the unit cells of TMACl-d_0 , TMABr-d_0 and TMAI-d_0 ; all are tetragonal at room temperature having space group D_{4h}^7 ($Z = 2$).

Compound	Unit cell dimension		Vol. unit cell (\AA^3)	Ionic radius of halide ion (\AA) ^b	Vol. occupied in unit cell by	
	a (\AA) ^a	c (\AA) ^a			Halide ions (\AA^3)	TMA ions (and free space) (\AA^3)
TMACl-d_0	7.78	5.53	334.72	0.26	0.148	334.57
TMABr-d_0	7.76	5.53	333.00	0.39	0.497	332.50
TMAI-d_0	7.941	5.749	362.53	0.50	1.047	361.48

^aValues taken from, J D H Donnay, Crystal Data, Am. Crystallogr. Assoc., 1963.

^bValues taken from Table of Periodic Properties of the Elements, Sargent-Welch Scientific Com., Chicago, 1968.

Table 4.3 : Observed band-positions (in cm^{-1}) in Raman spectra of selectively deuterated tetramethyl ammonium iodides (TMAI-d_n ; $d = 0, 1, 3, 9, 10, 11$ and 12) in polycrystalline form at room temperature with their assignment.

d_0	d_1	d_3	d_9	d_{10}	d_{11}	d_{12}	Assignment
449s	446m	438s	396m	390m	393s	382m	
460m	456m	454m	410m	396m	402m	390w	$\nu_{19}(\text{F}_2)$
...	466m	...	416m	408m	
...	492w, br
...	...	720vw	714w	694sh	$2\nu_8(\text{E})$
748s	743s	737vs	695vs	688vs	682vs	678s	$\nu_3(\text{A}_1)$
753m	
916vw	$2\nu_{19}(\text{F}_2)$
...	875m	842m	811m	808s	806s	806s	
940vs	946s	934m	837m	850w	858w	...	$\nu_{18}(\text{F}_2)$
...	1000w	994m	874m	868w	
1172vw, b...	955vw	936vw	918vw	923vw	
...	953vw	...	$\nu_7(\text{E})$
...	1000w	1016w	
...	1246w	
1278vw	1260w	1266m	1194m	1181s	$\nu_{17}(\text{F}_2)$
1282s	1292w	1295w	1249m	1188s	1189s	1184s	
1397s	1405s	1402s	1416w	
...	1310vw	...	$\nu_{16}(\text{F}_2)$
...	1334w	...	

Table 4.3 Contd....

d_0	d_1	d_3	d_9	d_{10}	d_{11}	d_{12}	Assignment
1448m	...	1086w	1034w	1052vw	...	1058vw	
...	1438w	1092w	1060vw	1064w	1070m	1066w	
1465m	1456w	1444m	1068w	1070vw	1080sh	1072w	$\nu_6(E)$ or $\nu_{15}(F_2)$
1468s	...	1464w	1078vw	
1471m	1472m	1469vw	
...	...	1478vw	1472m	
...	1174w	...	
...	1318w	
...	1334w	1328w	
...	1446w,b
...	...	1150vw	1118m	1108m	1117m	1132w	$\nu_2(A_1)$
...	2054sh
...	2194w
...	2194w	2204vw
2783m	2790w	2786m	2808w	$2\nu_{16}(F_2)$
2834vw	...	2826vw	$\nu_6(E)+\nu_{16}(F_2)$ or
2868m	2864vw	2854m	$\nu_{15}(F_2)+\nu_{16}(F_2)$
2892vw	2882sh	2895vw	2894w	
...	2906vw	2096sh	
...	...	2112vw	2110w	2111w	2104m	2108w	$2\nu_6(E)$ or
2914vw	...	2132w	2126w	2124vw	...	2124vw	$2\nu_{15}(F_2)$
...	2156sh	2148sh
...	...	2187m	2165s	2160s	2156s	2145s	$\nu_1(A_1)+\text{Lattice}$
...	2178vw	...	2164vw	
...	...	2078vw	2074vs	2078vs	2073vs	2077vs	$\nu_1(A_1)$
2938vs	2937s	2926s	2956s	

Table 4.3 Contd....

d_0	d_1	d_3	d_9	d_{10}	d_{11}	d_{12}	Assignment
...	2227w
...	2984s	...	ν (C-H)
...	2223m	2220m	ν (C-D)
...	2970m	2968vs	ν CH ₂ D sym.
...	3010s	ν CH ₂ D asym.
...	2174s	...	ν CHD ₂ sym.
...	2240vw	...	ν CHD ₂ asym.
...	...	2940w	ν_{14} (F ₂)
2973w, b	...	2952w	
3010s	...	2266vs	2266vs	2250sh	...	2250w	ν_5 (E) or
3015vs	3016vs	3010vs	3015vs	2267vs	2266vs	2269vs	ν_{13} (F ₂)
...	2300vw	2298vw
...	2885w
...	...	2976vw

v - very, s - strong, m - medium, w - weak, sh - shoulder and
b - broad.

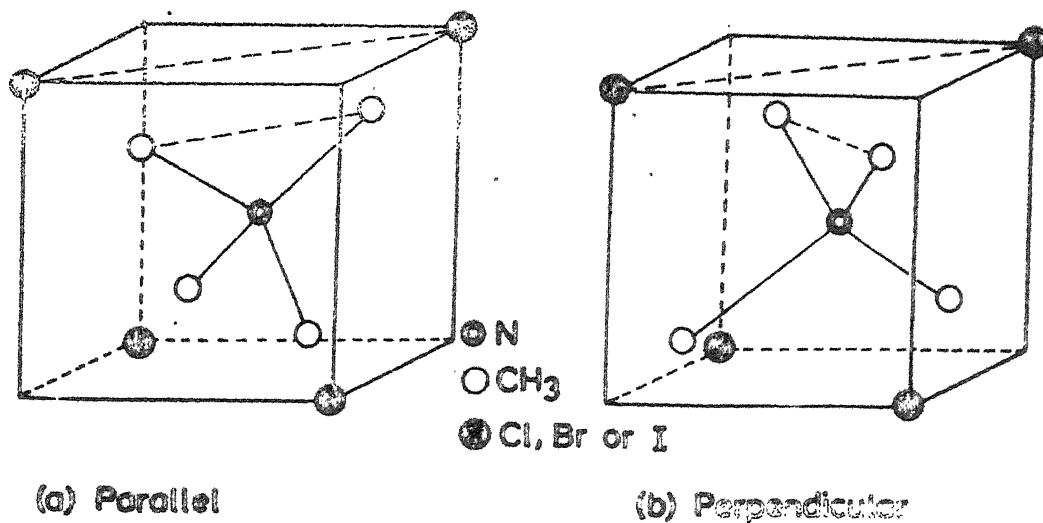


Fig. 4.1 Parallel and perpendicular orientations of the TMA ion in TMA halides (after Ohe [4]). Adjacent edges of the two tetrahedra (one formed by the methyl groups and the other by the four neighbour halide ions) are parallel (a), and perpendicular (b).

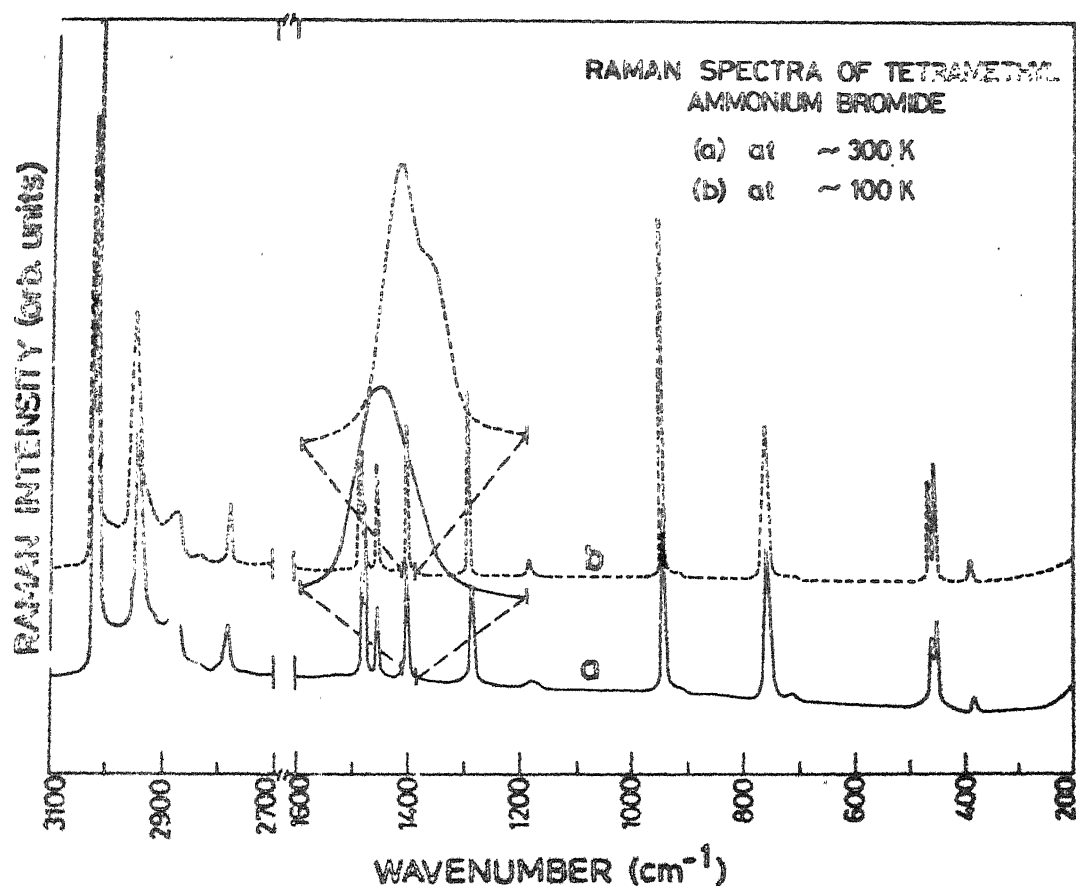


Fig. 4.2 Raman spectra of tetramethyl ammonium bromide (a) at 300 K and (b) at 100 K.

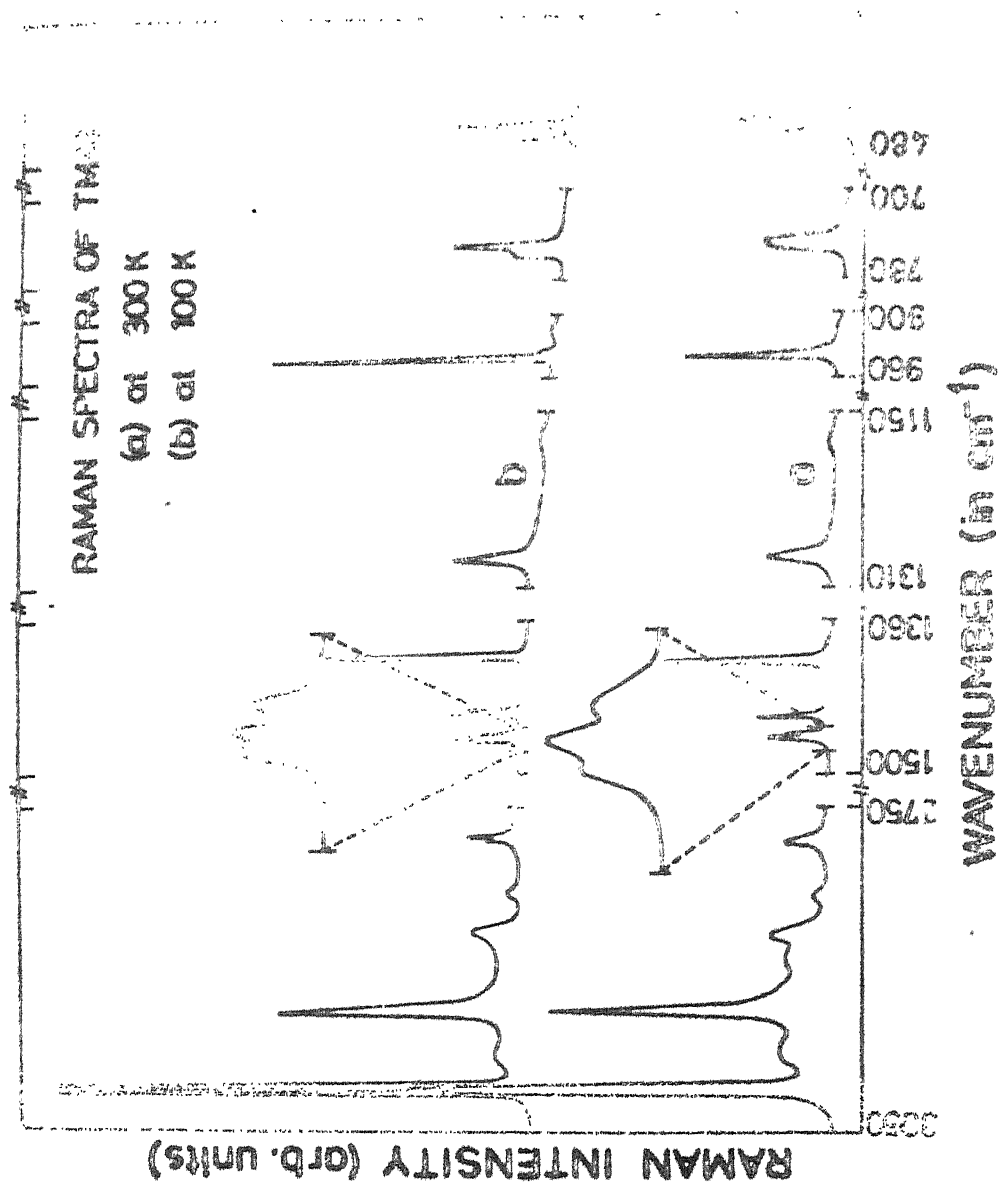


Fig. 4-3 Raman spectra of tetramethyl ammonium iodide (a) at 300 K and (b) at 100 K.

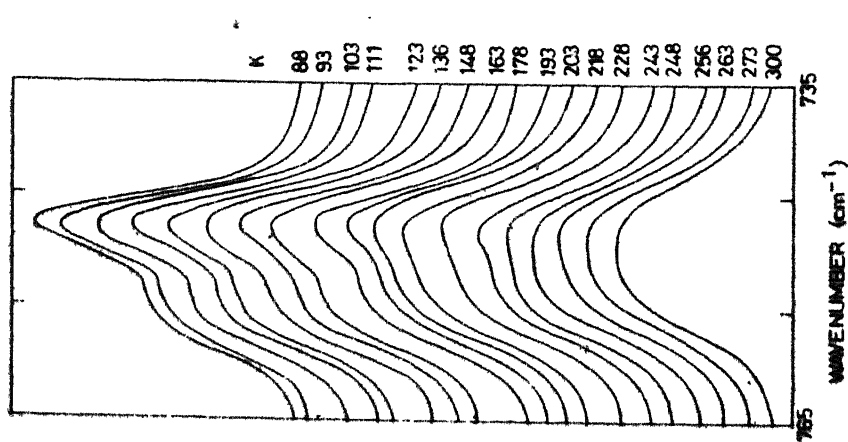


Fig. 4.4 Temperature dependence of the C_{2N} symmetric stretching mode $\nu_3(A_1)$ in tetramethyl ammonium iodide

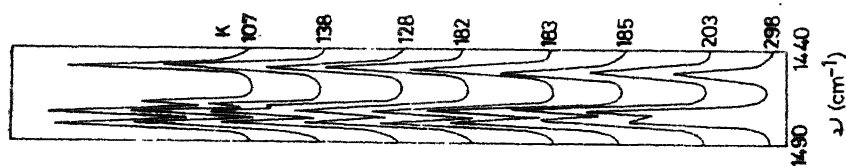


Fig. 4.5 The temperature dependence of CH_3 asymmetric deformation $\nu_6(E)$ and $\nu_{15}(F_2)$ in tetramethyl ammonium bromide.

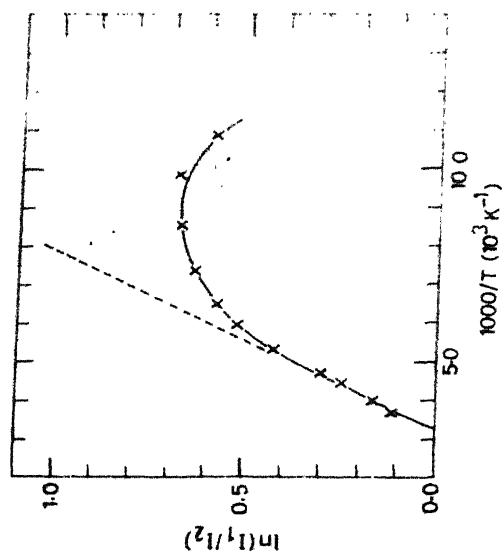


Fig. 4.6 Variation of intensities ratio of the components of C_{2N} symmetric stretching mode, $\nu_3(A_1)$ in tetramethyl ammonium iodide with temperature. The dotted line shows the slope in the higher temperature range.

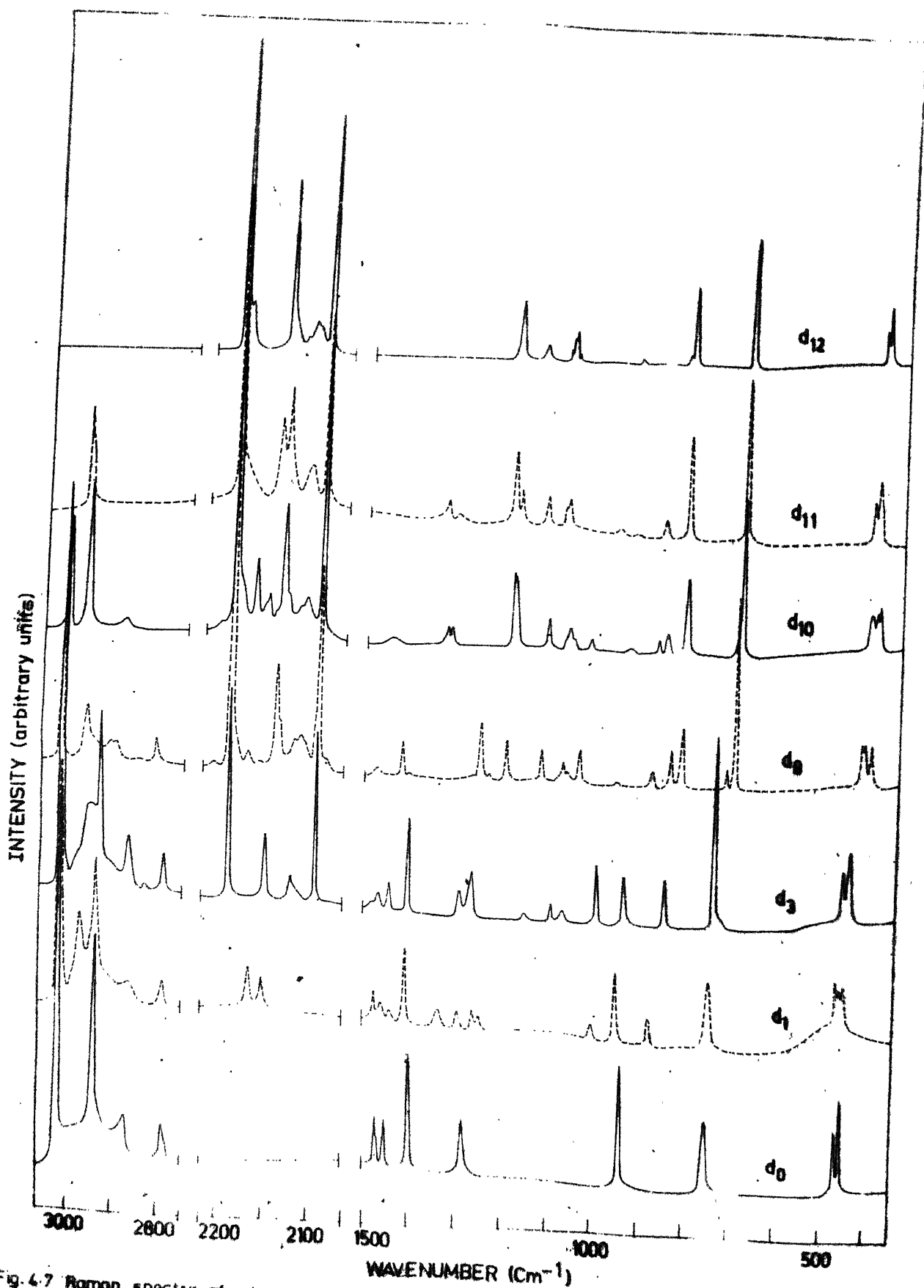


Fig. 4.7 Raman spectra of selectively deuterated tetramethyl ammonium iodide (TMAI- d_n , $n=0, 1, 3, 9, 10, 11$ and 12) at room temperature.

5. INCOMMENSURATE PHASE IN TETRAMETHYL AMMONIUM TETRACHLORO ZINCATE

In this chapter we present our vibrational Raman studies on tetramethyl ammonium tetrachloro zincate (abbreviated as $(\text{TMA})_2\text{ZnCl}_4$). We shall be mainly concerned with the behaviour of the internal modes in the incommensurate phase [1].

5.1 CRYSTAL STRUCTURE AND GROUP THEORETICAL ANALYSIS

The crystal structure of $(\text{TMA})_2\text{ZnCl}_4$ at room temperature was first determined by Morosin and Lingafelter [2]. Wiesner et al. [3] reperformed the X-ray studies and modified the lattice parameters. It has an orthorhombic structure with space group P_{nma} (D_{2h}^{16}) in which $a = 12.276 \text{ \AA}$, $b = 8.998 \text{ \AA}$, $c = 15.541 \text{ \AA}$ and $Z = 4$. The space group requires the ZnCl_4^{--} and TMA tetrahedra to lie on mirror planes parallel to (010) and at $y = \frac{1}{4}$. All the atoms are in the position $C_s(4)$ except Cl(2), Cl(3) and Cl(6) which are in the $C_1(8)$ position.

For group theoretical analysis the TMA and ZnCl_4^{--} have been considered as distinct groups which are at the site C_s . The total number of degrees of freedom for TMA in a unit cell are distributed as 24 translatory phonons + 24 rotatory phonons + 360 internal vibrations. For ZnCl_4^{--} there are 12 translatory phonons + 12 rotatory phonons + 36 internal vibrations.

Table 5.1 illustrates the correlation between the species of point group T_d and factor group D_{2h}^{16} through the site symmetry C_s . The internal vibrations of TMA and $ZnCl_4^{--}$ are distributed as follows:

$$\begin{aligned} \Gamma_{vib}^{TMA} &= 5A_g(R) + 4B_{1g}(R) + 5B_{2g}(R) + 4B_{3g}(R) \\ &\quad + 4A_u + 5B_{1u}(IR) + 4B_{2u}(IR) + 5B_{3u}(IR) \end{aligned} \quad (5.1)$$

$$\begin{aligned} \Gamma_{vib}^{ZnCl_4^{--}} &= 6A_g(R) + 3B_{1g}(R) + 6B_{2g}(R) + 3B_{3g}(R) \\ &\quad + 3A_u + 6B_{1u}(IR) + 3B_{2u}(IR) + 6B_{3u}(IR) \end{aligned} \quad (5.2)$$

The tensors associated with the Raman active species (A_g , B_{1g} , B_{2g} and B_{3g}) of the D_{2h} factor group in orthorhombic system are:

$$\begin{aligned} A_{1g}: & \begin{vmatrix} \alpha_{xx} & 0 & 0 \\ 0 & \alpha_{yy} & 0 \\ 0 & 0 & \alpha_{zz} \end{vmatrix} & B_{1g}: & \begin{vmatrix} 0 & 0 & 0 \\ 0 & 0 & \alpha_{yz} \\ 0 & \alpha_{yz} & 0 \end{vmatrix} \\ B_{2g}: & \begin{vmatrix} 0 & 0 & \alpha_{xz} \\ 0 & 0 & 0 \\ \alpha_{xz} & 0 & 0 \end{vmatrix} & \text{and } B_{3g}: & \begin{vmatrix} 0 & \alpha_{xy} & 0 \\ \alpha_{xy} & 0 & 0 \\ 0 & 0 & 0 \end{vmatrix} \end{aligned} \quad (5.3)$$

An orthorhombic crystal could be examined under the following geometries:

$$\begin{array}{llll}
A_g & Z(XX)Y & ; & Z(YY)X & ; & Y(ZZ)X \\
B_{1g} & Z(YX)Y & ; & Z(XY)X & ; & Y(XY)X \\
B_{2g} & Z(XZ)Y & ; & Z(XZ)X & ; & Y(XZ)X \\
B_{3g} & Z(YZ)Y & ; & Z(YZ)X & ; & Y(ZY)X
\end{array} \quad (5.4)$$

Out of these twelve geometries, those belonging to B_{1g} , B_{2g} and B_{3g} species give only one distinct spectrum each. Thus a maximum of six different polarization spectra are expected in an orthorhombic system.

5.2 RAMAN SPECTRA OF $(TMA)_2ZnCl_4$ CRYSTAL

The relevant portions of the observed Raman spectra of $(TMA)_2ZnCl_4$ at room temperature in six polarization geometries are shown in Fig. 5.1. The spectra are quite similar to those in aqueous solutions. Thus the vibrational (Raman) studies of $(TMA)_2ZnCl_4$ support the results of Blinc et al. [4] from nuclear magnetic resonance measurements. Blinc et al. proposed that at room temperature the TMA ion has a number of equivalent orientational positions due to which $(TMA)_2ZnCl_4$ behaves as a quasi-liquid. Our vibrational spectra reveal that $ZnCl_4^{--}$ too has a number of equivalent orientational positions like TMA ion. The assignment of TMA modes in aqueous solution has been discussed in detail earlier [see Chap. 3]. The observed band-positions in $(TMA)_2ZnCl_4$ and their assignment are given in Table 5.2.

The $\nu_1^Z(A_1)$ and $\nu_3^Z(F_2)$ modes of $ZnCl_4^{--}$ under point group symmetry T_d are falling nearly at the same positions.

A sharp and strong band at 280 cm^{-1} in the diagonal polarizations which appears as a weak band in cross polarizations is assigned to $\nu_1^Z(A_1)$. $\nu_3^Z(F_2)$ has negligible intensity in the Raman spectra and is covered by the overwhelming intensity of $\nu_1^Z(A_1)$. On the other hand, $\nu_1^Z(A_1)$ is forbidden in IR spectra. A very strong band at 272 cm^{-1} appears in IR spectra and is assigned to $\nu_3^Z(F_2)$. The band at 118 and 130 cm^{-1} in $X(ZZ)Y$ orientation are assigned $\nu_2^Z(Z)$ and $\nu_4^Z(F_2)$, respectively.

5.3 PHASE TRANSITIONS IN $(TMA)_2ZnCl_4$

The sequence of successive phase transitions in $(TMA)_2ZnCl_4$ has been extensively studied by several techniques such as differential thermal analysis [5,6], X-ray scattering [7-10], neutron inelastic scattering [11], electron spin resonance [12,13], proton magnetic relaxation [4,14], dielectric measurement [15], ultrasonic wave propagation [16] etc. Six transitions are known to occur in the salt from room temperature down to liquid nitrogen temperature. The details about the phases and transition temperatures are compiled in Table 5.3.

The temperature dependence of the Raman spectra from a single crystal of $(TMA)_2ZnCl_4$ in the $X(ZZ)Y$ orientation in the region $2750\text{--}3100\text{ cm}^{-1}$ is shown in Fig. 5.2. In this region we observed eight bands at 3027 , 2984 , 2958 , 2926 , 2894 , 2874 , 2826 and 2810 cm^{-1} . The band at 3027 cm^{-1} is associated with the CH_3 asymmetric stretching modes and the

other bands are associated with the CH_3 symmetric stretching mode and multiphonon transitions involving lower frequency bands.

The variation of the peak intensities with temperature of the four main bands at 3027, 2984, 2958, and 2926 cm^{-1} in $\text{X}(\text{ZZ})\text{Y}$ orientation is shown in Fig. 5.3. At the $\text{I} \rightarrow \text{II}$ transition point ($T_i \simeq 296\text{ K}$) the intensities of the symmetric mode bands start decreasing and achieve a minimum value at 293 K. Below this temperature they again gain intensities till the next commensurate phase comes ($T_c \simeq 281\text{ K}$). The CH_3 asymmetric band at 3027 cm^{-1} exhibits only marginal changes at the above transitions. The peak positions of all the bands remain unchanged. Such behaviour is observed for all the bands of species A_1 under point group symmetry T_d . In the $\text{X}(\text{YZ})\text{Y}$ geometry the behaviour is just the opposite, while in other geometries no temperature dependent variation of intensities is observed (Fig. 5.4) in this temperature range.

The existence of amplitudons and phasons is a specific feature of an incommensurate phase [17,18]. The phasons can only be detected either by neutron inelastic scattering or by Brillouin scattering [17]. The soft mode behaviour of amplitudons in the lattice region and appearance of a band only in the incommensurate phase have been understood as the Raman signatures of an incommensurate phase [17,18]. Bon et al. [19] have predicted the existence of a soft mode of species A_{1g} in the lattice region, but no such mode could be observed

in the lattice region in our spectra due to increase in the Rayleigh wing in going to low temperatures, which is perhaps related to the central peak problem.

As mentioned earlier Blinc et al. [4] have suggested that $(\text{TMA})_2\text{ZnCl}_4$ behaves as quasi-liquid, since it has a number of equally probable orientations. If one considers that in an incommensurate phase the orientations of $(\text{TMA})_2\text{ZnCl}_4$ are completely free relative to the X and Y directions, but with respect to the Z direction they have specific orientations which are governed by an incommensurate modulation in that direction, then a cosine term (cosine of angle between specific orientation and Z direction) will come in the expression for intensity of the bands and it may explain the abnormal behaviour of the intensity pattern. However, it could not so far be explained quantitatively. Efforts are in progress to understand theoretically the actual mechanism of such a behaviour of the internal modes in Raman scattering in the incommensurate phase.

5.4 CONCLUSION

$(\text{TMA})_2\text{ZnCl}_4$, even in its crystalline state, behaves as a quasi-liquid on account of many equivalent orientational positions of both of its ionic entities, i.e., TMA and ZnCl_4^{--} . It has many structurally distinct phases, out of which the incommensurate phase falling between the temperatures 290.6 and 280.9 K is of particular interest since all the totally

symmetric internal modes show an anomalous behaviour in this phase. A qualitative explanation for the observed anomaly is that the TMA and ZnCl_4^{--} ions have discrete orientations about the Z-direction governed by an incommensurate modulation but are free to be at any angle relative to the X and Y directions.

REFERENCES

1. Mahendra Pal, D P Khandelwal, V N Sarin and H D Bist, Proc. on Third Symposium on Lasers and Applications, Tata McGraw Hill, India (1984).
2. B Morosin and E C Lingafelter, Acta Crystallo. 12, 611 (1959).
3. J R Wiesner, R C Srivastava, C H L Kennard, M DiVaira and E C Lingafelter, Acta Crystallo. 23, 565 (1967).
4. R Blinc, M Burgar, J Slak, V Rutar and F Milia, Phys. Stat. Sol. A56, K65 (1979).
5. S Sawada, T Shiroishi, A Yamamoto, M. Takashige and M Matsuo, J. Phys. Soc. Jpn. 44, 687 (1978).
6. I R Larrea, A L Echarri and M J Tello, J. Phys. C14, 3171 (1981).
7. H Mashiyama and S Tanisaki, Phys. Lett. 76A, 347 (1980).
8. S Tanisaki and H Mashiyama, J. Phys. Soc. Jpn. 48, 339 (1980).
9. R Almairac, M Ribet, J L Ribet and M Bziouet, J. Physique 41, L315 (1980).
10. H Mashiyama, K Hasobe and S Tanisaki, J. Phys. Soc. Jpn. 49, 92 (1980).
11. K Gasi and M Iizumi, J. Phys. Soc. Jpn. 48, 1775 (1980).
12. J Chandrasekhar, K C Kumar and S Subramanian, J. Mag. Res. 18, 129 (1975).
13. I Suzuki, K Tsuchida, M Fukui and R Abe, Japanese J. Appl. Phys. 20, L840 (1981).
14. L K E Niemela and J E Heinila, Chem. Phys. Lett. 82, 192 (1981).

15. S Sawada, T Yamaguchi and N Shibayama, J. Phys. Jpn. 48, 1397 (1980).
16. H Hoshizaki, A Sawada and Y Ishibashi, J. Phys. Soc. Jpn. 47, 341 (1979).
17. M Quilichini, J P Mathieu, M Le Postollec and N Toupry, J. Physique 43, 787 (1982).
18. M Bertault, M Krauzman, M Le Postollec, R M Pick and M Scott, J. Physique 43, 755 (1982).
19. A M Bon, R Almairac, P Nassiri, C Benoit and J L Ribet, Phys. Stat. Sol. B101, K87 (1980).

Table 5.1 : Correlation of molecular symmetry T_d to factor group D_{2h} through the site symmetry C_s .

Molecular symmetry T_d	Site symmetry C_s	(XZ)	Factor group D_{2h}
A_1	A'		A_g
A_2	A'		B_{1g}
E	A'		B_{2g}
F_1	A'		B_{3g}
F_2	A''		A_u
	A''		B_{1u}
	A''		B_{2u}
	A''		B_{3u}

Table 5.2 : Observed band-positions (in cm^{-1}) in the Raman spectra of $(\text{TMA})_2\text{ZnCl}_4$ crystal at room temperature in six different polarization geometrics and their assignment.

Y(XX)Z	X(YY)Z	X(ZZ)Y	X(ZX)Y	X(YX)Y	X(YZ)Y	Assignment
102vw	96w	102vw	Lattice
...	118w	118w	118w	118w	120w	$\nu_2^Z(\text{E})$
138m	132w	130w	130w	130w	138w	$\nu_4^Z(\text{F}_2)$
280s	284s	284s	276m	280w	280w	$\nu_1^Z(\text{A}_1)$
372vw	376vw	372vw	370vw	376vw	372vw	$\nu_8(\text{E})$
460w	458w	464w	458w	458w	460w	$\nu_{19}(\text{F}_2)$
738w	736w	740w	736vw	$2\nu_8(\text{E})$
753vs	760vs	758vs	756w	756w	756m	$\nu_3(\text{A}_1)$
952m	956m	952m	953w	952w	952w	$\nu_{18}(\text{F}_2)$
1170vw	1176vw	1176vw	1170vw	1170vw	1176vw	$\nu_7(\text{E})$
1288vw	1292vw	1292vw	1288vw	1292vw	1292vw	$\nu_{17}(\text{F}_2)$
1416w	1412w	1412w	1412w	1412vw	1416w	$\nu_{16}(\text{F}_2)$
1452m	1456m	1454m	1452w	1456w	1456w	$\nu_6(\text{E})$
2808vw	2810vw	2810vw	2808vw	$2\nu_{16}(\text{F}_2)$
2826m	2824m	2826m	2828vw	2826vw	2828w	
2876vw	2874vw	2874vw	$\nu_{16}(\text{F}_2) + \nu_6(\text{E})$
2898vw	2898vw	2894vw	$2\nu_6(\text{E})$
2928s	2926s	2926s	2928vw	2928vw	2928m	$\nu_6(\text{E}) + \nu_{15}(\text{F}_2)$
2960m	2958m	2958m	2960vw	2960vw	2960w	$2\nu_{15}(\text{F}_2)$
2984s	2984s	2984s	2984vw	2984vw	2984w	$\nu_1(\text{A}_1)$
3027s	3028s	3027s	3028m	3027m	3026s	$\nu_5(\text{E}), \nu_{15}(\text{F}_2)$

Table 5.3 : The known phases and transition temperatures for $(\text{TMA})_2\text{ZnCl}_4^*$.

Phase	Transition temperature	Space group
I	296.65 \pm 0.05 K	$D_{2h}^{16} (P_{\text{nam}})$ $Z = 4$ orthorhombic
II	280.95 \pm 0.05	Incommensurate $K_z = \frac{2}{5} +$
III	277.40 \pm 0.06	$C_{2v}^9 (P_{2_1\text{cn}})$ $Z = 20$ orthorhombic $K_z = \frac{2}{5}$
IV	177.84 \pm 0.06	$C_{2h}^5 (P_{2_1/c})$ $Z = 12$ monoclinic
V	170.65 \pm 0.06	$C_{2h}^5 (P_{112_1/b})$ $Z = 4$ monoclinic or triclinic
VI	159.01 \pm 0.06	?
VII		$D_2^4 (P_{2_1 2_1 2_1})$ $Z = 12$ orthorhombic

*From ref. [6].

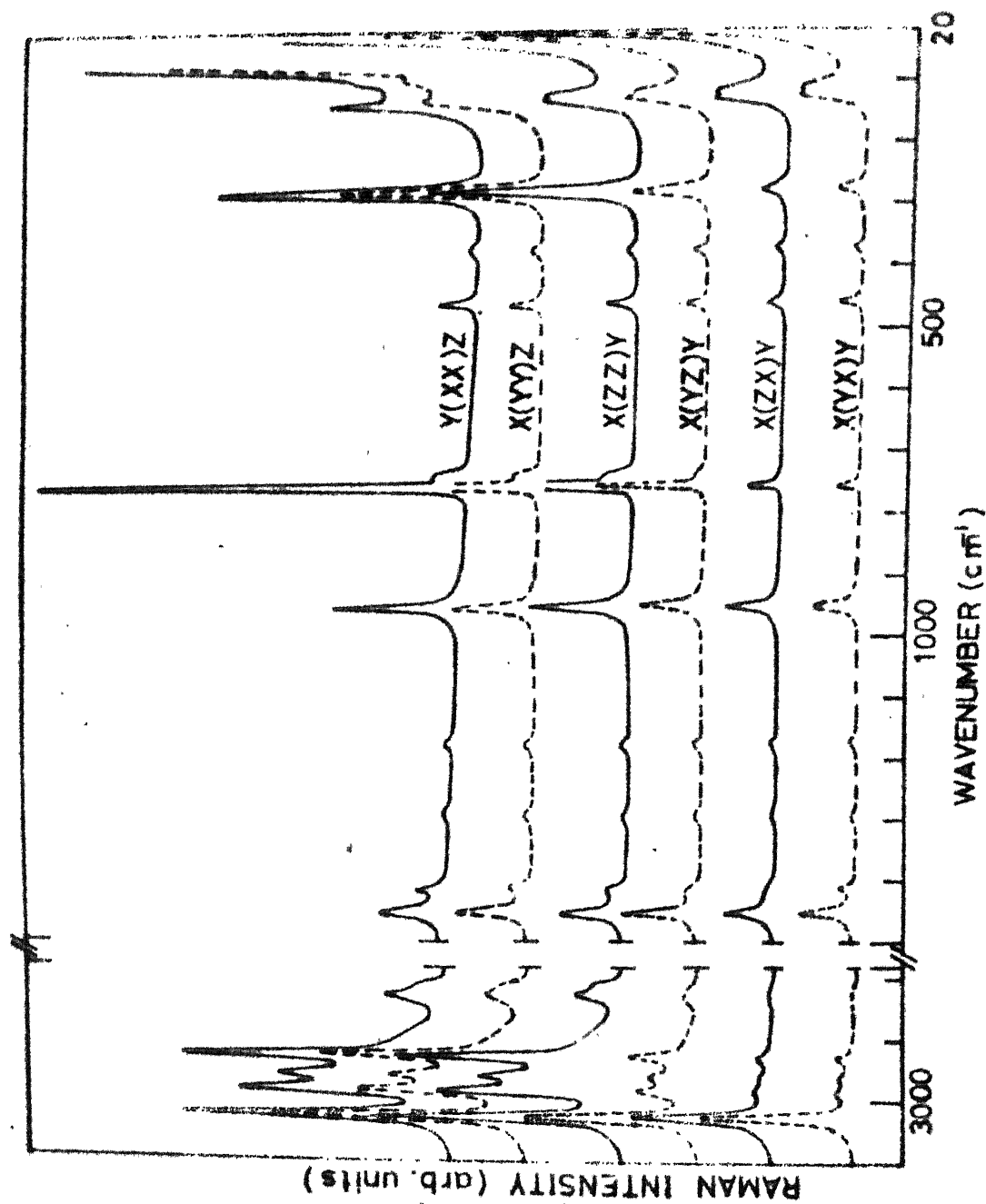


Fig.5.1 Raman spectra of $(\text{TMA})_2\text{ZnCl}_4$ at room temperature.

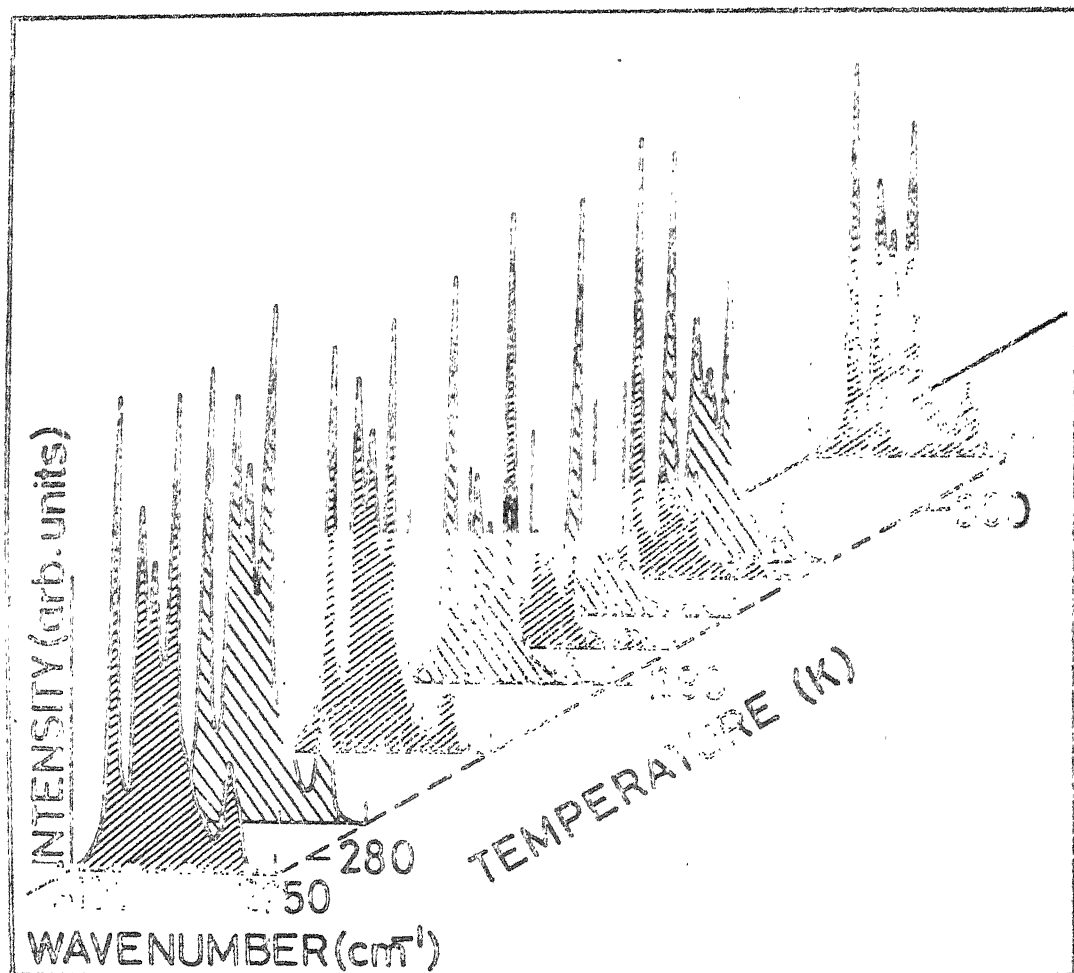


FIG.5-2 TEMPERATURE DEPENDENCE RAMAN SPECTRA OF $[(\text{CH}_3)_4\text{N}]_2\text{ZnCl}_4$ CRYSTAL IN X(ZZ)Y POLARIZATION.

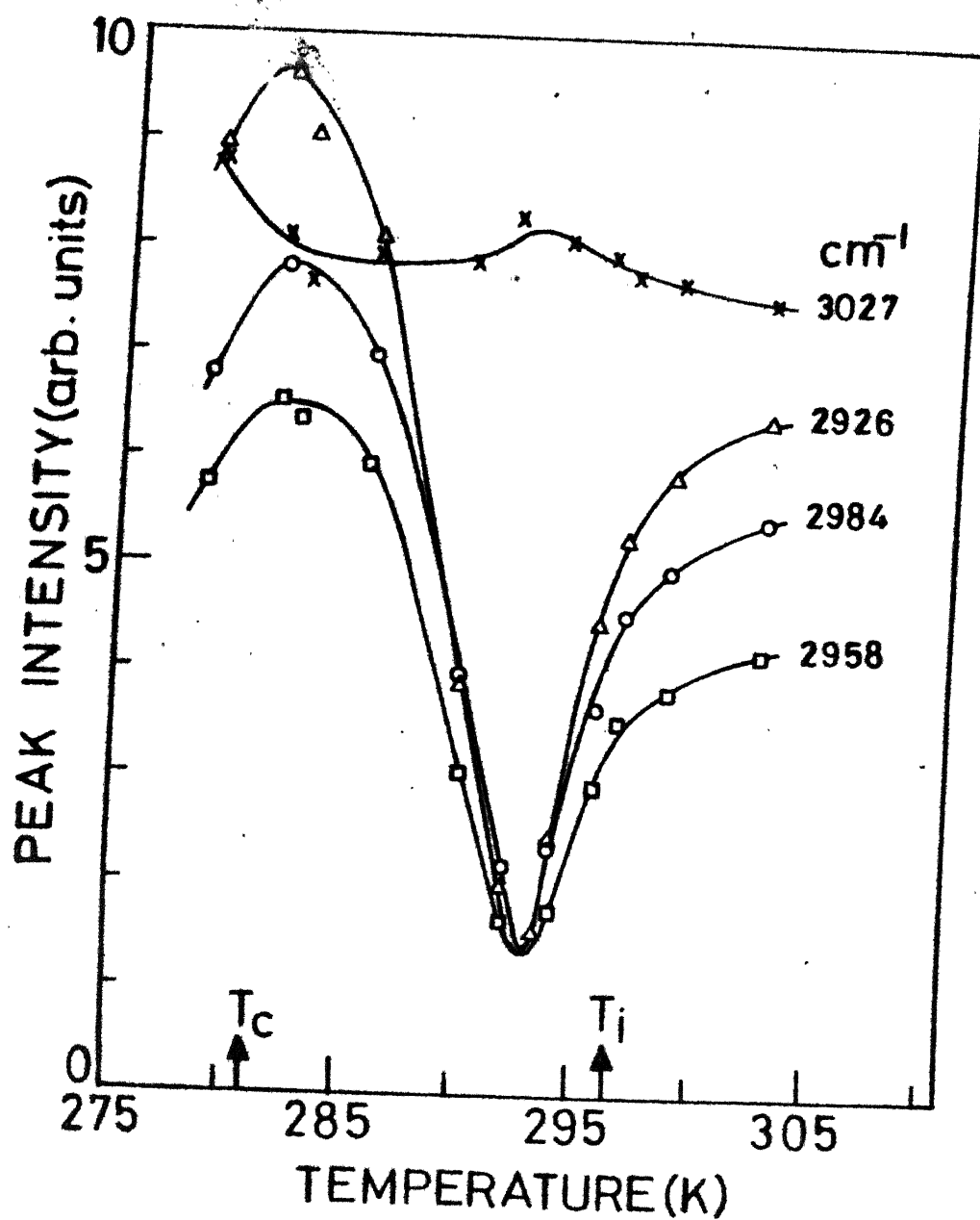


FIG.5.3 PEAK INTENSITY VERSUS TEMPERATURE OF THE BANDS IN X(ZZ)Y POLARIZATION.

6. CONCLUSION

In the work reported here the Raman and infrared absorption spectra of tetramethyl ammonium halides (chloride, bromide and iodide) and tetramethyl ammonium tetrachloro zincate have been studied with a view to understand the vibrational dynamics and the nature and mechanisms of the phase transitions in them. The observed bands in aqueous solutions and in solid phases have been characterized by considering the point group symmetry T_d of the tetramethyl ammonium (TMA) ion. The symmetric stretching mode of C_4N skeleton, $\nu_3(A_1)$ shows a two-fold splitting in the iodide TMAI- d_0 , unlike its single character in the corresponding chloride and bromide. This is attributed to reorientational disorder of TMA ion in the iodide between two inequivalent orientational positions - parallel and perpendicular; the reorientational energy has been calculated which turns out to be $0.43 \text{ KCal mol}^{-1}$. The tumbling would increase with the free space available in the lattice, and crystal data show it to be in the order TMAI > TMACl > TMABr. The maximum thermosensitivity of the bands is also found in TMAI for the same reason.

The asymmetric deformation modes of methyl group, $\nu_6(E)$ and $\nu_{15}(F_2)$, which appear very close together at room temperature have been separately identified and assigned with

the help of the temperature variation studies of their Raman spectra. The Raman spectra of TMA-d₀ halides in aqueous solutions show three intense polarized bands in the CH₃ stretching region. Two models have been proposed to explain this : (i) anharmonicity and Fermi resonance, and (ii) dynamic distortion of C₄N skeleton. However, both the models fail to explain the appearance of only a single strong band in the CH₃ symmetric stretching region in the Raman spectra of the polycrystalline TMA-d₀ halides.

The three known phase transitions in TMACl-d₀ above liquid nitrogen temperatures have been confirmed on the basis of these studies. Numbering the phases from high temperature downwards, the following inferences have been drawn about their mechanism from the spectral evidence : (i) the phase transition II → I, occurring at 536 K, is due to ionic diffusion in which H atoms of TMA-d₀ get relatively free, (ii) the transition III → II is irreversible and of the reconstructive type and this transition temperature depends on the rate of heating, T_c going up as the heating rate is decreased. The transition occurs at 367 ± 2 K on keeping the sample under vacuum during investigation, (iii) the transition III → IV occurs at 185 K and is due to reorientation of CH₃ groups and tumbling of the whole TMA-d₀ ion. In TMACl-d₁₂ a single phase transition (III → II) at 407 ± 5 K is observed which is irreversible and of the reconstructive type. It is concluded that TMACl-d₁₂ lies in between TMACl-d₀ and TMABr-d₀ in the generalized phase diagram.

of the TMA halides. TMABr and TMAI do not undergo any phase transition in the temperature range 540 - 90 K.

Our studies have suggested that at room temperature TMACl-d₀ and TMABr-d₀ are isostructural, whereas TMAI-d₀ possesses a different structure, though X-ray studies predicted the same space group for all the halides (D_{4h}^7 (Z = 2)). Further X-ray diffraction studies and inelastic neutron scattering studies are needed to resolve this discrepancy. A space group for phase IV in TMACl-d₀ is suggested to be D_4^1 (Z = 2) due to the splitting of bands of species F_2 of TMA-d₀ under molecular symmetry T_d into three components. In frame work of our studies the earlier suggested space group O_h^5 (Z = 4) for phase I is inherently inconsistent and has to be reinvestigated crystallographically.

(TMA)₂ZnCl₄, even in its crystalline state, behaves as a quasi-liquid on account of many equivalent orientational positions of both of its ionic entities, i.e., TMA and $ZnCl_4^{--}$. It has many structurally distinct phases and is incommensurate between the temperatures 290.6 and 280.9 K. In this phase, the totally symmetric modes behave anomalously in the z-direction due, probably, to discrete orientations of TMA and $ZnCl_4^{--}$ ions about the z-direction governed by an incommensurate modulation.

Thus in terms of the experimental investigations and interpretation of data, this work is a substantial advancement for understanding molecular vibrational dynamics in tetramethyl ammonium halides and the nature and mechanisms of the observed phase transitions. The additional investigation of

tetramethyl ammonium tetrachloro zincate, a representative example of the series compounds which undergo successive phase transitions including an incommensurate phase, justifies the potentiality of the approach.

The systems, which have been the subject of the present work, provide many aspects for future studies. The most promising is the normal coordinate analysis for the calculation of the force constants and the vibrational frequencies. Efforts are under progress to work out a computer program for this purpose. These calculations will be very helpful in verification of the vibrational assignment. Besides this, in $(\text{TMA})_2\text{ZnCl}_4$, the anomalous behaviour of the internal modes in the incommensurate phase seeks a theoretical justification. This, too, forms an interesting piece of work as the incommensurate phase transitions have, recently, attracted much attention for their peculiarity.

LIST OF PUBLICATIONS

(a) In Journal

- *₁ Dynamic distortion of C_4N skeleton in $(CH_3)_4NCl$
H D Bist, Mahendra Pal, G S Raghuvanshi and V N Sarin
Proc. Indian Acad. Sci. 91, 185 (1982).
- *₂. Vibrational studies and phase transitions in tetramethyl ammonium chloride
Mahendra Pal, G.S Raghuvanshi and H D Bist
Chem. Phys. Lett. 92, 85 (1982).
3. Fermi resonance in Raman infrared spectra of $Ni(CH_3COO)_2 \cdot 4H_2O$ and its deuterated analogue
G S Raghuvanshi, Mahendra Pal and H D Bist
J. Raman Spectros. 14, 1 (1983).
4. Vibrational spectra and phase transitions in $Ni(CH_3COO)_2 \cdot 4X_2O$ ($X = H, D$)
G S Raghuvanshi, Mahendra Pal, M B Patel and H D Bist
J. Mol. Struct. 00, 000 (1983).
- *₅. Raman spectra of III \rightarrow II phase transition in normal (d_0) and deuterated (d_{12}) tetramethyl ammonium chlorides
Mahendra Pal, A Agarwal, M B Patel and H D Bist
J. Raman Spectros. 00, 000 (1984).
- *₆. Dynamic disorder of $(CH_3)_4N^+$ ion in $(CH_3)_4NX$ ($X = Cl, Br$ and I)
Mahendra Pal, A Agarwal, D P Khandelwal and H D Bist
J. Mol. Struct. 112, 309 (1984).

(b) In Proceedings

1. Phase transitions in ammonium tetrachlorozincate by Raman technique
A Agarwal, Mahendra Pal and H D Bist
Proc. of Nuclear Physics and Solid State Physics Symposium 25C, 000 (1982).

2. Laser Raman studies of incommensurate phase in
 $[(CH_3)_4N]_2ZnCl_4$
Mahendra Pal, D P Khandelwal, V N Sarin and H D Bist
Proc. on Third Symposium on Laser and Applications,
Tata McGraw Hill, India (1984).

*Paper forming a part of the thesis.

A 87525

PHY-1984-D-PAL-VIB